



Exclusive dimuon production in ultraperipheral Pb+Pb collisions at $\sqrt{s_{\text{NN}}} = 5.02 \text{ TeV}$ with ATLAS

The ATLAS Collaboration

Exclusive dimuon production in ultraperipheral collisions (UPC), resulting from photon–photon interactions in the strong electromagnetic fields of colliding high-energy lead nuclei, $\text{PbPb}(\gamma\gamma) \rightarrow \mu^+\mu^- (\text{Pb}^{(\star)}\text{Pb}^{(\star)})$, is studied using $\mathcal{L}_{\text{int}} = 0.48 \text{ nb}^{-1}$ of $\sqrt{s_{\text{NN}}} = 5.02 \text{ TeV}$ lead–lead collision data at the LHC with the ATLAS detector. Dimuon pairs are measured in the fiducial region $p_{\text{T},\mu} > 4 \text{ GeV}$, $|\eta_\mu| < 2.4$, invariant mass $m_{\mu\mu} > 10 \text{ GeV}$, and $p_{\text{T},\mu\mu} < 2 \text{ GeV}$. The primary background from single-dissociative processes is extracted from the data using a template fitting technique. Differential cross sections are presented as a function of $m_{\mu\mu}$, absolute pair rapidity ($|y_{\mu\mu}|$), scattering angle in the dimuon rest frame ($|\cos \vartheta_{\mu\mu}^\star|$) and the colliding photon energies. The total cross section of the UPC $\gamma\gamma \rightarrow \mu^+\mu^-$ process in the fiducial volume is measured to be $\sigma_{\text{fid}}^{\mu\mu} = 34.1 \pm 0.3(\text{stat.}) \pm 0.7(\text{syst.}) \mu\text{b}$. Generally good agreement is found with calculations from STARlight, which incorporate the leading-order Breit–Wheeler process with no final-state effects, albeit differences between the measurements and theoretical expectations are observed. In particular, the measured cross sections at larger $|y_{\mu\mu}|$ are found to be about 10–20% larger in data than in the calculations, suggesting the presence of larger fluxes of photons in the initial state. Modification of the dimuon cross sections in the presence of forward and/or backward neutron production is also studied and is found to be associated with a harder incoming photon spectrum, consistent with expectations.

Contents

1	Introduction	3
2	ATLAS detector	5
3	Trigger and luminosity	7
3.1	Event trigger	7
3.2	Luminosity and electromagnetic (EM) pileup	7
4	Theoretical background	8
5	Monte Carlo samples	10
5.1	STARlight	10
5.2	Simulated samples: single muons and STARlight	10
5.3	QED showering with STARlight+PYTHIA8	11
5.4	LPAIR	11
6	Event characterization	11
6.1	Event selection	11
6.2	ZDC event class definition	12
7	Data analysis	13
7.1	Cross-section definitions	13
7.2	Trigger efficiencies	13
7.3	Reconstruction efficiencies and scale factors	15
7.4	Outflow from fiducial region	15
7.5	Dissociative background corrections	16
7.6	Forward neutron topology fractions	17
7.7	Unfolding of the acoplanarity distribution	19
8	Systematic uncertainties	20
8.1	Trigger efficiency	20
8.2	Reconstruction scale factors	20
8.3	Muon momentum scale and resolution	20
8.4	Fiducial acceptance definition	20
8.5	Dissociative background	21
8.6	Luminosity	21
8.7	ZDC neutron topology fractions	21
8.8	Unfolded acoplanarity distributions	22
9	Results	22
10	Conclusion	28

1 Introduction

Collisions of nuclei at ultrarelativistic energies are typically studied for processes in which the nucleons interact hadronically at impact parameters less than twice the nuclear radius ($b < 2R_A$), producing a large volume of hot, dense quark–gluon plasma in the overlap region, which can decay into thousands of outgoing hadrons. Events with the smallest impact impact parameters ($b \approx 0$) are referred to as “central” events, while those with the largest ($b \approx 2R_A$) are called “peripheral” events. However, the strong electromagnetic (EM) fields of large nuclei can also induce interactions in “ultraperipheral” collisions (UPC), events with impact parameters well beyond twice the nuclear radius ($b > 2R_A$), where any contributions from strong interactions are negligible. In the Weizsäcker–Williams approach [1, 2], based on a proposal from Fermi [3], also referred to as the “equivalent photon approximation” (EPA), the Lorentz-contracted EM fields act as a source of high-energy, nearly real photons. In nuclear collisions, photons with wavelengths larger than the nuclear size are produced coherently from the entire nucleus, and thus their flux is enhanced by a factor of Z^2 for each nucleus, relative to incoherent emission. While the photon energy in the rest frame is limited to $O(\hbar c/R_A) \approx 25$ MeV, where R_A is the nuclear radius, the longitudinal boost leads to photons of up to 75–100 GeV at the highest-available LHC nuclear beam energies (2.51 TeV per beam, corresponding to a Lorentz boost of $\gamma = 2595$). At such high energies, UPC can induce a wide variety of exclusive final states in lead–lead (Pb+Pb) collisions – dileptons, dijets, and diphotons being the most commonly measured – for which no other activity is observed, except for nucleons emitted at very small angles relative to the beam direction. The photons are also characterized by small transverse momenta of $O(\hbar c/R_A)$, such that high-energy decay products in these exclusive final states are almost perfectly balanced in the transverse direction.

Exclusive dimuon final states can be produced in Pb+Pb collisions via two primary UPC processes: 1) resonant diffractive photon–pomeron scattering which produces a vector meson that subsequently decays muonically, and 2) nonresonant exclusive two-photon scattering to dimuons, $\text{PbPb}(\gamma\gamma) \rightarrow \mu^+\mu^-(\text{Pb}^{(*)}\text{Pb}^{(*)})$, inclusive in the excitation of the outgoing nuclei (indicated by the $*$). UPC dimuon production is often referred to as the Breit–Wheeler process [4]. The leading-order Feynman diagram for UPC dimuons is shown in Figure 1(a). Once the invariant mass of the dileptons exceeds 10 GeV, the nonresonant two-photon contributions are by far the dominant contributions to the cross section. Although these purely EM interactions have a small cross section relative to strong interactions, the two-photon luminosity in UPC is enhanced over the nuclear luminosity by Z^4 . Thus, substantial rates of such processes are expected in heavy-ion collisions, and they are directly sensitive to the number and momentum distributions of photons emitted from a single nucleus. Precise measurements of the incoming photon fluxes are of great value for calibrating the rates of other hard processes involving UPC, such as the photonuclear production of hadrons and jets [5], and for improving predictions for purely EM processes such as light-by-light scattering [6, 7]. UPC dimuons can also be a non-negligible background for vector-boson production in peripheral heavy-ion collisions, where the EM fluxes exceed the partonic fluxes [8]. Comprehensive reviews of UPC physics, and two-photon physics in particular, can be found in Refs. [9–11].

Several groups have performed calculations of exclusive dilepton production at RHIC and the LHC [12–17]. In all calculations, the photon flux from each nucleus is usually modeled starting with a point source, but the finite extent of the nuclei is handled in different ways. The most widely used model is STARlight, the dilepton formalism of which is discussed in Ref. [12]. It has a sophisticated handling of the nuclear charge distributions, but it is missing several processes relevant for describing both signal and background in experimental data. None of the calculations to date include higher-order final-state QED effects, an

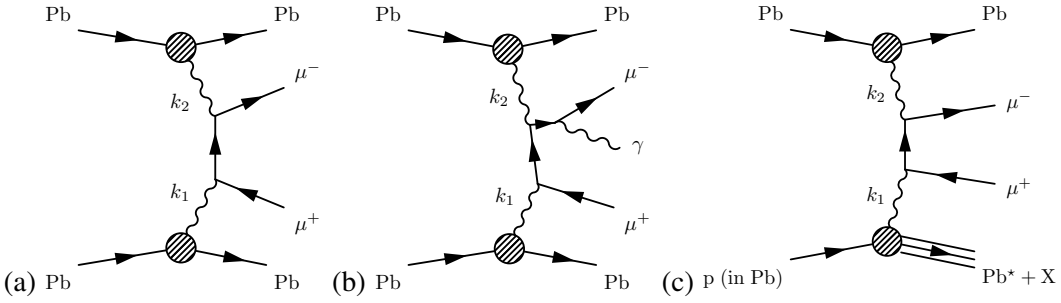


Figure 1: Diagrams for the (a) leading-order $\text{PbPb}(\gamma\gamma) \rightarrow \mu^+\mu^-$ (PbPb) and (b) next-to-leading-order $\text{PbPb}(\gamma\gamma) \rightarrow \mu^+\mu^- + \gamma$ (PbPb) (middle) Breit–Wheeler process in $\text{Pb}+\text{Pb}$ collisions, and (c) the dissociative $\text{PbPb}(\gamma\gamma^*) \rightarrow \mu^+\mu^- + X$ (Pb^*Pb) process where one photon is emitted from the substructure of one of the nucleons, leading to nucleon fragmentation in the far-forward direction.

example of which is shown in Figure 1(b), where the muons are accompanied by additional resolved soft photons in the final state. Dissociative processes, where one photon is emitted by charged constituents of a nucleon, as shown in Figure 1(c), are also neglected by most models, in part due to the fact that these processes are not coherently enhanced.

The study of exclusive dimuon cross sections, conditional on observations of forward neutron production in the direction of one or both incoming nuclei, provides an additional experimental handle on the impact parameter range sampled in the observed events [12, 18–20]. In any particular collision, soft photons emitted by one lead nucleus (Pb) can excite the other (Pb^*), typically through the giant dipole resonance [21], and induce the emission of one or more neutrons, each of which carry, on average, the full per-nucleon beam energy. Since the probability of these excitations, as well as the overall hardness of the photon spectrum, is correlated with the nucleus–nucleus impact parameter b [12], events with neutron excitation are typically correlated with harder photon collisions. In STARlight, dilepton cross sections associated with forward neutron production are calculated by convolving differential cross sections for low-energy photonuclear neutron production with the expected photon fluxes, thus in principle providing an essentially parameter-free prediction. Of course, the contribution from nucleonic dissociative processes must be subtracted before comparisons with data.

Exclusive dimuon cross sections are usually presented as a function of the following quantities of the dimuon final state:

- The dimuon invariant mass $m_{\mu\mu}$, which is equivalent to W , the center-of-mass energy of the colliding $\gamma\gamma$ system.
- The dimuon pair rapidity $y_{\mu\mu}$, which is the rapidity of the four-vector sum of the two muons. Conservation of longitudinal momentum implies that $y_{\mu\mu}$ is equal to the rapidity of the $\gamma\gamma$ system.
- The cosine of the dimuon scattering angle ϑ^* in the $\gamma\gamma$ center-of-mass frame, $|\cos \vartheta_{\mu\mu}^*|$. This is calculated from the rapidities of the two muons, y_+ and y_- , as $\tanh [(y_+ - y_-)/2]$.
- The acoplanarity $\alpha = 1 - |\Delta\phi_{\mu\mu}|/\pi$ which reflects, in part, the initial dimuon $p_{\text{T},\mu\mu}$.

While these are all final-state observables, the fact that the final state consists of only the two muons allows the initial photon energies (k_1 and k_2) to be determined from the final-state muons. This is described in

detail in Section 9, and these variables are perhaps the most transparent way to compare the experimental data with yields determined by the nuclear photon fluxes assumed by the models.

The ALICE and CMS experiments have performed several measurements of exclusive vector-meson production in Pb+Pb collisions, for which the Breit–Wheeler process is one of the backgrounds. Reference [22] presents the measured contribution from the dilepton continuum out to invariant mass $m_{\mu\mu} = 10$ GeV. They found no observable contribution from the Υ , which is expected to have a cross section at least an order of magnitude below the continuum at LHC energies. ALICE has also measured J/ψ in UPC in p +Pb collisions [23]. ATLAS [24, 25] and CMS [26] have both measured exclusive high-mass dileptons in proton–proton (pp) collisions, and LHCb has measured exclusive Υ production [27]. At RHIC, where the maximum photon energy is about 3 GeV, STAR has measured low-mass continuum electron pairs [28, 29], ρ^0 photoproduction [30]. PHENIX has measured the cross section for J/ψ and the continuum below the J/ψ peak [31]. CDF has observed exclusive electron pair production out to $m_{ee} = 30$ GeV [32] and exclusive muons [33] in $3 < m_{\mu\mu} < 4$ GeV. CMS has measured modifications of α distributions, but not cross sections, as a function of the forward neutron topology [34]. In no case has a heavy-ion cross section measurement of the dilepton pair continuum been performed above 10 GeV, which impedes precise predictions for higher-mass $\gamma\gamma$ processes, particularly light-by-light scattering [35–38].

This paper presents measurements of cross sections for exclusive dimuon production in UPC with lead nuclei, $PbPb(\gamma\gamma) \rightarrow \mu^+\mu^- (Pb^{(*)}Pb^{(*)})$, using $\mathcal{L}_{int} = 0.48 \text{ nb}^{-1}$ of data taken in 2015. The measurements are performed for a fiducial region matched to the optimal performance for measuring muons in ATLAS. This requires single muons with transverse momentum $p_{T,\mu} > 4$ GeV and pseudorapidity $|\eta_\mu| < 2.4$, a pair invariant mass range $10 < m_{\mu\mu} < 200$ GeV, and a pair $p_{T,\mu\mu} < 2$ GeV. The cross sections are measured by selecting events using a single-muon trigger, in association with an otherwise low-multiplicity event. The events are required to consist only of two oppositely charged muons, with no other measured activity in the ATLAS inner detector. Events are then corrected for muon trigger and reconstruction efficiencies, migration relative to the fiducial region, and for dissociative backgrounds. The cross sections are presented as a function of the final-state dimuon pair mass ($m_{\mu\mu}$), pair rapidity ($y_{\mu\mu}$), $\gamma\gamma$ center-of-mass scattering angle ($|\cos \vartheta_{\mu\mu}^*|$), and the dimuon acoplanarity. The two muon four-momenta can be combined to present cross sections as a function of the maximum and minimum energies of the incoming photons. Detailed comparisons of these data with predictions from STARlight provide the first detailed comparison at LHC energies of the various aspects of STARlight – from the nuclear photon fluxes to the implementation of the exclusivity condition – with experimental data over a very wide range in initial photon energies (up to 100 GeV). To vary the impact parameter range sampled by the dimuon events, events are classified according to their forward neutron topology, i.e. whether or not the neutrons are emitted in the forward or backward direction, or both, and corrected for the presence of EM pileup processes. Finally, cross sections for events with no forward neutron activity, which removes dissociative events, are presented as a function of dimuon acoplanarity. These data can be used to study the impact of QED showering on the final-state muons in an environment with very low backgrounds.

2 ATLAS detector

The ATLAS detector [39] at the LHC covers nearly the entire solid angle around the collision point. It consists of an inner tracking detector surrounded by a thin superconducting solenoid, electromagnetic and hadronic calorimeters, and a muon spectrometer incorporating three large superconducting toroidal magnets with eight coils each.

The inner detector (ID) is immersed in a 2 T axial magnetic field and provides charged-particle tracking in the range $|\eta| < 2.5$. The ID is composed of three major subsystems. The high-granularity silicon pixel detector covers the vertex region and typically provides four measurement points per track. It is followed by the silicon microstrip tracker, which usually provides four two-dimensional measurement points per track. These silicon detectors are complemented by the transition radiation tracker, which covers the pseudorapidity¹ interval $|\eta| < 2$ and thus enables radially extended track reconstruction in that range.

The calorimeter system covers the pseudorapidity range $|\eta| < 4.9$. Within the region $|\eta| < 3.2$, electromagnetic calorimetry is provided by barrel and endcap high-granularity lead/liquid-argon (LAr) electromagnetic calorimeters, with an additional thin LAr presampler covering $|\eta| < 1.8$ to correct for energy loss in material upstream of the calorimeters. Hadronic calorimetry is provided by the steel/scintillator-tile calorimeter, segmented into three barrel structures within $|\eta| < 1.7$, and two copper/LAr hadronic endcap calorimeters. The solid angle coverage is completed with forward copper/LAr and tungsten/LAr calorimeter modules optimized for electromagnetic and hadronic measurements respectively.

The muon spectrometer (MS) comprises separate trigger and high-precision tracking chambers measuring the deflection of muons in a magnetic field generated by the superconducting air-core toroids. The field integral of the toroids ranges between 2.0 and 6.0 T m across most of the detector. A set of precision chambers covers the region $|\eta| < 2.7$ with three layers of monitored drift tubes, with the innermost chambers replaced by cathode strip chambers in the forward region ($|\eta| > 2$), where the background is highest. The muon trigger system covers the range $|\eta| < 2.4$ with resistive plate chambers in the barrel, and thin gap chambers in the endcap regions.

Muon reconstruction is first performed independently in the ID and MS. The information from the individual subdetectors is then combined to form the muon tracks that are used in the analysis [40].

A multi-level trigger system is used to select interesting events [41]. The first-level (L1) trigger is implemented in hardware and uses a subset of detector information to reduce the event rate to a design value of at most 75 kHz. This is followed by a software-based high-level trigger (HLT) which reduces the event rate to several kHz.

To reject hadronic interactions, this measurement makes use of the minimum-bias trigger scintillators (MBTS), which cover $2.08 < |\eta| < 3.75$ with two rings of scintillator counters positioned at $z = \pm 3.28$ m from the ATLAS IP. The inner MBTS ring covers $2.78 < |\eta| < 3.75$ with eight slats, each subtending approximately 45° in azimuth.

During heavy-ion running, two zero-degree calorimeters (ZDC) are installed at $z = \pm 140$ m, upstream and downstream of the IP in both directions, each covering approximately $|\eta| > 8.3$ for neutral particles, which are primarily neutrons and photons. Each detector side (labeled ZDC+ for $\eta > 8.3$ and ZDC- for $\eta < -8.3$) consists of four modules, each with approximately one interaction length of tungsten absorber surrounding layers of vertical quartz rods. Hadronic showers induce Cherenkov photons in the quartz which are transported to a photomultiplier tube about 35 cm above the top edge of the absorber. The ZDC calibration is performed in each set of four modules using photonuclear processes that deposit one or more neutrons on one side, used for triggering, and a single neutron, carrying the full per-nucleon beam energy, on the other. Time-dependent module weights are determined in short time intervals to minimize the

¹ ATLAS uses a right-handed coordinate system with its origin at the nominal interaction point (IP) in the center of the detector and the z -axis along the beam pipe. The x -axis points from the IP to the centre of the LHC ring, and the y -axis points upwards. Cylindrical coordinates (r, ϕ) are used in the transverse plane, ϕ being the azimuthal angle around the z -axis. The pseudorapidity is defined in terms of the polar angle θ as $\eta = -\ln \tan(\theta/2)$. Angular distance is measured in units of $\Delta R \equiv \sqrt{(\Delta\eta)^2 + (\Delta\phi)^2}$.

variance around the nominal per-nucleon beam energy. Energy resolutions achieved are typically around $\Delta E/E \approx 16\%$.

3 Trigger and luminosity

The data analyzed in this paper are from the 2015 Pb+Pb run at the LHC. The primary event trigger used in this work utilized nearly the full ATLAS detector system: the MS trigger, the full calorimeter system, the ID, and the MBTS.

3.1 Event trigger

To collect a large sample of exclusive dimuon events, the L1 trigger signature was a coincidence of a muon track in the MS, with no specific transverse momentum selection, for events with a maximum transverse energy of 50 GeV registered in the entire calorimeter system. The MBTS detectors were used in the HLT to reject events with more than one hit in the inner ring in either the forward or backward direction. Finally, the ID was used in the HLT to select events with a well-reconstructed track with $p_T > 200$ MeV. The efficiency of the HLT track trigger is estimated to be approximately 100%. The MBTS veto in the trigger could potentially lead to inefficiencies if the noise rate is sufficiently high. Using events triggered on empty bunch crossings, it is found that the fraction of events failing the MBTS selection is negligible. Thus, the efficiency of the trigger is driven primarily by the efficiency of the L1 MS trigger requirement for single muons. This was determined using minimum-bias data, and cross-checked using exclusive dimuon events, as described below in Section 7.2.

All selected events are also required to pass standard quality preselections. Events are required to be taken during periods where ATLAS is fully operational. Furthermore, events with identified problems associated with the ID, calorimeter, or data acquisition are removed. This only occurs in 0.15% of the total number of events, so no correction for this procedure is applied.

3.2 Luminosity and electromagnetic (EM) pileup

The primary trigger provided rejection against hadronic events using the MBTS requirement. Thus, it sampled the full luminosity of the 2015 heavy-ion run. The total integrated luminosity used for this analysis is found to be $\mathcal{L}_{\text{int}} = 0.48 \text{ nb}^{-1}$ with an uncertainty of $\Delta \mathcal{L}_{\text{int}}/\mathcal{L}_{\text{int}} = 1.5\%$ [42].

The peak instantaneous luminosity during the run reached $\mathcal{L} = 3 \times 10^{27} \text{ cm}^{-2}\text{s}^{-1}$, while the average luminosity was about half of that. Using the total hadronic cross section for Pb+Pb predicted by Glauber calculations [43] $\sigma_{\text{AA}} = 7.7 \text{ b}$, one expects an interaction rate per bunch crossing of about $\mu = 0.004$. Averaging over the full 2015 running period gives a mean interaction rate per bunch crossing of $\mu = 0.0022$. However, the hadronic interaction rate is not the relevant one when considering the impact of EM pileup on forward neutron production. The large photon fluxes at very low photon energies give a cross section for forward neutron production from EM dissociation (EMD) in each arm of about 200 barns. This cross section has not yet been measured at 5.02 TeV, but it has been measured by ALICE in Run 1 at 2.76 TeV to be $181.3 \pm 0.3(\text{stat.})^{+12.8}_{-10.9}(\text{syst.})$ barns [44]. The RELDIS model [19] predicts a relative increase of 11% in the cross section between 2.76 TeV and 5.02 TeV. Applying this correction to the ALICE cross section gives a predicted cross section of $201.2 \pm 0.3(\text{stat.})^{+14.2}_{-12.1}(\text{syst.})$ barns for single

inclusive EMD, where one or more neutrons are detected in one direction, independent of the other. A similar scaling, utilizing predictions at 2.76 TeV and 5.02 TeV, predicts a cross section for mutual EMD, where neutrons are detected in both directions, of $6.0 \pm 0.1(\text{stat.}) \pm 0.4(\text{syst.})$ barns. The computed cross sections for 5.02 TeV can be used to extrapolate the mean number of EM interactions per bunch crossing by scaling μ by the ratio of cross sections $201.2/7.7 = 26.1$. This gives $\mu_{\text{1EMD}} = 0.0583$ for exclusive single EMD, which can be converted to the probability of at least one interaction per crossing as $p_S = 1 - P(0) = 1 - \exp(-\mu) = (5.59^{+0.38}_{-0.33}) \cdot 10^{-2}$. Similarly, the mutual interaction probability per event based on rescaling using the RELDIS ratio is $p_M = (0.174 \pm 0.011) \cdot 10^{-2}$. These quantities are used in Section 7.6 to correct the observed fractions of events with a particular forward neutron topology.

4 Theoretical background

Analytic calculations of dilepton rates, which are used as the basis for Monte Carlo (MC) generators, typically involve an integral over the factorized product of a two-photon flux (which acts as an effective luminosity) and the $\gamma\gamma \rightarrow \mu^+\mu^-$ cross section from perturbative QED. An event-by-event sampling of the scattering angle, as well as the transverse momenta of the scattering photons, is performed to generate a sample of events satisfying the fiducial selection.

Primarily following the discussion in Ref. [12], the two-photon flux is the joint distribution of the incoming photon energies k_1 and k_2

$$\frac{d^2N_{\gamma\gamma}}{dk_1 dk_2} \propto \int_{b_1 > R_A} d^2 b_1 \int_{b_2 > R_A} d^2 b_2 n(k_1, b_1) n(k_2, b_2) P(b) \quad (1)$$

where the functions $n(k_i, b_i)$ are single-nucleus photon differential fluxes $d^3N/d^2b_i dk_i$, which depend on the magnitudes of \vec{b}_1 or \vec{b}_2 , the position vectors relative to each nucleus, with the origin at the nuclear barycenter. The function $P(b)$ encodes the interaction probability as a function of the nucleus–nucleus impact parameter b , which is the magnitude of the impact parameter vector $\vec{b} = \vec{b}_2 - \vec{b}_1$. This function is a product of different contributions, the two most important being the probability of having no hadronic interaction and the probability of a particular configuration of forward neutron production. For ultrarelativistic nuclei, the photon flux for each nucleus $n(k_i, b_i)$ can be approximated as

$$n(k_i, b_i) = \frac{d^3N_\gamma}{dk_i d^2b_i} = \frac{Z^2 \alpha}{\pi^2 b_i^2 k_i} x^2 K_1^2(x)$$

where $x = b_i k_i / \gamma$ (γ is the Lorentz factor), K_1 is a modified Bessel function of the second kind, and α is the fine structure constant.

To present the flux in a form that best matches the dilepton production cross section, the photon energies need to be presented in terms of their invariant mass (W) and pair rapidity (Y), defined as: $k_{1,2} = (W/2) \exp(\pm Y)$ and $Y = (1/2) \ln(k_1/k_2)$.

The observed rate of dimuon events is then the product of the two-photon flux and the dilepton cross section

$$\frac{d^2\sigma_{\mu\mu}}{dW dY} = \frac{d^2N_{\gamma\gamma}}{dW dY} \sigma(\gamma\gamma \rightarrow \mu^+ \mu^-),$$

where $\sigma(\gamma\gamma \rightarrow \mu^+ \mu^-)$ is the dimuon production cross section calculated from perturbative QED. Most UPC calculations use the lowest-order version of this: the Breit–Wheeler process [4]. The rapidities of the

final-state muons also depend on the distribution of the center-of-mass scattering angle (ϑ^*), calculated using lowest-order QED [45].

While the formalism shown here is shared between most theoretical groups, there are differences both in how the integrals are restricted to exclude hadronic events, and where dimuon pairs are allowed to form. This affects the integration limits over \vec{b}_1 and \vec{b}_2 , as well as the impact-parameter-dependent function $P(b)$:

- The photon flux from each nucleus always scales with Z^2 but its dependence on the radial coordinate (b_i) has to be regulated to account for the extent of the nuclear charge distribution. In some calculations [16], this is done by convolving the point charge with a form factor derived from the measured nuclear densities. In others, the nuclear radius is imposed as a minimum radial distance for each nucleus, such that a dilepton pair cannot be produced inside it [12].
- At small impact parameters, hadronic processes occur simultaneously with a $\gamma\gamma$ process and contaminate the exclusive process with additional hadrons. To avoid needing to disentangle these two processes, most calculations exclude the impact parameter range where the nuclei overlap. This is sometimes approximated as a step function imposing a condition on b , the relative impact parameter between the two nuclei, $b > R_1 + R_2$, where R_1 and R_2 are the radii of the two nuclei. For realistic nuclear densities, the condition is imposed as the impact-parameter-dependent probability of not interacting, so $P(b) \propto 1 - P_H(b)$, where $P_H(b)$ is the probability of a hadronic interaction at a given b :

$$P_H(b) = 1 - \exp \left(-\sigma_{nn} \int d^2\vec{r} T_A(|\vec{r}|) T_A(|\vec{r} - \vec{b}|) \right),$$

where the nuclear thickness function $T_A(|\vec{r}|)$ is the integral over z (the longitudinal coordinate along the beam axis) of the nuclear density $\rho(\vec{b}_i, z)$. This function is essentially unity for impact parameters less than the sum of the radii of the colliding objects, e.g. $b \leq 2R_A$ for symmetric nuclei, and drops to zero rapidly above it.

- Until recently (e.g. Ref. [46, 47]), most calculations did not account for the final-state radiation (FSR) from the outgoing charged leptons, and none include contributions from dissociative $\gamma\gamma$ processes. This process, shown diagrammatically in Figure 1(c), also produces dileptons, but one of the incoming photons is radiated from a charged constituent of a nucleon, and this radiative process is associated with a momentum scale large enough to break up the nucleus. Both of these effects tend to populate the dimuon acoplanarity distribution in the region $\alpha > 0.01$. However, dissociative processes also induce nuclear breakup, allowing a systematic disentangling of these two processes in the experimental data by the comparison of different ZDC selections.
- The presence or absence of forward neutrons also affects the impact parameter dependence of the two-photon flux. STARlight implements this using $P_{fn}(b)$, an additional contribution to $P(b)$. The function $P_{fn}(b)$ is the probability of a dissociative photonuclear interaction, where the precise form depends on the desired forward neutron topology. This can be nondissociative (“0n0n”, with no neutrons in either direction); single dissociative (“Xn0n”, with neutrons in only one direction and not the other); or double dissociative (“XnXn”, with neutrons emitted in both directions). The primary quantity which determines $P_{fn}(b)$ is $P_{Xn}^1(b)$, the rate of photodissociation of one nucleus ($\gamma A \rightarrow A^*$) as a function of the distance between the two nuclei:

$$P_{Xn}^1(b) = \int_{k_{\min}}^{k_{\max}} dk n(k, b) \sigma_{\gamma A \rightarrow A^*}(k)$$

where $\sigma_{\gamma A \rightarrow A^*}(k)$ are measured photonuclear cross sections [48], parameterized by k , the incoming photon energy measured in the target rest frame. Using this, the probability of neutrons being emitted toward each ZDC arm is $P_{Xn}(b) = 1 - \exp(-P_{Xn}^1(b))$. In STARlight the probability for exclusive single-arm $Xn0n$ events is $2P_{Xn}(1 - P_{Xn})$; two-arm $XnXn$ events occur with probability P_{Xn}^2 ; and $0n0n$ events without neutrons have probability $(1 - P_{Xn})^2$. For the beam energy and kinematic selections studied in this paper, typical probabilities (for example, from STARlight) for zero, one or two ZDC arms are 60%, 35% and 5% respectively.

- The transverse dimensions of the nuclear charge distributions are reflected in the transverse momenta of the incoming photons. There are different ways to implement this, but the most common approach is to provide a transverse momentum kick to each photon with a distribution determined primarily by the nuclear form factor. These are then summed vectorially to give the intrinsic photon-pair p_T that is imparted to the lepton pair. While STARlight does not implement an impact-parameter dependence of the photon-pair p_T , recent calculations suggest that this may be an observable quantity [49].

These differences are relevant to all cross-section calculations. However, it should be noted that while the most widely used framework for this, the STARlight model, has the most sophisticated handling of the nuclear photon fluxes as well as the nuclear overlap, it has no higher-order QED or nucleon dissociative processes.

5 Monte Carlo samples

Several different models are used to simulate signal and background processes, as well as to add FSR. Fully simulated samples are used to calculate experimental corrections using single muons, and to test their accuracy on simulated dimuon events. Fast simulations are used to study the impact of QED showering on the measured dimuon final state. Finally generator-level samples of dissociative pair production are used to estimate the background contributions.

5.1 STARlight

STARlight [50] implements calculations of both the nuclear photon flux (including the nuclear form factor) and the lowest-order QED cross sections for exclusive processes [51], such as the process $\gamma\gamma \rightarrow \mu^+\mu^-$ studied in this paper. Reference [12] provides the most complete presentation of the STARlight formalism, including the modifications of the dimuon spectrum when selecting on the number of ZDC arms (zero, one or two) with forward neutrons. Each dimuon event is fully determined by $m_{\mu\mu}$, $y_{\mu\mu}$, $|\cos\vartheta_{\mu\mu}^*|$ and $p_{T,\mu\mu}$.

5.2 Simulated samples: single muons and STARlight

A large sample of single muons, distributed uniformly in the ranges $|\eta_\mu| < 3$, $-\pi < \phi_\mu < \pi$ and $2 < p_{T,\mu} < 50$ GeV, is utilized to evaluate the muon reconstruction efficiencies $\varepsilon_R(q\eta_\mu, p_{T,\mu})$ as a function of $q\eta_\mu$ (the product of the muon charge and pseudorapidity) and $p_{T,\mu}$. To perform detailed comparisons of data with simulated exclusive dimuon events, a sample of STARlight 1.1 events is passed through a detector simulation [52] based on GEANT4 [53] and is reconstructed with the standard ATLAS reconstruction software.

5.3 QED showering with STARlight+PYTHIA8

STARlight does not implement final-state radiation (FSR), which is observed in the acoplanarity distributions in data as a notable tail that is absent in the STARlight simulations. STARlight only provides initial-state transverse momentum from the nuclear form factors. Higher-order contributions have been calculated in Ref. [46] in a Sudakov formalism and are found to qualitatively compare well with the preliminary version of this analysis. To include this effect, STARlight dimuon events were provided as input into PYTHIA8 (version 8.226 [54, 55]) for QED showering, with the hard scale set to one muon’s p_T (the standard choice in PYTHIA8 for a t -channel process). By construction, the showering process conserves the overall cross section, but the FSR can lead to a fraction of the events migrating in and out (but primarily out) of the selected fiducial region used here. The sensitivity of the showering to the assumptions used in PYTHIA8 was tested by varying the available phase space for the radiation, relative to the selected hard scale, and no change in the final distributions was observed for the kinematic regions explored in this paper.

5.4 LPAIR

The LPAIR 4.0 generator [56] is used to calculate the dissociative process $pp^* \rightarrow \gamma\gamma \rightarrow \mu^+\mu^-$, a well-known background in proton–proton collisions [57]. LPAIR models single-dissociative proton–proton collisions using an EPA spectrum for the nondissociated nucleon, and the Suri–Yennie form factor [58] for the dissociated nucleon. This leads to the production of dimuons, many of which are emitted into the central region, as well as forward hadron production, although the hadrons are typically not emitted into the region covered by the ATLAS ID. Since the only observable from LPAIR used in this analysis is the acoplanarity, and this is determined primarily by the much larger initial-state p_T associated with the dissociated proton, no attempt is made to reweight the initial photon spectra. However, comparisons of LPAIR with STARlight+PYTHIA8 are made only after identical selections in $m_{\mu\mu}$ and $y_{\mu\mu}$.

6 Event characterization

6.1 Event selection

The signal process $PbPb(\gamma\gamma) \rightarrow \mu^+\mu^-(Pb^{(*)}Pb^{(*)})$ that can be treated using the EPA is only straightforward to calculate when the two nuclei do not interact hadronically. In this case, there is no potential background from hadronic processes and the full nuclear charge contributes to the two-photon flux. To suppress hadronic processes, the ATLAS ID is used to require no activity beyond that associated with the two oppositely charged muons. Of the triggered events passing all quality selections, events are selected with two “tight” muons [40]. Only a single event has a third tight muon, so this event is discarded as potential background. One of the two muons is required to match the L1 trigger muon that caused the event to be recorded. Next the single muon and muon pair kinematics are required to satisfy the fiducial selection criteria:

- The two muons must have opposite charges.
- Each muon must have $p_{T,\mu} > 4 \text{ GeV}$, $|\eta_\mu| < 2.4$, and a transverse impact parameter relative to the beamspot of less than 1.5 mm.

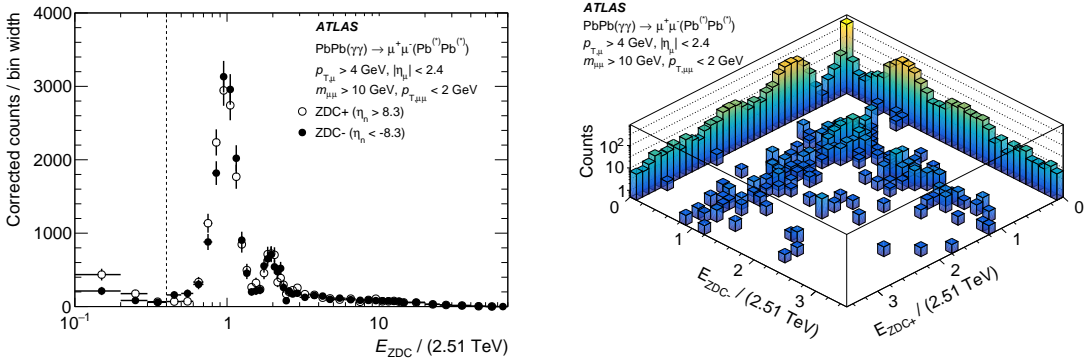


Figure 2: Distribution of ZDC energies in events selected in the fiducial region, normalized by the beam energy per-nucleon of 2.51 TeV, for each ZDC direction. The left panel shows the distributions for each of the two ZDC directions superimposed, while the right panel shows their correlation.

- The muon pair must have invariant mass $m_{\mu\mu} > 10$ GeV, and a transverse momentum of the dimuon system $p_{T,\mu\mu} < 2$ GeV.

The fiducial criteria remove about two-thirds of the triggered events containing two good muons. Of the remaining events, none are observed to have more than one reconstructed vertex, so no vertex requirement (for either a single vertex or multiple vertices) is imposed. Finally, events are rejected if there are any other well-reconstructed tracks in the acceptance with $p_T > 100$ MeV; this removes only 2% of the events. As a cross-check, a more restrictive condition was also considered – to reject events with any additional track of any track quality – but this was found to only reject 3% of the selected events. For the selected events, the distributions of track transverse impact parameter are consistent with simulated STARlight events, implying that there is no residual contribution from heavy-flavor production.

In fully simulated STARlight events, the requirement of having a reconstructed vertex leads to a selection inefficiency of approximately 5% while providing no additional background rejection. This was demonstrated by noting that after the vertex requirement, the fraction of events with an additional good track (2%) is found to be the same as for the event selection without it. Thus, the vertex requirement is considered only as a cross-check and is not part of the primary event selection.

After all fiducial selections, 12132 candidate events passing fiducial selections are utilized in the analysis.

6.2 ZDC event class definition

Each selected exclusive dimuon event can be classified according to its forward neutron topology, utilizing the two ZDCs. The ZDC energies are reconstructed by extracting the signal amplitude for each of the four modules in each direction and then applying a time-dependent weight to each module. These weights are determined so as to minimize the width of the energy distribution in the single-neutron region. The energy resolution is sufficient to clearly separate the one-neutron peak from the distribution at lower energies, which is mainly a combination of electronic noise and forward photons. The presence of ZDC activity on either side is defined as an energy greater than 40% of the single-neutron peak position. This is indicated in the individual energy distributions in the left panel of Figure 2. The correlation of energies in the right panel of Figure 2 illustrates the three primary topologies available for these events: 1) the most probable

configuration is no activity in either ZDC (“0n0n”), 2) the next mostly likely configuration is observing one or more forward neutrons in one ZDC, and none in the other (“Xn0n”), and 3) finally, the rarest configuration is observing one or more forward neutrons in both ZDC arms (“XnXn”).

Due to EM pileup in the LHC (as discussed above in Section 3.2) the neutrons detected in one or both arms of the ZDC are not necessarily associated with the observed dimuon pair. However, the rate of additional neutrons can be predicted when the single and mutual dissociation probabilities are known. Corrections associated with this are calculated below in Section 7.6.

7 Data analysis

7.1 Cross-section definitions

After the exclusive dimuon event selection, cross sections are derived by scaling the dimuon yields by the Pb+Pb collision luminosity (\mathcal{L}_{int}). This is done after correcting the observed number of events ($N_{\mu\mu}$) for: 1) muon pair trigger and reconstruction efficiencies (ε_T and ε_R , respectively), 2) bin migration at the edge of the $p_{T,\mu} > 4$ GeV fiducial region (C_{mig}) and 3) backgrounds from dissociative processes (f_{dis}). This is represented by the following formula:

$$\frac{d\sigma_{\mu\mu}}{dX_{\mu\mu}} = \frac{C_{\text{mig}}}{\mathcal{L}_{\text{int}}} \sum_{\text{events}} \frac{(1 - f_{\text{dis}})}{\varepsilon_{R\mu\mu} \varepsilon_{T\mu\mu}}$$

where $X_{\mu\mu}$ is one of the dimuon kinematic variables, described in Section 1. These include $m_{\mu\mu}$, $y_{\mu\mu}$, $|\cos \vartheta_{\mu\mu}^*|$ and the initial energies of the photons, inferred by combining $m_{\mu\mu}$ and $y_{\mu\mu}$.

The efficiencies and background corrections are applied as event-level weights, while C_{mig} is applied to the final spectra. The trigger efficiency, first discussed in Section 3.1 is derived using Pb+Pb data, using both minimum-bias hadronic events with reconstructed muons and UPC dimuon events. The muon reconstruction efficiency is based on simulation, but corrected by an η -dependent scale factor (SF) based on data.

7.2 Trigger efficiencies

The single-muon L1 trigger efficiencies used for final corrections are derived using the minimum-bias data as a function of the product of the muon charge and pseudorapidity, $q\eta_\mu$, and the muon transverse momentum $p_{T,\mu}$. The trigger efficiency does not depend on the overall event activity, which was checked by comparing different centrality intervals in the data. The efficiency values were also cross-checked by an independent tag-and-probe method using the selected exclusive dimuon events. In these events, only one of the muons is required to be associated with a L1 muon object. Thus, one can use each muon associated with a trigger as a tag, and then measure the probability of the other muon being emitted into an angular region, opposite in azimuth, that also has a L1 trigger muon. This gives an independent estimate of the trigger efficiency, which is found to compare well with the minimum-bias data. For application to the data, the single-trigger efficiencies are smoothed using a Fermi function.

The total event-level trigger efficiency is the probability that at least one of the muons led to the recording of the event:

$$\varepsilon_{T\mu\mu} = 1 - (1 - \varepsilon_T(\eta^+))(1 - \varepsilon_T(-\eta^-))$$

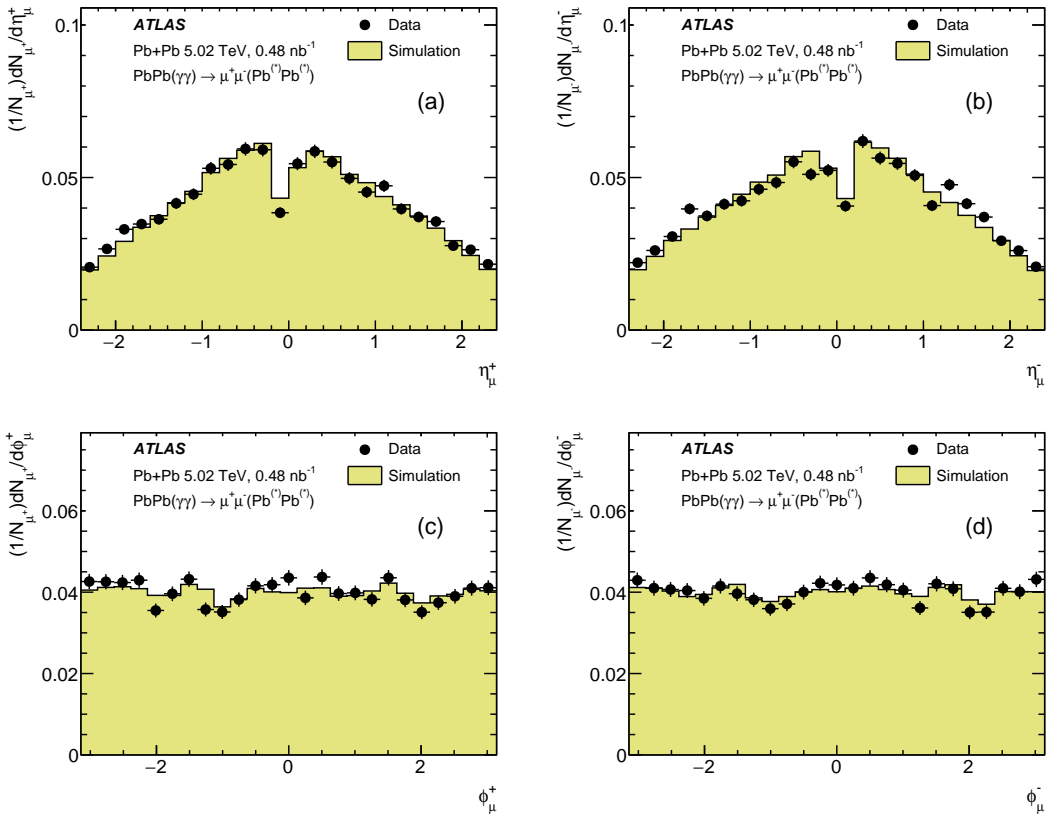


Figure 3: Distributions of single muons, corrected for trigger efficiency, with positive (panels (a) and (c)) and negative (panels (b) and (d)) charge, as a function of $\eta^{(\pm)}$ and $\phi^{(\pm)}$, the pseudorapidity and azimuthal coordinate for positive and negative muons, each normalized by the integral. Data are compared with fully simulated STARlight events. Error bars are the statistical uncertainties of the data points.

where ε_T^+ and ε_T^- are the single-trigger efficiencies for positive and negative muons, respectively. The typical trigger efficiency is 93% at smaller $m_{\mu\mu}$ (less than 20 GeV) and $|y_{\mu\mu}|$ (less than 1), and increases to 97% at larger values of $m_{\mu\mu}$ (greater than 40 GeV) and $|y_{\mu\mu}|$ (greater than 1.5).

To assess the overall level of agreement between data and simulation after trigger efficiency corrections, the normalized pseudorapidity and azimuthal distributions of single muons in data and simulation are compared separately for both positive and negative charges, for all events in the fiducial acceptance. While the data are corrected for the trigger efficiency, neither data nor simulation are corrected for the reconstruction efficiency. This is to provide a low-level comparison of data and MC simulation, as it should also be noted that the data are not yet corrected for dissociative backgrounds. Figure 3 shows that the distributions in η_μ and ϕ_μ are in good agreement for both charges, with the overall shape and some smaller-scale features of the data also seen in the simulations.

7.3 Reconstruction efficiencies and scale factors

The muon reconstruction efficiency is defined as the probability for a generated muon to be fully reconstructed and characterized as a “tight” muon [40]. It is determined as a function of the muon pseudorapidity times its charge ($q\eta_\mu$) using single-muon MC samples as described in Section 5.2, with a per-muon scale factor determined using UPC events in a tag-and-probe approach. In events with fewer than three tracks, a “tag” muon is selected using the single-muon trigger, and is required to satisfy tight selection criteria. Two types of “probes” can then be selected, track probes (reconstructed ID tracks with a transverse impact parameter $|d_0| < 1.5$ mm and passing selections identical to those for muons) and extrapolated MS track probes. Both are required to have a reconstructed charge opposite to the tag, to have an acoplanarity of less than 0.02, and a pair $p_T < 2$ GeV. For each ID track probe, one searches for a muon passing tight selections, which defines $\varepsilon(\mu|\text{ID})$. For each extrapolated MS track probe, one searches for the closest track passing the same spectrometer and impact parameter selections, and $\varepsilon(\text{ID}|\text{MS})$ is the matching probability. In each case, the two objects are considered matched if they are separated by a relative $\eta-\phi$ distance of $\Delta R < 0.1$. The full reconstruction efficiency is the product $\varepsilon(\mu|\text{ID})\varepsilon(\text{ID}|\text{MS})$, and this can be compared directly between data and STARlight simulations. The ratio of the full reconstruction efficiency in data to that in simulation is defined as the SF, which is a multiplicative correction to the simulated efficiency to account for differences between data and MC simulation that depend on emission angle. The SF is measured as a function of the muon pseudorapidity, and for each range in η_μ is found to be constant with $p_{T,\mu}$. Thus, only one SF is extracted for each η_μ range. It is found to be within -1% of unity for $|\eta_\mu| > 1.5$ and to decrease systematically toward $|\eta_\mu| = 0$, with a maximum deviation of around -4% near $\eta_\mu = 0$.

Since the muons are well separated in emission angle, the pair efficiency is the product of the two individual efficiencies:

$$\varepsilon_{R\mu\mu} = \varepsilon_R(p_T^+, \eta^+) \text{SF}(\eta^+) \varepsilon_R(p_T^-, -\eta^-) \text{SF}(\eta^-)$$

where each individual muon efficiency is multiplied by the appropriate SF. Due to the turn-on of the efficiency at $p_{T,\mu} = 4$ GeV, the impact of correcting for the reconstruction efficiency is about 40–50% for $m_{\mu\mu} < 20$ GeV and $|y_{\mu\mu}| < 0.8$, decreasing to 15% at larger values.

The combined weight, including both the trigger and reconstruction efficiency corrections, is applied as a per-event weight $w = 1/(\varepsilon_{T\mu\mu}\varepsilon_{R\mu\mu})$.

7.4 Outflow from fiducial region

Migration between bins in the dimuon variables was checked and found to be negligible, due to the high precision of the ATLAS MS. Despite the excellent reconstruction performance of the MS, the fact that the fiducial acceptance region requires a two-dimensional cut in the joint transverse momentum distribution of both μ^+ and μ^- leads to some net loss owing to momentum resolution. For events within the fiducial volume, but just at the boundary with both muon $p_{T,\mu} > 4$ GeV, if either muon’s transverse momentum fluctuates even slightly below 4 GeV, due to finite momentum resolution, then the event is rejected, while both muon transverse momenta would have to fluctuate upward to remain in the fiducial volume. This effect is exacerbated by the strong p_T correlations induced by the UPC initial state, with nearly vanishing total transverse momentum. This can be seen clearly by reconstructing simulated STARlight events, and applying the reconstruction efficiency weights event by event. While most of the spectrum in pair rapidity and pair mass is reconstructed correctly, within 1%, a systematic depletion is observed when one or both of the muon $p_{T,\mu}$ values approach 4 GeV. This depletion, quantified as a function of the different kinematic

variables, is derived using the STARlight simulation, and is found to lead to corrections of 2–3%, but only for $|y_{\mu\mu}| < 1.6$ and $m_{\mu\mu} < 20$ GeV. The edges of the acceptance in $|\cos \vartheta_{\mu\mu}^*|$ vs. $m_{\mu\mu}$ are affected somewhat more, with typical corrections of about 10%.

Since these corrections are calculated as a function of the dimuon kinematic variables, they are applied to the multidimensional yields (e.g. $m_{\mu\mu}$ vs. $y_{\mu\mu}$ or $|\cos \vartheta_{\mu\mu}^*|$ vs. $m_{\mu\mu}$) before the final results are calculated.

7.5 Dissociative background corrections

After all corrections are applied, there remains an irreducible background from the presence of dissociative events. This process is expected to contribute at large values of acoplanarity ($\alpha > 0.01$). However, one cannot simply select only events with small acoplanarity, since the large-acoplanarity region also has a non-negligible contribution from QED radiative effects. For each dimuon kinematic selection, a binned maximum-likelihood fitting procedure applied to the dimuon acoplanarity distribution is used to estimate the fraction of dissociative events. Due to the limited size of the data sample, it was split into coarse intervals in $m_{\mu\mu}$ (three intervals with boundaries at 10, 20, 40 and 80 GeV) and absolute pair rapidity (three intervals with boundaries at 0, 0.8, 1.6 and 2.4).

The fit model utilizes two templates, where the signal distribution is calculated using STARlight + PYTHIA8, and the background is from LPAIR. The PDF of the acoplanarity distribution, in a particular selection of $m_{\mu\mu}$ and $y_{\mu\mu}$, $P(\alpha, m_{\mu\mu}, y_{\mu\mu})$, is a sum of the signal and LPAIR contributions, parameterized by the fraction f_{dis} :

$$P(\alpha, m_{\mu\mu}, y_{\mu\mu}) = (1 - f_{\text{dis}})P_{\text{EPA}}(\alpha, m_{\mu\mu}, y_{\mu\mu}) + f_{\text{dis}}P_{\text{dis}}(\alpha, m_{\mu\mu}, y_{\mu\mu}).$$

For the nominal determination of the correction factors, no weights are applied to the events during the fitting, since the corrections do not vary strongly within each individual dimuon kinematic interval and they are independent of α . The fits are applied to distributions both for a specific forward neutron topology (OnOn, XnOn, and XnXn) and for ZDC-inclusive data. Figure 4 shows the outputs of the fits for the selection with the largest number of events: $10 < m_{\mu\mu} < 20$ GeV and $|y_{\mu\mu}| < 0.8$. Two notable features are observed. First, the OnOn selection is very well described by the STARlight+PYTHIA8 distribution, with no significant contribution from LPAIR 4.0 needed. This suggests that events with no ZDC activity (OnOn) have no dissociation, and the tails in the acoplanarity distributions derive only from higher-order QED contributions. By contrast, the XnOn and XnXn selections have a much less steep falloff at larger acoplanarity values. Inclusion of the LPAIR contribution gives a good description in the region beyond $\alpha > 0.02$. The overall contributions to the XnOn and XnXn integrals from the dissociative contribution are 7% and 12%, respectively. Finally, the distribution inclusive in forward neutron topology has an overall contribution of about 3% for this kinematic selection. Intervals with much higher pair mass or pair rapidity have fewer events that can be utilized in the fit, giving larger statistical uncertainties to the extracted f_{dis} . These uncertainties are propagated into the final results as systematic uncertainties.

The dissociative contributions come primarily from the process $\gamma\gamma \rightarrow \mu^+\mu^-$ where one photon comes from a lead ion (and thus has $p_T \approx 25$ MeV), while the other is emitted by the charged constituents of an individual nucleon with a GeV-scale transverse momentum. Of the two, the nucleon has the smaller radius, so its photon spectrum is much harder, and thus a strong asymmetry is expected in the dimuon rapidity distribution, with more pairs emitted in the nucleon-going direction. One can test this expectation after assigning the pair rapidity a sign based on the direction of the ZDC signal in XnOn events, as one expects

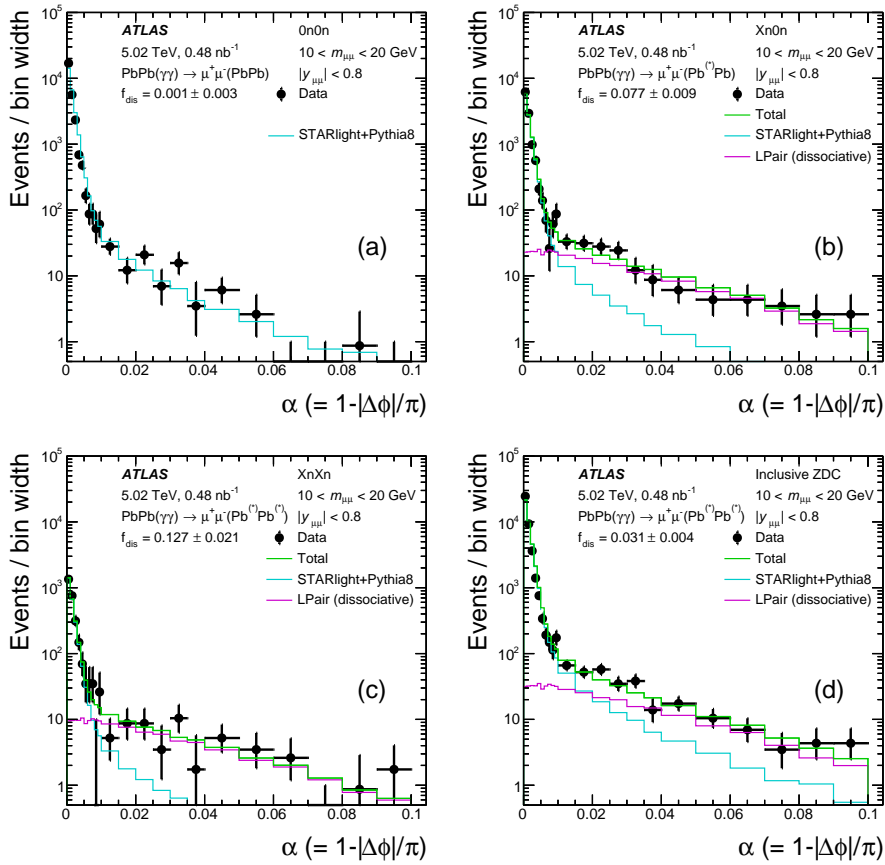


Figure 4: Combined fits to the three ZDC selections ((a) $0n0n$, (b) $Xn0n$, (c) $XnXn$) as well as (d) ZDC-inclusive data for $|y_{\mu\mu}| < 0.8$ and $10 < m_{\mu\mu} < 20$ GeV, as well as all other fiducial acceptance cuts. The signal distribution is obtained using STARlight + PYTHIA8, while the background prediction is obtained using LPAIR in the same kinematic selections. No efficiency corrections are applied. The fraction of dissociative events is given as f_{dis} . The error bars on the data points are the statistical uncertainties.

to observe nuclear dissociation in the direction of the dissociated nucleon. The fractions of dissociative events are shown as a function of signed $y_{\mu\mu}$ in Figure 5. It is observed that the extracted dissociative contribution increases with pair rapidity in the direction of the dissociated nucleus, consistent with being induced by a dissociated nucleon.

7.6 Forward neutron topology fractions

In Section 4, it is shown that the ZDC selection modifies the impact parameter profile $P(b)$ found in the integral for the two-photon luminosity. Due to the increasing photon flux at smaller radial distances from the nuclear center (b_i), events with a ZDC signal (either $Xn0n$ or $XnXn$) typically have smaller impact parameters than for $0n0n$. The smaller impact parameters lead to interactions involving higher photon energies from one or both nuclei. This tends to harden the observed diphoton (and thus dimuon) invariant mass spectrum for a fixed interval in pair rapidity. Conversely, for a fixed interval in dimuon mass, the rapidity distribution gets narrower. To measure this in each dimuon kinematic selection, the fractions

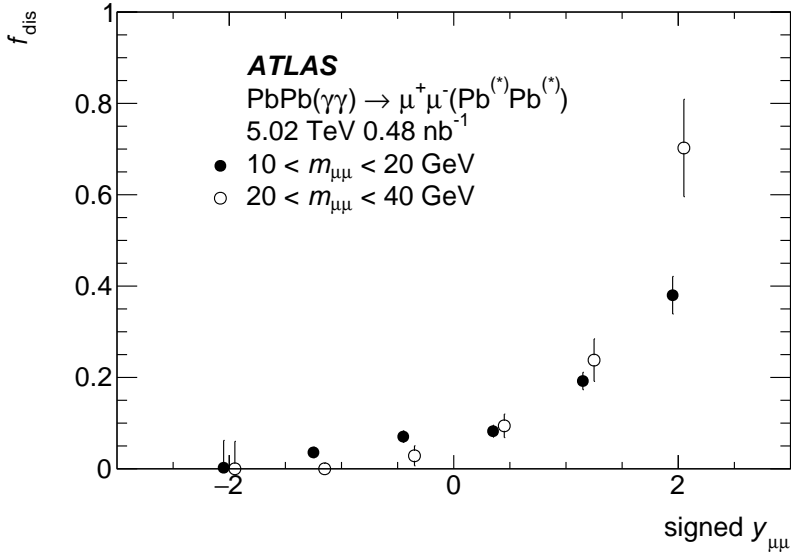


Figure 5: Dissociative background fractions in $Xn0n$ events as a function of signed rapidity, where positive $y_{\mu\mu}$ is in the direction of the ZDC signal. Two invariant mass ranges are shown, and the $10 < m_{\mu\mu} < 20 \text{ GeV}$ range is shifted slightly in the horizontal direction for clarity. Error bars are statistical uncertainties.

of events with $Xn0n$ and $XnXn$ (f_{Xn0n} and f_{XnXn} , respectively) are estimated with a single fit over all three ZDC topologies that includes the contribution from dissociative background, as discussed previously. Once the measured ZDC fractions are determined, they must be corrected for EM pileup processes and, in principle, for any ZDC inefficiency. However, while the ZDC is only 4.6 interaction lengths deep, which implies an approximately 2% inefficiency for single neutrons, more than half of the EMD events on a single side produce more than one neutron. This leads to an estimate of an overall efficiency of over 99%. Accounting for this sub-percent inefficiency is addressed in the systematic uncertainties.

The combined fit model is formulated as a set of three equations for each kinematic region, with a total number of events in each ZDC category (N_Z , where Z is an index corresponding to $0n0n$, $Xn0n$, or $XnXn$) given by

$$N_Z(\alpha, y_{\mu\mu}, m_{\mu\mu}) = f'_Z(y_{\mu\mu}, m_{\mu\mu}) N_{\text{EPA}}(y_{\mu\mu}, m_{\mu\mu}) P_{\text{EPA}}(\alpha, y_{\mu\mu}, m_{\mu\mu}) + N_Z^{\text{dis}}(y_{\mu\mu}, m_{\mu\mu}) P_{\text{dis}}(\alpha, y_{\mu\mu}, m_{\mu\mu})$$

with parameters N_{EPA} , the overall yield of dimuons from the signal distributions, f'_Z the measured fraction of events for each ZDC class (i.e. $Z = 0n0n$, $Xn0n$, and $XnXn$), and N_Z^{dis} the background contribution for each ZDC selection. The fractions are subject to the constraint $f'_{0n0n} + f'_{Xn0n} + f'_{XnXn} = 1$ since all events have to fall into one of the categories. The simultaneous fit incorporates the statistical correlations between the samples. The choice of using the same template PDFs P_{EPA} and P_{dis} for all three ZDC selections is motivated by direct comparisons of the acoplanarity distributions, and validated by the good quality of the fits.

EM pileup processes (as discussed in Section 3.2) generate neutrons that are detected in one or both arms of the ZDC but are not associated with the scattering process that generated the dimuon pair. This leads to an outflow from $0n0n$ and $Xn0n$ events to both the $Xn0n$ and $XnXn$ events. The two fundamental parameters

are p_S and p_M , the probabilities for exclusive single (for each arm) and mutual (two arm) dissociation per bunch crossing. The probability of pileup preserving a $0n0n$ configuration is $(1 - p_S)(1 - p_S)(1 - p_M)$, i.e. the joint probability of having no single pileup in each arm, as well as no mutual process occurring. Conversely, the probability of pileup turning $0n0n$ into $XnXn$ is $p_M + p_S^2$, i.e. the sum of probabilities of mutual breakup or two independent single breakup processes, one in each arm. The probability turning $0n0n$ into $Xn0n$ is just the complement of the other two quantities. Similarly, the probability of preserving $Xn0n$ is $(1 - p_S)(1 - p_M)$, since one arm has already seen activity, and its complement is the probability for converting $Xn0n$ to $XnXn$. Finally, $XnXn$ is unaffected by the presence of any pileup. Putting these together, one gets the migration matrix:

$$\begin{bmatrix} f'_{0n0n} \\ f'_{Xn0n} \\ f'_{XnXn} \end{bmatrix} = \begin{bmatrix} (1 - p_S)(1 - p_S)(1 - p_M) & 0 & 0 \\ 2p_S(1 - p_S - p_M + p_M p_S/2) & (1 - p_S)(1 - p_M) & 0 \\ p_M + p_S^2 & p_M + p_S - p_M p_S & 1 \end{bmatrix} \begin{bmatrix} f_{0n0n} \\ f_{Xn0n} \\ f_{XnXn} \end{bmatrix}.$$

Here the fractions f' are the measured ones extracted from the combined fits, and the fractions f are the corrected values reported in the results. The terms which go as p_S^2 reflect the possibility that a pileup event can be composed of two separate pileup interactions in addition to the primary physics event. While not identical, as assumed by STARlight, p_S^2 is of similar order to the p_M estimated using measured cross sections, as discussed in Section 3.2. This matrix is inverted to transform the measured ZDC fractions into the corrected ones. The statistical uncertainty of the corrected values includes the full fit covariance information.

7.7 Unfolding of the acoplanarity distribution

In order to facilitate comparisons of QED calculations with the experimental acoplanarity (α) distribution, a bin-by-bin unfolding procedure is applied to the measured values. To maximize the statistical precision, the entire fiducial region with $m_{\mu\mu} > 10$ GeV is included. The response used in the unfolding is derived from a large sample of events produced with STARlight + PYTHIA8, with each muon's azimuthal angle smeared in accord with parameterizations of the full GEANT4 simulations. The unfolding corrections range from an upward correction of about 3% for $\alpha < 0.0001$ to a downward correction of a bit less than 4% around $\alpha = 0.005$. Around $\alpha = 0.01$, the corrections converge rapidly to zero, as the underlying spectrum becomes flatter. The net effect is to slightly narrow the measured peak near $\alpha = 0$, which is smeared slightly by detector effects. The corrections were also compared with those for a sample in which the simulated α spectrum is reweighted to agree with data, a procedure which is limited by the size of the data sample, and while they are generally similar to each other, they disagree in some α intervals by up to 2%, which sets the overall scale for the systematic uncertainty. The corrections were checked against a fully simulated sample of STARlight events and the corrections agree to better than 0.4% for $\alpha < 0.01$. To eliminate the contribution from dissociative events, only the $0n0n$ selection is used, and the results are normalized to the pileup-corrected $0n0n$ cross section. This is done by scaling the measured total cross section (reported in the next section) by the $0n0n$ fraction $f_{0n0n} = (72.1 \pm 0.6)\%$ after correcting the measured fraction of 64% for the time-averaged EM pileup.

8 Systematic uncertainties

8.1 Trigger efficiency

The trigger selection is based on four contributions: the L1 muon trigger, the rejection of events with total transverse energy greater than 50 GeV, the MBTS veto in the HLT, and the track selection in the HLT. The muon trigger efficiency has been measured directly in peripheral minimum-bias data and is parameterized by a Fermi function. The assigned systematic error is the statistical uncertainty of the fits, propagated using 200 replicas, and is about 0.2%. The tag-and-probe results are consistent with the minimum-bias results, so either could be used in principle, but the minimum-bias data have better statistical precision and are thus preferred. The transverse energy veto has a negligible inefficiency, as there are no selected dimuon events with a L1 transverse energy above 15 GeV, far from the veto threshold. The HLT track selection is determined to have 100% efficiency, with an uncertainty of 0.4%, using a support trigger based on the MS accompanied by a total transverse energy requirement of $E_T < 50$ GeV. Finally, the false-positive rate for the MBTS veto was checked using empty events, where neither LHC ring had filled bunches colliding in a particular bunch crossing. In these events, the rate of false positives is at the 10^{-5} level, indicating that this contribution is negligible.

8.2 Reconstruction scale factors

The uncertainty in the reconstruction SFs has two contributions. The statistical uncertainties of the SF are propagated by constructing 200 replicas, with the SF in each interval varied according to its statistical uncertainty, and the variance in the yields determines the uncertainty. The sensitivity to the details of the procedure was checked by changing the selection criteria for the events used in the SF calculation, as well as the matching between the ID and MS. Given that the dimuon selection is quite pure, these changes have only a small impact, and a constant 1% systematic uncertainty is assigned to cover this. This uncertainty also includes a small deviation of the reconstruction efficiency determined in the simulation using tag-and-probe from the one extracted directly from the simulated muons for $2.0 < |\eta_\mu| < 2.4$.

8.3 Muon momentum scale and resolution

The muon momentum scale and momentum resolution are studied using a set of weights that vary the transverse momentum of simulated muons to determine a set of modified corrections that encapsulate the known uncertainties in muon performance in pp collisions [40]. The extracted corrections have a negligible impact on this analysis, and so are neglected. The impact of possible bias on the momentum measurement due to relative detector misalignment between data and MC simulation is studied by comparing the transverse momentum of each muon as measured in the ID with that measured in the MS. The differences observed in data and MC simulation are found to agree to better than 1% and no specific uncertainty is assigned to this contribution.

8.4 Fiducial acceptance definition

The correction factors determined using the fully reconstructed STARlight events account for the net outflow of one or both reconstructed muons from the $p_{T,\mu} > 4$ GeV fiducial acceptance. This correction is

up to 3% for $m_{\mu\mu} < 20$ GeV and decreases with increasing pair mass and pair rapidity. This is sensitive to the photon spectral shape. Thus, the uncertainty in this correction was estimated by reweighting the MC spectrum to resemble the data, as a function of k_1 and k_2 , the energies of the incoming photons. The difference between these two sets of corrections is at the 0.1% level, and no systematic uncertainty is assigned.

8.5 Dissociative background

The background from dissociative processes is estimated directly from data. The uncertainties in this derive both from the fit statistical uncertainties, and from the sensitivity to variations of the fitting procedure. As a cross-check, the fits are also performed using an unbinned fitting procedure, instead of the binned procedure used by default, and no significant differences are found. In addition, several other variations are performed:

1. Signal α templates are allowed to be rescaled, in the fitting procedure, to better agree with the distributions near $\alpha = 0$.
2. The measured distribution for the $0n0n$ selection is used as the signal distribution for $Xn0n$ and $XnXn$ selections. This is justified by the observed dissociative fraction being consistent with zero, e.g. as shown in Figure 4.
3. Applying reconstruction and trigger efficiency corrections before the fit.

The impact of these changes is quite small, since the dissociative tail has a distinct shape, especially when requiring forward neutrons in either ZDC arm. The differences turn out to be about 1% (absolute), constant in $m_{\mu\mu}$ and $y_{\mu\mu}$. A 1% uncertainty is applied to the yields to cover this.

The statistical contributions to the background correction are propagated by keeping track of the sum of background correction weights, i.e. $\sum(\Delta(1 - f_{\text{dis}}))^2 = \sum(\Delta f_{\text{dis}})^2$, for each kinematic selection. The final uncertainty associated with this is then $\sqrt{\sum(\Delta f_{\text{dis}})^2}$.

8.6 Luminosity

The uncertainty in the integrated luminosity for the 2015 Pb+Pb run at $\sqrt{s_{\text{NN}}} = 5.02$ TeV is 1.5%. It is derived from the calibration of the luminosity scale using x - y beam-separation scans, following a methodology similar to that detailed in Ref. [42], and using the LUCID-2 detector for the baseline luminosity measurements [59].

8.7 ZDC neutron topology fractions

The analysis of forward neutron topology fractions involves ratios of selected distributions, classifying them by the presence or absence of a signal in one or both ZDCs. As neither the event trigger nor the muon reconstruction is affected by the ZDC event class ($0n0n$, $Xn0n$ or $XnXn$), all of these uncertainties cancel out. The systematic uncertainties related to the fitting procedure itself are the same as in the previous subsection, and are at most 1% on an absolute scale. The impact of EM pileup on the extracted ZDC fractions depends on our knowledge of the measured EMD cross sections, which have not been measured for $\sqrt{s_{\text{NN}}} = 5.02$ TeV, but only for $\sqrt{s_{\text{NN}}} = 2.76$ TeV. Thus, the cross sections used to extrapolate to the

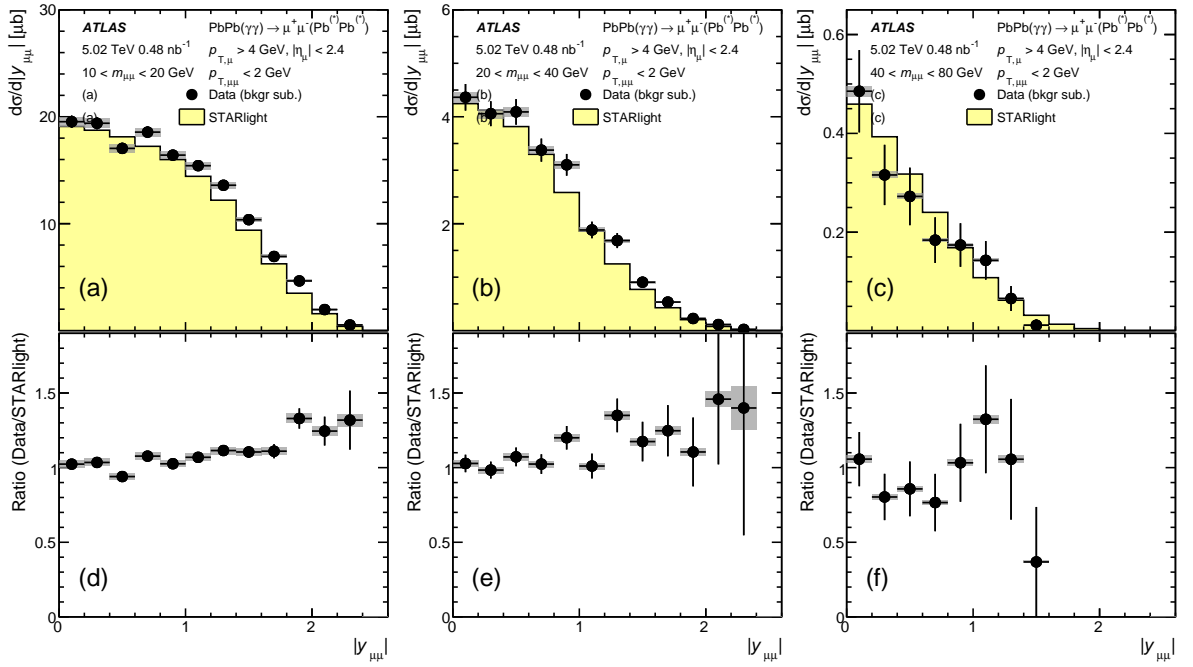


Figure 6: (a-c) Differential cross sections shown as a function of $|y_{\mu\mu}|$ in bins of $m_{\mu\mu}$ (a) $10 < m_{\mu\mu} < 20$ GeV, (b) $20 < m_{\mu\mu} < 40$ GeV, and (c) $40 < m_{\mu\mu} < 80$ GeV compared with cross sections from STARlight and (d-f) the ratio of data to STARlight. Statistical uncertainties are shown as error bars while total systematic uncertainties are shown as gray bands.

higher energy are varied by their experimental uncertainties. The uncertainties associated with this have a magnitude of about 1%, on an absolute scale.

8.8 Unfolded acoplanarity distributions

The primary systematic uncertainties applicable to the unfolded differential cross sections are those that apply to all cross sections, but now integrated over the full fiducial region $m_{\mu\mu} > 10$ GeV. Besides the luminosity uncertainty (1.5%), the $OnOn$ cross section has an uncertainty of 0.8%, dominated by the extrapolation of the EM pileup expectations to 5.02 TeV. Finally, there is an overall 2% uncertainty, constant in α , which contains the variations testing the sensitivity to the input spectrum (nominal compared with reweighted) as well as the resolution model (full simulation compared with fast simulation). Combining these uncertainties in quadrature, the total systematic uncertainty is estimated to be 2.6%, which is applied uniformly to the unfolded acoplanarity distribution.

9 Results

This section presents comparisons of data with STARlight 2.0, which implements all of the primary physics mechanisms, except dissociative processes and QED FSR. All of the systematic uncertainties presented in Section 8 are combined in quadrature, and are typically about 2.2%. The dissociative processes are

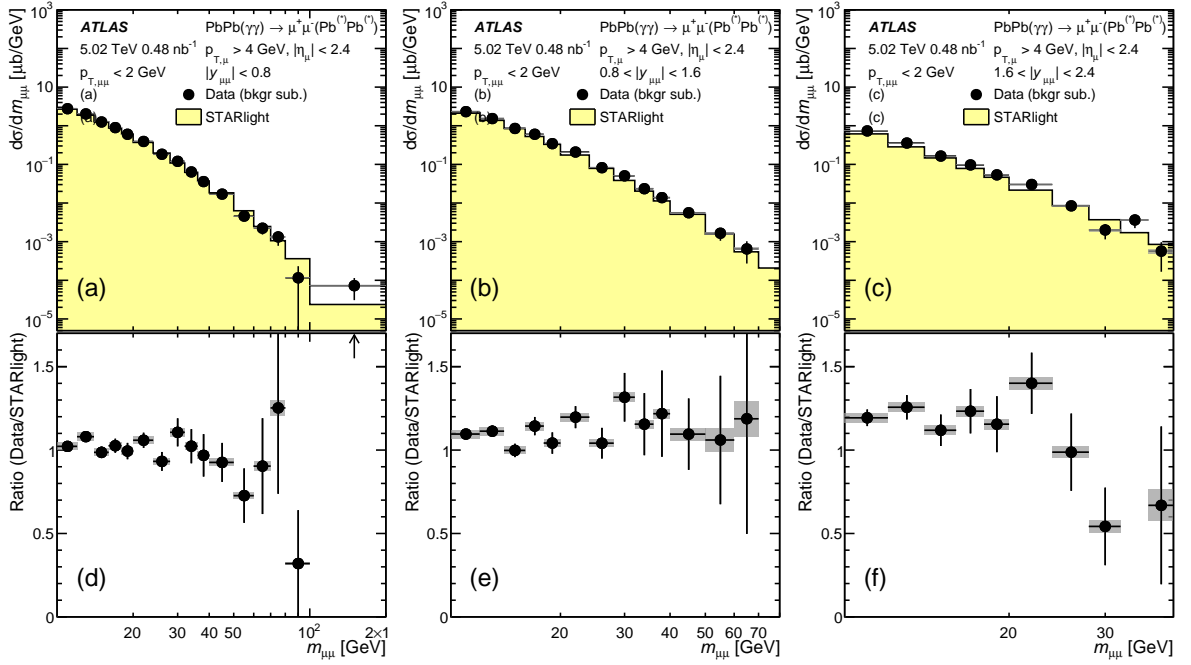


Figure 7: (a-c) Differential cross sections shown as a function of $m_{\mu\mu}$ in bins of $|y_{\mu\mu}|$, (a) $|y_{\mu\mu}| < 0.8$, (b) $0.8 < |y_{\mu\mu}| < 1.6$, and (c) $1.6 < |y_{\mu\mu}| < 2.4$ compared with cross sections from STARlight and (d-f) the ratio of data to STARlight. Statistical uncertainties are shown as error bars while total systematic uncertainties are shown as gray bands.

explicitly corrected for by the fitting procedure described in Section 7.5, but the FSR is necessarily included in the signal yields. It should be noted that only 1.5% of the data are removed by the $p_{T,\mu\mu} < 2$ GeV selection, which was chosen to limit the dissociative contributions. The same p_T selection only removes a small fraction of STARlight events even including FSR effects. However, the FSR separately has the effect of reducing the STARlight cross sections by about 4%, due to the reduction in p_T of one or both muons from the extra radiation. This effect is not included in the nominal STARlight comparisons, except in comparisons of data with the full α distribution.

After integrating over the full fiducial phase space ($p_{T,\mu} > 4$ GeV, $|\eta_\mu| < 2.4$, $m_{\mu\mu} > 10$ GeV, $p_{T,\mu\mu} < 2$ GeV), the measured total cross section is $\sigma_{\text{fid}}^{\mu\mu} = 34.1 \pm 0.3(\text{stat.}) \pm 0.7(\text{syst.}) \mu\text{b}$. This should be compared with 32.1 μb for STARlight and 30.8 μb for STARlight + PYTHIA8.

Figure 6 shows the absolute dimuon rapidity distributions for three mass intervals ($10 < m_{\mu\mu} < 20$ GeV, $20 < m_{\mu\mu} < 40$ GeV, $40 < m_{\mu\mu} < 80$ GeV). It is observed that while the measured cross sections are consistent with predictions near $|y_{\mu\mu}| = 0$, there is an excess in the data which increases monotonically with increasing $|y_{\mu\mu}|$. There are too few events in the higher $m_{\mu\mu}$ bins to allow any strong statements to be made about whether the increase remains the same as in the lowest mass bin.

The mass distributions are presented in three pair rapidity bins ($|y_{\mu\mu}| < 0.8$, $0.8 < |y_{\mu\mu}| < 1.6$, and $1.6 < |y_{\mu\mu}| < 2.4$) in Figure 7. It is observed that the overall shape of the spectra is well described out to the highest masses in the available event sample (which limits the mass range for higher values of $|y_{\mu\mu}|$). The invariant mass interval extending from 100 to 200 GeV contains only four events, including the highest-mass candidate with $m_{\mu\mu} = 173$ GeV.

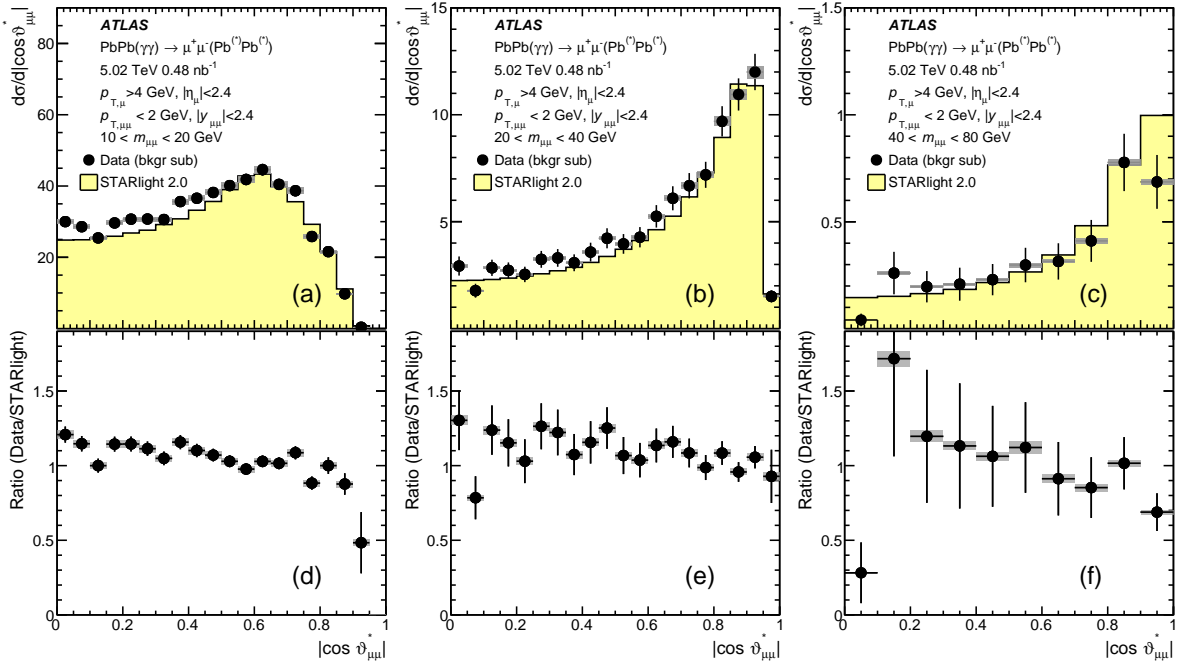


Figure 8: (a-c) Differential cross sections shown as a function of $|\cos \vartheta_{\mu\mu}^*|$ in bins of $m_{\mu\mu}$, (a) $10 < m_{\mu\mu} < 20$ GeV, (b) $20 < m_{\mu\mu} < 40$ GeV, and (c) $40 < m_{\mu\mu} < 80$ GeV, after integrating over the full range in $|y_{\mu\mu}|$, compared with cross sections from STARlight and (d-f) the ratio of data to STARlight. Statistical uncertainties are shown as error bars while total systematic uncertainties are shown as gray bands.

While the pair mass and rapidity distributions are clearly important for characterizing the interaction between the two photons, the scattering angle in the initial center-of-mass system is particularly important for assessing the compatibility of the data with QED. Without the fiducial selection, these distributions would have a steep rise at large $|\cos \vartheta_{\mu\mu}^*|$. However, the restriction on muon pseudorapidity ($|\eta_\mu| < 2.4$) strongly cuts into the acceptance for $|\cos \vartheta_{\mu\mu}^*|$ near unity, i.e. at small scattering angles. Since the differential cross section calculated in leading-order QED is only a function of $m_{\mu\mu}$ [45], the disagreement already observed as an enhancement of the cross section at forward $|y_{\mu\mu}|$ makes comparisons of data and STARlight nontrivial. If one compares the differential cross sections $d\sigma/d|\cos \vartheta_{\mu\mu}^*|$ for the same $m_{\mu\mu}$ selections as in Figure 6, one arrives at the distributions shown in Figure 8. STARlight calculations show that events with smaller values of $|\cos \vartheta_{\mu\mu}^*|$ also span a large range in $|y_{\mu\mu}|$, while these large values of $|\cos \vartheta_{\mu\mu}^*|$ are only accessible in a more limited range, close to $|y_{\mu\mu}| = 0$. The cross sections are recalculated for $|y_{\mu\mu}| < 0.8$, the region where data and STARlight agree well. With this selection, there is a better description of the $|\cos \vartheta_{\mu\mu}^*|$ distributions in the lowest mass range, as is observed in Figure 9. The systematic enhancement at smaller $|\cos \vartheta_{\mu\mu}^*|$ can thus be attributed to the residual disagreement in the pair rapidity distributions.

Since the observed final state consists of just the final-state muons, and two-photon invariant mass and rapidity are conserved in the final-state dimuon system, the muon kinematics can be used to estimate the initial photon energies, k_1 and k_2 (as discussed in Section 4): $k_{1,2} = (1/2)m_{\mu\mu} \exp(\pm y_{\mu\mu})$. No corrections are applied for the presence of a soft final-state photon, but the impact on the extracted mass and rapidity is generally found to be quite small.

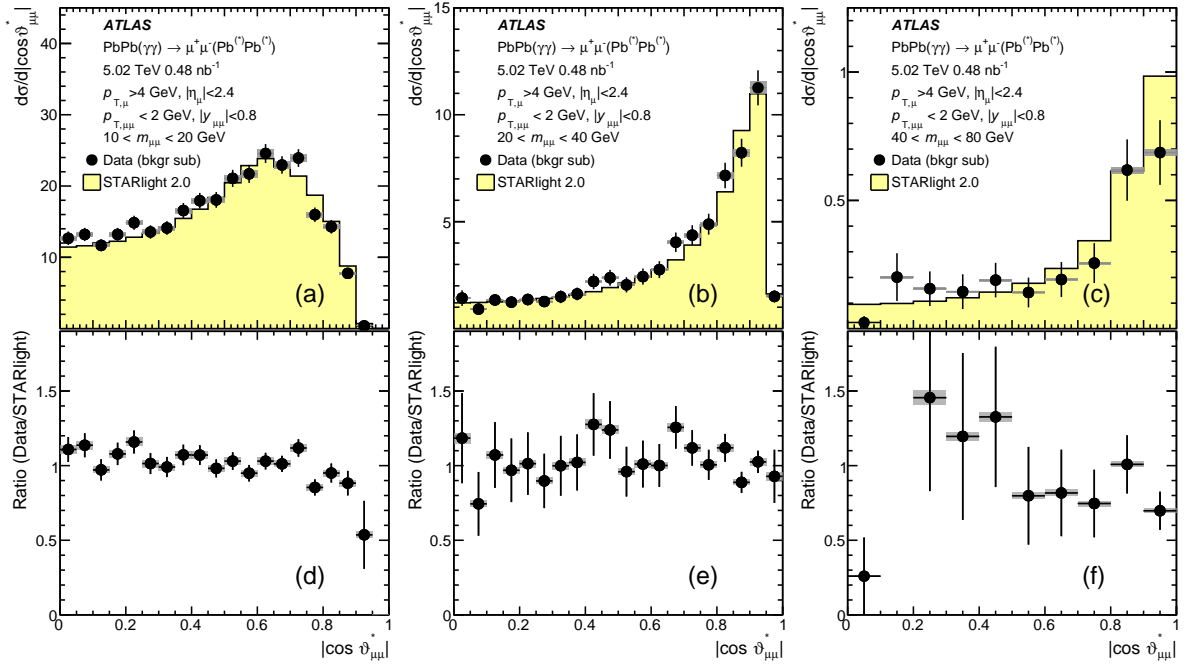


Figure 9: (a-c) Differential cross sections shown as a function of $|\cos \vartheta_{\mu\mu}^*|$ in bins of $m_{\mu\mu}$, (a) $10 < m_{\mu\mu} < 20$ GeV, (b) $20 < m_{\mu\mu} < 40$ GeV, and (c) $40 < m_{\mu\mu} < 80$ GeV, after requiring $|y_{\mu\mu}| < 0.8$ to exclude the regions where the rapidity distributions disagree, compared with cross sections from STARlight and (d-f) the ratio of data to STARlight. Statistical uncertainties are shown as error bars while total systematic uncertainties are shown as gray bands, which are typically smaller than the data points.

Since the two photons are emitted independently, each event can be characterized by the maximum and minimum photon energies k_{\max} and k_{\min} , where k_{\max} is the larger of the two photon energies. The corrected differential cross sections in k_{\max} and k_{\min} are presented in Figure 10, for both data and STARlight in the top panel, and their ratio is provided in the bottom panel.

It is observed that the ratio is near unity for photon energies (both minimum and maximum) around 10–20 GeV, but is significantly higher at both lower and higher energies. The disagreement for $75 < k_{\max} < 100$ GeV is approximately 40%, while an enhancement of about 15% is observed for $k_{\min} < 2$ GeV. In the region between 5 and 20 GeV, the distributions for k_{\max} and k_{\min} are also observed to overlap, within uncertainties, suggesting that the distributions factorize (as represented in Eq. (1), i.e. it does not matter whether a 10 GeV photon has the larger or smaller energy). They also have the smallest difference relative to STARlight, with an excess of only around 5%. Combined, these suggest that a systematic modification of the initial energy spectrum is necessary to explain the differences between the data and STARlight calculations.

One possible avenue to explore is whether the integration limits in Eq. (1) could be relaxed without violating any important physics constraints. In particular, the authors of Ref. [12] note in their derivation that this restriction against production inside the two nuclei is to avoid the produced particles scattering off the nuclei. Dileptons have a very small probability of interacting with the nuclei, and this is even less likely within the nuclear skin. Thus, this condition could be weakened somewhat, so long as $1 - P_H$ (as defined in Section 4) is not too small. If the integration limits are decreased slightly, by one nuclear skin

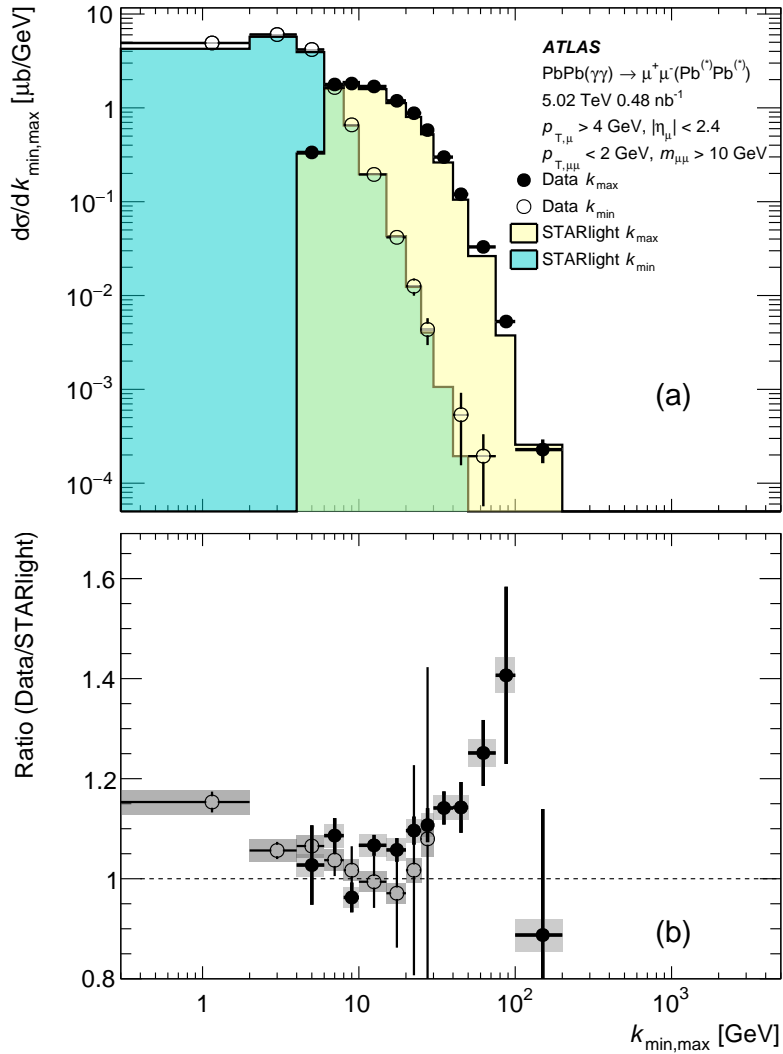


Figure 10: (a) Differential cross sections presented as a function of the maximum photon energy (k_{\max}) and minimum photon energy (k_{\min}), compared with cross sections from STARlight. Statistical uncertainties are shown as error bars while total systematic uncertainties are shown as gray bands. (b) Ratio of experimental cross sections to STARlight calculations.

depth, it is observed that, relative to STARlight, the distribution of k_{\min} is enhanced below 2 GeV, and the distribution of k_{\max} is enhanced above 20 GeV.

All of the results shown so far are inclusive of the different ZDC topologies, which indicate either no activity ($OnOn$), activity in either the forward or backward side ($Xn0n$), or activity on both sides ($XnXn$). Events with smaller impact parameters, where the nuclei are closer together, are more likely to be accompanied by neutron dissociation in one or both arms and to have photons with higher energies. The procedure to extract the ZDC event class fractions is discussed in detail in Section 7.6, and is based on a simultaneous fit to the acoplanarity distributions for all three ZDC selections, assuming that all events arise from partitioning the original selection of signal events, along with backgrounds from dissociative processes that can be

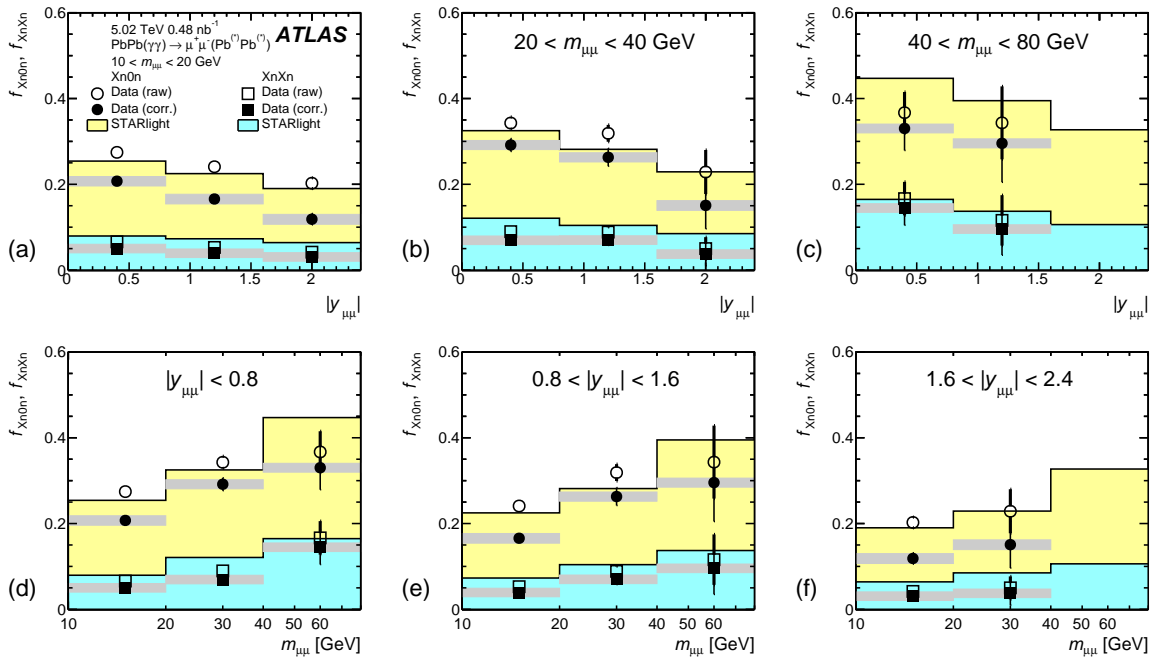


Figure 11: Fractions of events with $Xn0n$ and $XnXn$, as a function of $|y_{\mu\mu}|$ (a-c), or $m_{\mu\mu}$ (d-f). Data are shown as raw (open circles) and corrected for EM pileup (closed circles). Theory predictions from STARlight are shown as histograms. Systematic uncertainties are shown for the corrected data, as grey bands, and error bars are statistical uncertainties.

different for each forward neutron topology ($Xn0n$ and $XnXn$). The EM-pileup-corrected results are shown in Figure 11, which displays f_{Xn0n} and f_{XnXn} , the fraction of events with $Xn0n$ and $XnXn$, as functions of $m_{\mu\mu}$ and $|y_{\mu\mu}|$. It should be noted that the two sets of results are different representations of the same data, but it is useful to see them plotted separately vs. $m_{\mu\mu}$ and $|y_{\mu\mu}|$. The uncorrected data are also shown, to indicate the size of the EM pileup corrections. The data compared with STARlight suggest overall agreement, but STARlight generally tends to predict too large a fraction of events with forward neutrons, which is consistent with previously reported ALICE data at 2.76 TeV [60].

The unfolded differential cross sections $d\sigma/d\alpha$ for the $0n0n$ topology are shown in Figure 12. The measured cross sections are compared with predictions of both generator-level STARlight and generator-level STARlight + PYTHIA8, both for an inclusive ZDC selection, but scaled by the same $0n0n$ fraction as observed in data. The STARlight α distributions have no dependence on impact parameter, and thus no dependence on the ZDC selection. It is observed that the shape of the spectrum at large $\alpha > 0.01$, which reflects only the QED showering after applying the $0n0n$ condition, agrees well with STARlight + PYTHIA8. However, a difference in shape is observed for smaller values $\alpha < 0.01$. This could be explained by a small change in the p_T spectrum assumed by STARlight, which controls the width of the α distribution.

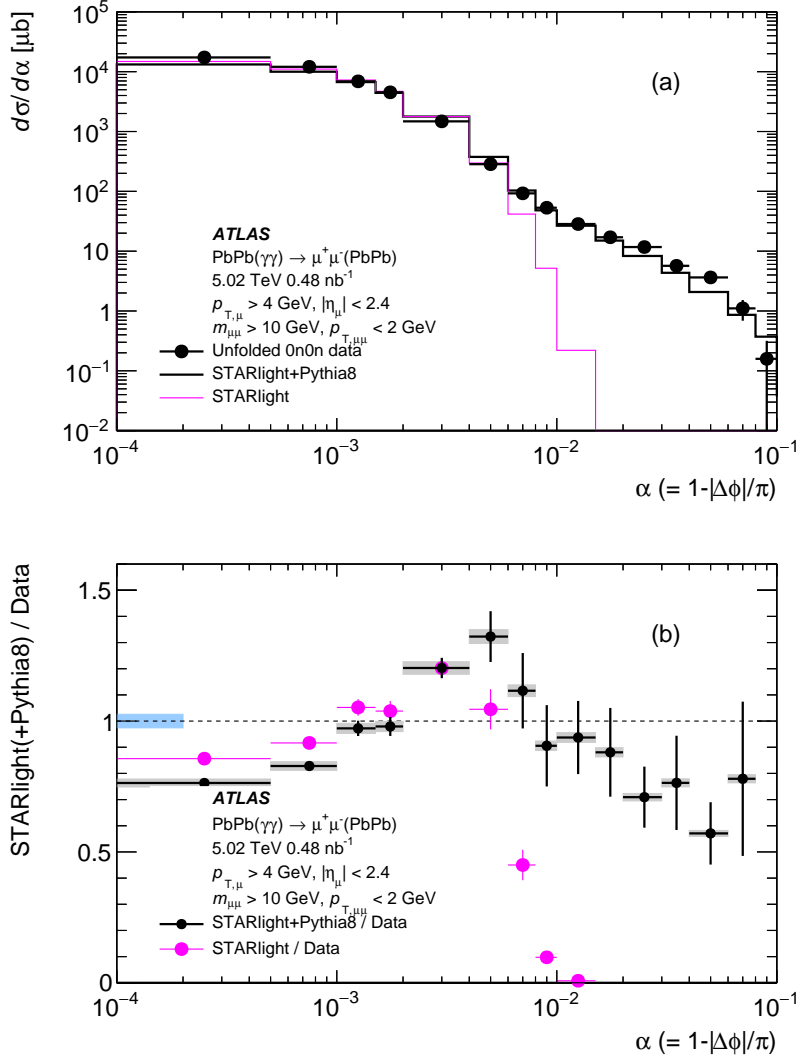


Figure 12: (a) Fully corrected differential cross sections $d\sigma/d\alpha$ for 0n0n-selected data. Data are compared with absolute cross sections from STARlight with, and without, PYTHIA8 QED showering. Statistical uncertainties are shown as error bars. (b) Ratios of STARlight + PYTHIA8 cross sections (black circles) and STARlight cross sections (magenta circles) to the data. The STARlight ratios do not extend beyond $\alpha = 0.01$ due to the absence of higher-order QED effects. The blue band around unity indicates the overall systematic uncertainty, while the gray bands around the data points reflect the uncertainties associated with the bin-by-bin unfolding.

10 Conclusion

The ATLAS experiment at the LHC has performed a measurement of cross sections for exclusive dimuon production in the process $\text{PbPb}(\gamma\gamma) \rightarrow \mu^+\mu^- (\text{Pb}^{(*)}\text{Pb}^{(*)})$ using 0.48 nb^{-1} of Pb+Pb collision data taken at $\sqrt{s_{\text{NN}}} = 5.02 \text{ TeV}$. This reaction directly probes the quasi-real photon fluxes surrounding the highly boosted nuclei. The cross section of dimuons is corrected for detector effects, as well as for backgrounds from dissociative processes. The acoplanarity distributions are used to subtract dissociative backgrounds

using fits incorporating contributions from signal and background. The signal is modeled by STARlight 2.0 with QED showering using PYTHIA8, and backgrounds are modeled using the single dissociative process from LPAIR 4.0. After all corrections, differential cross sections in a fiducial acceptance ($p_{T,\mu} > 4$ GeV, $|\eta_\mu| < 2.4$, $m_{\mu\mu} > 10$ GeV, $p_{T,\mu\mu} < 2$ GeV) are presented as a function of $m_{\mu\mu}$, $|y_{\mu\mu}|$, $|\cos \vartheta_{\mu\mu}^\star|$, k_{\max} and k_{\min} , and compared with STARlight 2.0 calculations. Generally, good agreement is found but some systematic differences are seen, which may be explained by deficiencies in the modeling of the incoming photon flux. In particular, allowing dilepton pairs to be produced deeper within the nuclear skin may be sufficient to explain the observed differences, something which could be addressed systematically within the currently available models. Progress in modeling this process, using the data presented here, will be important in reducing uncertainties in the photon fluxes. These reduced uncertainties will be needed for precision studies of QED and QCD in nuclear collisions, as well as to probe physics beyond the Standard Model, both at the LHC, especially with the increased luminosity expected, and at future machines.

Acknowledgments

We thank CERN for the very successful operation of the LHC, as well as the support staff from our institutions without whom ATLAS could not be operated efficiently.

We acknowledge the support of ANPCyT, Argentina; YerPhI, Armenia; ARC, Australia; BMWFW and FWF, Austria; ANAS, Azerbaijan; SSTC, Belarus; CNPq and FAPESP, Brazil; NSERC, NRC and CFI, Canada; CERN; ANID, Chile; CAS, MOST and NSFC, China; COLCIENCIAS, Colombia; MSMT CR, MPO CR and VSC CR, Czech Republic; DNRF and DNSRC, Denmark; IN2P3-CNRS and CEA-DRF/IRFU, France; SRNSFG, Georgia; BMBF, HGF and MPG, Germany; GSRT, Greece; RGC and Hong Kong SAR, China; ISF and Benoziyo Center, Israel; INFN, Italy; MEXT and JSPS, Japan; CNRST, Morocco; NWO, Netherlands; RCN, Norway; MNiSW and NCN, Poland; FCT, Portugal; MNE/IFA, Romania; JINR; MES of Russia and NRC KI, Russian Federation; MESTD, Serbia; MSSR, Slovakia; ARRS and MIZŠ, Slovenia; DST/NRF, South Africa; MICINN, Spain; SRC and Wallenberg Foundation, Sweden; SERI, SNSF and Cantons of Bern and Geneva, Switzerland; MOST, Taiwan; TAEK, Turkey; STFC, United Kingdom; DOE and NSF, United States of America. In addition, individual groups and members have received support from BCKDF, CANARIE, Compute Canada, CRC and IVADO, Canada; Beijing Municipal Science & Technology Commission, China; COST, ERC, ERDF, Horizon 2020 and Marie Skłodowska-Curie Actions, European Union; Investissements d’Avenir Labex, Investissements d’Avenir Idex and ANR, France; DFG and AvH Foundation, Germany; Herakleitos, Thales and Aristeia programmes co-financed by EU-ESF and the Greek NSRF, Greece; BSF-NSF and GIF, Israel; La Caixa Banking Foundation, CERCA Programme Generalitat de Catalunya and PROMETEO and GenT Programmes Generalitat Valenciana, Spain; Göran Gustafssons Stiftelse, Sweden; The Royal Society and Leverhulme Trust, United Kingdom.

The crucial computing support from all WLCG partners is acknowledged gratefully, in particular from CERN, the ATLAS Tier-1 facilities at TRIUMF (Canada), NDGF (Denmark, Norway, Sweden), CC-IN2P3 (France), KIT/GridKA (Germany), INFN-CNAF (Italy), NL-T1 (Netherlands), PIC (Spain), ASGC (Taiwan), RAL (UK) and BNL (USA), the Tier-2 facilities worldwide and large non-WLCG resource providers. Major contributors of computing resources are listed in Ref. [61].

References

- [1] C. F. von Weizsäcker, *Ausstrahlung bei Stößen sehr schneller Elektronen*, *Z. Phys.* **88** (1934) 612.
- [2] E. J. Williams, *Correlation of certain collision problems with radiation theory*, Kong. Dan. Vid. Sel. Mat. Fys. Medd. **13N4** (1935) 1.
- [3] E. Fermi, *Über die Theorie des Stoßes zwischen Atomen und elektrisch geladenen Teilchen*, *Z. Phys.* **29** (1924) 315.
- [4] G. Breit and J. A. Wheeler, *Collision of Two Light Quanta*, *Phys. Rev.* **46** (1934) 1087.
- [5] M. Strikman, R. Vogt, and S. N. White, *Probing Small x Parton Densities in Ultraperipheral AA and pA Collisions at the CERN Large Hadron Collider*, *Phys. Rev. Lett.* **96** (2006) 082001, arXiv: [hep-ph/0508296](#).
- [6] D. d'Enterria and G. G. da Silveira, *Observing Light-by-Light Scattering at the Large Hadron Collider*, *Phys. Rev. Lett.* **111** (2013) 080405, [Erratum: *Phys. Rev. Lett.* **116**, 129901 (2016)], arXiv: [1305.7142 \[hep-ph\]](#).
- [7] M. Kłusek-Gawenda, P. Lebiedowicz, and A. Szczurek, *Light-by-light scattering in ultraperipheral Pb-Pb collisions at energies available at the CERN Large Hadron Collider*, *Phys. Rev. C* **93** (2016) 044907, arXiv: [1601.07001 \[nucl-th\]](#).
- [8] ATLAS Collaboration, *Z boson production in Pb+Pb collisions at $\sqrt{s_{NN}} = 5.02$ TeV measured by the ATLAS experiment*, *Phys. Lett. B* **802** (2020) 135262, arXiv: [1910.13396 \[nucl-ex\]](#).
- [9] C. A. Bertulani, S. R. Klein, and J. Nystrand, *Physics of ultra-peripheral nuclear collisions*, *Ann. Rev. Nucl. Part. Sci.* **55** (2005) 271, arXiv: [nucl-ex/0502005](#).
- [10] A. J. Baltz et al., *The Physics of ultraperipheral Collisions at the LHC*, *Phys. Rept.* **458** (2008) 1, arXiv: [0706.3356 \[nucl-ex\]](#).
- [11] S. Klein and P. Steinberg, *Photonuclear and Two-photon Interactions at High-Energy Nuclear Colliders*, (2020), arXiv: [2005.01872 \[nucl-ex\]](#).
- [12] A. J. Baltz, Y. Gorbunov, S. R. Klein, and J. Nystrand, *Two-photon interactions with nuclear breakup in relativistic heavy ion collisions*, *Phys. Rev. C* **80** (2009) 044902, arXiv: [0907.1214 \[nucl-ex\]](#).
- [13] M. Vysotsky and E. Zhemchugov, *Equivalent photons in proton–proton and ion–ion collisions at the Large Hadron Collider*, *Phys. Usp.* **62** (2019) 910, arXiv: [1806.07238 \[hep-ph\]](#).
- [14] M. Y. Şengül, M. C. Güçlü, Ö. Mercan, and N. G. Karakuş, *Electromagnetic heavy-lepton pair production in relativistic heavy-ion collisions*, *Eur. Phys. J. C* **76** (2016) 428, arXiv: [1508.07051 \[hep-ph\]](#).
- [15] M. Vidović, M. Greiner, C. Best, and G. Soff, *Impact-parameter dependence of the electromagnetic particle production in ultrarelativistic heavy-ion collisions*, *Phys. Rev. C* **47** (1993) 2308.
- [16] M. Kłusek-Gawenda and A. Szczurek, *Exclusive muon-pair productions in ultrarelativistic heavy-ion collisions: Realistic nucleus charge form factor and differential distributions*, *Phys. Rev. C* **82** (2010) 014904, arXiv: [1004.5521 \[nucl-th\]](#).
- [17] C. Azevedo, V. Gonçalves, and B. Moreira, *Exclusive dilepton production in ultraperipheral PbPb collisions at the LHC*, *Eur. Phys. J. C* **79** (2019) 432, arXiv: [1902.00268 \[hep-ph\]](#).
- [18] M. Kłusek-Gawenda, M. Ciemala, W. Schäfer, and A. Szczurek, *Electromagnetic excitation of nuclei and neutron evaporation in ultrarelativistic ultraperipheral heavy ion collisions*, *Phys. Rev. C* **89** (2014) 054907, arXiv: [1311.1938 \[nucl-th\]](#).

- [19] I. A. Pshenichnov, J. P. Bondorf, I. N. Mishustin, A. Ventura, and S. Masetti, *Mutual heavy ion dissociation in peripheral collisions at ultrarelativistic energies*, *Phys. Rev. C* **64** (2001) 024903, arXiv: [nucl-th/0101035](#).
- [20] I. A. Pshenichnov, *Electromagnetic excitation and fragmentation of ultrarelativistic nuclei*, *Phys. Part. Nucl.* **42** (2011) 215.
- [21] A. Veyssiére, H. Beil, R. Bergere, P. Carlos, and A. Lepretre, *Photoneutron cross sections of ^{208}Pb and ^{197}Au* , *Nucl. Phys. A* **159** (1970) 561.
- [22] ALICE Collaboration, *Charmonium and e^+e^- pair photoproduction at mid-rapidity in ultra-peripheral Pb-Pb collisions at $\sqrt{s_{\text{NN}}}=2.76$ TeV*, *Eur. Phys. J. C* **73** (2013) 2617, arXiv: [1305.1467 \[nucl-ex\]](#).
- [23] ALICE Collaboration, *Exclusive J/ψ Photoproduction off Protons in Ultraperipheral $p - \text{Pb}$ collisions at $\sqrt{s_{\text{NN}}} = 5.02$ TeV*, *Phys. Rev. Lett.* **113** (2014) 232504, arXiv: [1406.7819 \[nucl-ex\]](#).
- [24] ATLAS Collaboration, *Measurement of exclusive $\gamma\gamma \rightarrow \ell^+\ell^-$ production in proton-proton collisions at $\sqrt{s} = 7$ TeV with the ATLAS detector*, *Phys. Lett. B* **749** (2015) 242, arXiv: [1506.07098 \[hep-ex\]](#).
- [25] ATLAS Collaboration, *Measurement of the exclusive $\gamma\gamma \rightarrow \mu^+\mu^-$ process in proton-proton collisions at $\sqrt{s} = 13$ TeV with the ATLAS detector*, *Phys. Lett. B* **777** (2018) 303, arXiv: [1708.04053 \[hep-ex\]](#).
- [26] CMS Collaboration, *Exclusive $\gamma\gamma \rightarrow \mu^+\mu^-$ production in proton-proton collisions at $\sqrt{s} = 7$ TeV*, *JHEP* **01** (2012) 052, arXiv: [1111.5536 \[hep-ex\]](#).
- [27] LHCb Collaboration, *Measurement of the exclusive Υ production cross-section in pp collisions at $\sqrt{s} = 7$ TeV and 8 TeV*, *JHEP* **09** (2015) 084, arXiv: [1505.08139 \[hep-ex\]](#).
- [28] STAR Collaboration, *Production of e^+e^- pairs accompanied by nuclear dissociation in ultra-peripheral heavy-ion collision*, *Phys. Rev. C* **70** (2004) 031902, arXiv: [nucl-ex/0404012 \[nucl-ex\]](#).
- [29] STAR Collaboration, *Probing Extreme Electromagnetic Fields with the Breit-Wheeler Process*, (2019), arXiv: [1910.12400 \[nucl-ex\]](#).
- [30] STAR Collaboration, *ρ^0 photoproduction in ultraperipheral relativistic heavy ion collisions at $\sqrt{s_{\text{NN}}} = 200$ GeV*, *Phys. Rev. C* **77** (2008) 034910, arXiv: [0712.3320 \[nucl-ex\]](#).
- [31] PHENIX Collaboration, *Photoproduction of J/ψ and of high mass e^+e^- in ultra-peripheral Au+Au collisions at $\sqrt{s_{\text{NN}}} = 200$ GeV*, *Phys. Lett. B* **679** (2009) 321, arXiv: [0903.2041 \[nucl-ex\]](#).
- [32] CDF Collaboration, *Observation of Exclusive Electron-Positron Production in Hadron-Hadron Collisions*, *Phys. Rev. Lett.* **98** (2007) 112001, arXiv: [hep-ex/0611040](#).
- [33] CDF Collaboration, *Observation of Exclusive Charmonium Production and $\gamma + \gamma$ to $\mu^+\mu^-$ in $p\bar{p}$ Collisions at $\sqrt{s} = 1.96$ TeV*, *Phys. Rev. Lett.* **102** (2009) 242001, arXiv: [0902.1271 \[hep-ex\]](#).
- [34] CMS Collaboration, *Observation of forward neutron multiplicity dependence of dimuon acoplanarity in ultraperipheral PbPb collisions at $\sqrt{s_{\text{NN}}} = 5.02$ TeV*, (2020), arXiv: [2011.05239 \[hep-ex\]](#).
- [35] ATLAS Collaboration, *Evidence for light-by-light scattering in heavy-ion collisions with the ATLAS detector at the LHC*, *Nature Phys.* **13** (2017) 852, arXiv: [1702.01625 \[hep-ex\]](#).
- [36] CMS Collaboration, *Evidence for light-by-light scattering and searches for axion-like particles in ultraperipheral PbPb collisions at $\sqrt{s_{\text{NN}}} = 5.02$ TeV*, *Phys. Lett. B* **797** (2019) 134826, arXiv: [1810.04602 \[hep-ex\]](#).

- [37] ATLAS Collaboration, *Observation of Light-by-Light Scattering in Ultraperipheral Pb+Pb Collisions with the ATLAS Detector*, *Phys. Rev. Lett.* **123** (2019) 052001, arXiv: [1904.03536 \[hep-ex\]](#).
- [38] ATLAS Collaboration, *Measurement of light-by-light scattering and search for axion-like particles with 2.2 nb^{-1} of Pb+Pb data with the ATLAS detector*, (2020), arXiv: [2008.05355 \[hep-ex\]](#).
- [39] ATLAS Collaboration, *The ATLAS Experiment at the CERN Large Hadron Collider*, *JINST* **3** (2008) S08003.
- [40] ATLAS Collaboration, *Muon reconstruction performance of the ATLAS detector in proton–proton collision data at $\sqrt{s} = 13 \text{ TeV}$* , *Eur. Phys. J. C* **76** (2016) 292, arXiv: [1603.05598 \[hep-ex\]](#).
- [41] ATLAS Collaboration, *Performance of the ATLAS trigger system in 2015*, *Eur. Phys. J. C* **77** (2017) 317, arXiv: [1611.09661 \[hep-ex\]](#).
- [42] ATLAS Collaboration, *Luminosity determination in pp collisions at $\sqrt{s} = 8 \text{ TeV}$ using the ATLAS detector at the LHC*, *Eur. Phys. J. C* **76** (2016) 653, arXiv: [1608.03953 \[hep-ex\]](#).
- [43] M. L. Miller, K. Reygers, S. J. Sanders, and P. Steinberg, *Glauber Modeling in High-Energy Nuclear Collisions*, *Ann. Rev. Nucl. Part. Sci.* **57** (2007) 205, arXiv: [nucl-ex/0701025](#).
- [44] ALICE Collaboration, *Measurement of the Cross Section for Electromagnetic Dissociation with Neutron Emission in Pb-Pb Collisions at $\sqrt{s_{NN}} = 2.76 \text{ TeV}$* , *Phys. Rev. Lett.* **109** (2012) 252302, arXiv: [1203.2436 \[nucl-ex\]](#).
- [45] S. J. Brodsky, T. Kinoshita, and H. Terazawa, *Two-Photon Mechanism of Particle Production by High-Energy Colliding Beams*, *Phys. Rev. D* **4** (1971) 1532.
- [46] S. Klein, A. H. Mueller, B.-W. Xiao, and F. Yuan, *Acoplanarity of a Lepton Pair to Probe the Electromagnetic Property of Quark Matter*, *Phys. Rev. Lett.* **122** (2019) 132301, arXiv: [1811.05519 \[hep-ph\]](#).
- [47] S. Klein, A. Mueller, B.-W. Xiao, and F. Yuan, *Lepton Pair Production Through Two Photon Process in Heavy Ion Collisions*, (2020), arXiv: [2003.02947 \[hep-ph\]](#).
- [48] A. J. Baltz, M. J. Rhoades-Brown, and J. Wenner, *Heavy-ion partial beam lifetimes due to Coulomb induced processes*, *Phys. Rev. E* **54** (1996) 4233.
- [49] J. D. Brandenburg et al., *Acoplanarity of QED pairs accompanied by nuclear dissociation in ultra-peripheral heavy ion collisions*, (2020), arXiv: [2006.07365 \[hep-ph\]](#).
- [50] S. R. Klein, J. Nystrand, J. Seger, Y. Gorbunov, and J. Butterworth, *STARlight: A Monte Carlo simulation program for ultra-peripheral collisions of relativistic ions*, *Comput. Phys. Commun.* **212** (2017) 258, arXiv: [1607.03838 \[hep-ph\]](#).
- [51] F. Krauss, M. Greiner, and G. Soff, *Photon and gluon induced processes in relativistic heavy-ion collisions*, *Prog. Part. Nucl. Phys.* **39** (1997) 503.
- [52] ATLAS Collaboration, *The ATLAS Simulation Infrastructure*, *Eur. Phys. J. C* **70** (2010) 823, arXiv: [1005.4568 \[physics.ins-det\]](#).
- [53] S. Agostinelli et al., *GEANT4 – A Simulation toolkit*, *Nucl. Instrum. Meth. A* **506** (2003) 250.
- [54] T. Sjöstrand, S. Mrenna, and P. Z. Skands, *PYTHIA 6.4 Physics and Manual*, *JHEP* **05** (2006) 026, arXiv: [hep-ph/0603175](#).
- [55] T. Sjöstrand et al., *An Introduction to PYTHIA 8.2*, *Comput. Phys. Commun.* **191** (2015) 159, arXiv: [1410.3012 \[hep-ph\]](#).
- [56] J. A. M. Vermaasen, *Two-photon processes at very high-energies*, *Nucl. Phys. B* **229** (1983) 347.

- [57] ATLAS Collaboration, *Measurement of the exclusive $\gamma\gamma \rightarrow \mu^+\mu^-$ process in proton-proton collisions at $\sqrt{s} = 13$ TeV with the ATLAS detector*, *Phys. Lett. B* **777** (2018) 303, arXiv: [1708.04053](https://arxiv.org/abs/1708.04053) [hep-ex].
- [58] A. Suri and D. R. Yennie, *The space-time phenomenology of photon absorption and inelastic electron scattering*, *Annals Phys.* **72** (1972) 243.
- [59] G. Avoni et al., *The new LUCID-2 detector for luminosity measurement and monitoring in ATLAS*, *JINST* **13** (2018) P07017.
- [60] ALICE Collaboraton, *Coherent ρ^0 photoproduction in ultra-peripheral Pb-Pb collisions at $\sqrt{s_{NN}} = 2.76$ TeV*, *JHEP* **09** (2015) 095, arXiv: [1503.09177](https://arxiv.org/abs/1503.09177) [nucl-ex].
- [61] ATLAS Collaboration, *ATLAS Computing Acknowledgements*, ATL-SOFT-PUB-2020-001, URL: <https://cds.cern.ch/record/2717821>.

The ATLAS Collaboration

G. Aad¹⁰², B. Abbott¹²⁸, D.C. Abbott¹⁰³, A. Abed Abud³⁶, K. Abeling⁵³, D.K. Abhayasinghe⁹⁴, S.H. Abidi¹⁶⁷, O.S. AbouZeid⁴⁰, N.L. Abraham¹⁵⁶, H. Abramowicz¹⁶¹, H. Abreu¹⁶⁰, Y. Abulaiti⁶, B.S. Acharya^{67a,67b,n}, B. Achkar⁵³, L. Adam¹⁰⁰, C. Adam Bourdarios⁵, L. Adamczyk^{84a}, L. Adamek¹⁶⁷, J. Adelman¹²¹, M. Adersberger¹¹⁴, A. Adiguzel^{12c,ad}, S. Adorni⁵⁴, T. Adye¹⁴³, A.A. Affolder¹⁴⁵, Y. Afik¹⁶⁰, C. Agapopoulou⁶⁵, M.N. Agaras³⁸, A. Aggarwal¹¹⁹, C. Agheorghiesei^{27c}, J.A. Aguilar-Saavedra^{139f,139a,ac}, A. Ahmad³⁶, F. Ahmadov⁸⁰, W.S. Ahmed¹⁰⁴, X. Ai¹⁸, G. Aielli^{74a,74b}, S. Akatsuka⁸⁶, M. Akbiyik¹⁰⁰, T.P.A. Åkesson⁹⁷, E. Akilli⁵⁴, A.V. Akimov¹¹¹, K. Al Khoury⁶⁵, G.L. Alberghini^{23b,23a}, J. Albert¹⁷⁶, M.J. Alconada Verzini¹⁶¹, S. Alderweireldt³⁶, M. Aleksa³⁶, I.N. Aleksandrov⁸⁰, C. Alexa^{27b}, T. Alexopoulos¹⁰, A. Alfonsi¹²⁰, F. Alfonsi^{23b,23a}, M. Alhoob¹²⁸, B. Ali¹⁴¹, S. Ali¹⁵⁸, M. Aliev¹⁶⁶, G. Alimonti^{69a}, C. Allaire³⁶, B.M.M. Allbrooke¹⁵⁶, B.W. Allen¹³¹, P.P. Allport²¹, A. Aloisio^{70a,70b}, F. Alonso⁸⁹, C. Alpigiani¹⁴⁸, E. Alunno Camelia^{74a,74b}, M. Alvarez Estevez⁹⁹, M.G. Alviggi^{70a,70b}, Y. Amaral Coutinho^{81b}, A. Ambler¹⁰⁴, L. Ambroz¹³⁴, C. Amelung²⁶, D. Amidei¹⁰⁶, S.P. Amor Dos Santos^{139a}, S. Amoroso⁴⁶, C.S. Amrouche⁵⁴, F. An⁷⁹, C. Anastopoulos¹⁴⁹, N. Andari¹⁴⁴, T. Andeen¹¹, J.K. Anders²⁰, S.Y. Andrean^{45a,45b}, A. Andreazza^{69a,69b}, V. Andrei^{61a}, C.R. Anelli¹⁷⁶, S. Angelidakis⁹, A. Angerami³⁹, A.V. Anisenkov^{122b,122a}, A. Annovi^{72a}, C. Antel⁵⁴, M.T. Anthony¹⁴⁹, E. Antipov¹²⁹, M. Antonelli⁵¹, D.J.A. Antrim¹⁷¹, F. Anulli^{73a}, M. Aoki⁸², J.A. Aparisi Pozo¹⁷⁴, M.A. Aparo¹⁵⁶, L. Aperio Bella⁴⁶, N. Aranzabal³⁶, V. Araujo Ferraz^{81a}, R. Araujo Pereira^{81b}, C. Arcangeletti⁵¹, A.T.H. Arce⁴⁹, F.A. Arduh⁸⁹, J.-F. Arguin¹¹⁰, S. Argyropoulos⁵², J.-H. Arling⁴⁶, A.J. Armbruster³⁶, A. Armstrong¹⁷¹, O. Arnaez¹⁶⁷, H. Arnold¹²⁰, Z.P. Arrubarrena Tame¹¹⁴, G. Artoni¹³⁴, H. Asada¹¹⁷, K. Asai¹²⁶, S. Asai¹⁶³, T. Asawatavonvanich¹⁶⁵, N.A. Asbah⁵⁹, E.M. Asimakopoulou¹⁷², L. Asquith¹⁵⁶, J. Assahsah^{35d}, K. Assamagan²⁹, R. Astalos^{28a}, R.J. Atkin^{33a}, M. Atkinson¹⁷³, N.B. Atlay¹⁹, H. Atmani⁶⁵, K. Augsten¹⁴¹, V.A. Aastrup¹⁸², G. Avolio³⁶, M.K. Ayoub^{15a}, G. Azuelos^{110,al}, D. Babal^{28a}, H. Bachacou¹⁴⁴, K. Bachas¹⁶², F. Backman^{45a,45b}, P. Bagnaia^{73a,73b}, H. Bahrasemani¹⁵², A.J. Bailey¹⁷⁴, V.R. Bailey¹⁷³, J.T. Baines¹⁴³, C. Bakalis¹⁰, O.K. Baker¹⁸³, P.J. Bakker¹²⁰, E. Bakos¹⁶, D. Bakshi Gupta⁸, S. Balaji¹⁵⁷, R. Balasubramanian¹²⁰, E.M. Baldin^{122b,122a}, P. Balek¹⁸⁰, F. Balli¹⁴⁴, W.K. Balunas¹³⁴, J. Balz¹⁰⁰, E. Banas⁸⁵, M. Bandieramonte¹³⁸, A. Bandyopadhyay²⁴, Sw. Banerjee^{181,i}, L. Barak¹⁶¹, W.M. Barbe³⁸, E.L. Barberio¹⁰⁵, D. Barberis^{55b,55a}, M. Barbero¹⁰², G. Barbour⁹⁵, T. Barillari¹¹⁵, M.-S. Barisis³⁶, J. Barkeloo¹³¹, T. Barklow¹⁵³, R. Barnea¹⁶⁰, B.M. Barnett¹⁴³, R.M. Barnett¹⁸, Z. Barnovska-Blenessy^{60a}, A. Baroncelli^{60a}, G. Barone²⁹, A.J. Barr¹³⁴, L. Barranco Navarro^{45a,45b}, F. Barreiro⁹⁹, J. Barreiro Guimarães da Costa^{15a}, U. Barron¹⁶¹, S. Barsov¹³⁷, F. Bartels^{61a}, R. Bartoldus¹⁵³, G. Bartolini¹⁰², A.E. Barton⁹⁰, P. Bartos^{28a}, A. Basalaev⁴⁶, A. Basan¹⁰⁰, A. Bassalat^{65,ai}, M.J. Basso¹⁶⁷, R.L. Bates⁵⁷, S. Batlamous^{35e}, J.R. Batley³², B. Batool¹⁵¹, M. Battaglia¹⁴⁵, M. Bauce^{73a,73b}, F. Bauer^{144,*}, P. Bauer²⁴, H.S. Bawa³¹, A. Bayirli^{12c}, J.B. Beacham⁴⁹, T. Beau¹³⁵, P.H. Beauchemin¹⁷⁰, F. Becherer⁵², P. Bechtle²⁴, H.C. Beck⁵³, H.P. Beck^{20,p}, K. Becker¹⁷⁸, C. Becot⁴⁶, A. Beddall^{12d}, A.J. Beddall^{12a}, V.A. Bednyakov⁸⁰, M. Bedognetti¹²⁰, C.P. Bee¹⁵⁵, T.A. Beermann¹⁸², M. Begalli^{81b}, M. Begel²⁹, A. Behera¹⁵⁵, J.K. Behr⁴⁶, F. Beisiegel²⁴, M. Belfkir⁵, A.S. Bell⁹⁵, G. Bella¹⁶¹, L. Bellagamba^{23b}, A. Bellerive³⁴, P. Bellos⁹, K. Beloborodov^{122b,122a}, K. Belotskiy¹¹², N.L. Belyaev¹¹², D. Benchekroun^{35a}, N. Benekos¹⁰, Y. Benhammou¹⁶¹, D.P. Benjamin⁶, M. Benoit²⁹, J.R. Bensinger²⁶, S. Bentvelsen¹²⁰, L. Beresford¹³⁴, M. Beretta⁵¹, D. Berge¹⁹, E. Bergeaas Kuutmann¹⁷², N. Berger⁵, B. Bergmann¹⁴¹, L.J. Bergsten²⁶, J. Beringer¹⁸, S. Berlendis⁷, G. Bernardi¹³⁵, C. Bernius¹⁵³, F.U. Bernlochner²⁴, T. Berry⁹⁴, P. Berta¹⁰⁰, A. Berthold⁴⁸, I.A. Bertram⁹⁰, O. Bessidskaia Bylund¹⁸², N. Besson¹⁴⁴, A. Bethani¹⁰¹, S. Bethke¹¹⁵, A. Betti⁴², A.J. Bevan⁹³, J. Beyer¹¹⁵, D.S. Bhattacharya¹⁷⁷, P. Bhattacharai²⁶, V.S. Bhopatkar⁶, R. Bi¹³⁸, R.M. Bianchi¹³⁸, O. Biebel¹¹⁴, D. Biedermann¹⁹, R. Bielski³⁶, K. Bierwagen¹⁰⁰, N.V. Biesuz^{72a,72b}, M. Biglietti^{75a}, T.R.V. Billoud¹⁴¹, M. Bindi⁵³, A. Bingul^{12d}, C. Bini^{73a,73b},

S. Biondi^{23b,23a}, C.J. Birch-sykes¹⁰¹, M. Birman¹⁸⁰, T. Bisanz³⁶, J.P. Biswal³, D. Biswas^{181,i},
 A. Bitadze¹⁰¹, C. Bittrich⁴⁸, K. Bjørke¹³³, T. Blazek^{28a}, I. Bloch⁴⁶, C. Blocker²⁶, A. Blue⁵⁷,
 U. Blumenschein⁹³, G.J. Bobbink¹²⁰, V.S. Bobrovnikov^{122b,122a}, S.S. Bocchetta⁹⁷, D. Bogavac¹⁴,
 A.G. Bogdanchikov^{122b,122a}, C. Bohm^{45a}, V. Boisvert⁹⁴, P. Bokan^{172,53}, T. Bold^{84a}, A.E. Bolz^{61b},
 M. Bomben¹³⁵, M. Bona⁹³, J.S. Bonilla¹³¹, M. Boonekamp¹⁴⁴, C.D. Booth⁹⁴, A.G. Borbely⁵⁷,
 H.M. Borecka-Bielska⁹¹, L.S. Borgna⁹⁵, A. Borisov¹²³, G. Borissov⁹⁰, D. Bortoletto¹³⁴, D. Boscherini^{23b},
 M. Bosman¹⁴, J.D. Bossio Sola¹⁰⁴, K. Bouaouda^{35a}, J. Boudreau¹³⁸, E.V. Bouhova-Thacker⁹⁰,
 D. Boumediene³⁸, A. Boveia¹²⁷, J. Boyd³⁶, D. Boye^{33c}, I.R. Boyko⁸⁰, A.J. Bozson⁹⁴, J. Bracinik²¹,
 N. Brahimi^{60d,60c}, G. Brandt¹⁸², O. Brandt³², F. Braren⁴⁶, B. Brau¹⁰³, J.E. Brau¹³¹,
 W.D. Breaden Madden⁵⁷, K. Brendlinger⁴⁶, R. Brener¹⁶⁰, L. Brenner³⁶, R. Brenner¹⁷², S. Bressler¹⁸⁰,
 B. Brickwedde¹⁰⁰, D.L. Briglin²¹, D. Britton⁵⁷, D. Britzger¹¹⁵, I. Brock²⁴, R. Brock¹⁰⁷, G. Brooijmans³⁹,
 W.K. Brooks^{146d}, E. Brost²⁹, P.A. Bruckman de Renstrom⁸⁵, B. Brüers⁴⁶, D. Bruncko^{28b}, A. Bruni^{23b},
 G. Bruni^{23b}, M. Bruschi^{23b}, N. Bruscino^{73a,73b}, L. Bryngemark¹⁵³, T. Buanes¹⁷, Q. Buat¹⁵⁵, P. Buchholz¹⁵¹,
 A.G. Buckley⁵⁷, I.A. Budagov⁸⁰, M.K. Bugge¹³³, F. Bührer⁵², O. Bulekov¹¹², B.A. Bullard⁵⁹,
 T.J. Burch¹²¹, S. Burdin⁹¹, C.D. Burgard¹²⁰, A.M. Burger¹²⁹, B. Burghgrave⁸, J.T.P. Burr⁴⁶, C.D. Burton¹¹,
 J.C. Burzynski¹⁰³, V. Büscher¹⁰⁰, E. Buschmann⁵³, P.J. Bussey⁵⁷, J.M. Butler²⁵, C.M. Buttar⁵⁷,
 J.M. Butterworth⁹⁵, P. Butti³⁶, W. Buttinger¹⁴³, C.J. Buxo Vazquez¹⁰⁷, A. Buzatu¹⁵⁸,
 A.R. Buzykaev^{122b,122a}, G. Cabras^{23b,23a}, S. Cabrera Urbán¹⁷⁴, D. Caforio⁵⁶, H. Cai¹³⁸, V.M.M. Cairo¹⁵³,
 O. Cakir^{4a}, N. Calace³⁶, P. Calafiura¹⁸, G. Calderini¹³⁵, P. Calfayan⁶⁶, G. Callea⁵⁷, L.P. Caloba^{81b},
 A. Caltabiano^{74a,74b}, S. Calvente Lopez⁹⁹, D. Calvet³⁸, S. Calvet³⁸, T.P. Calvet¹⁰², M. Calvetti^{72a,72b},
 R. Camacho Toro¹³⁵, S. Camarda³⁶, D. Camarero Munoz⁹⁹, P. Camarri^{74a,74b}, M.T. Camerlingo^{75a,75b},
 D. Cameron¹³³, C. Camincher³⁶, S. Campana³⁶, M. Campanelli⁹⁵, A. Camplani⁴⁰, V. Canale^{70a,70b},
 A. Canesse¹⁰⁴, M. Cano Bret⁷⁸, J. Cantero¹²⁹, T. Cao¹⁶¹, Y. Cao¹⁷³, M.D.M. Capeans Garrido³⁶,
 M. Capua^{41b,41a}, R. Cardarelli^{74a}, F. Cardillo¹⁷⁴, G. Carducci^{41b,41a}, I. Carli¹⁴², T. Carli³⁶, G. Carlino^{70a},
 B.T. Carlson¹³⁸, E.M. Carlson^{176,168a}, L. Carminati^{69a,69b}, R.M.D. Carney¹⁵³, S. Caron¹¹⁹, E. Carquin^{146d},
 S. Carra⁴⁶, G. Carratta^{23b,23a}, J.W.S. Carter¹⁶⁷, T.M. Carter⁵⁰, M.P. Casado^{14,f}, A.F. Casha¹⁶⁷,
 E.G. Castiglia¹⁸³, F.L. Castillo¹⁷⁴, L. Castillo Garcia¹⁴, V. Castillo Gimenez¹⁷⁴, N.F. Castro^{139a,139e},
 A. Catinaccio³⁶, J.R. Catmore¹³³, A. Cattai³⁶, V. Cavaliere²⁹, V. Cavasinni^{72a,72b}, E. Celebi^{12b}, F. Celli¹³⁴,
 K. Cerny¹³⁰, A.S. Cerqueira^{81a}, A. Cerri¹⁵⁶, L. Cerrito^{74a,74b}, F. Cerutti¹⁸, A. Cervelli^{23b,23a}, S.A. Cetin^{12b},
 Z. Chadi^{35a}, D. Chakraborty¹²¹, J. Chan¹⁸¹, W.S. Chan¹²⁰, W.Y. Chan⁹¹, J.D. Chapman³²,
 B. Chargeishvili^{159b}, D.G. Charlton²¹, T.P. Charman⁹³, M. Chatterjee²⁰, C.C. Chau³⁴, S. Che¹²⁷,
 S. Chekanov⁶, S.V. Chekulaev^{168a}, G.A. Chelkov^{80,ag}, B. Chen⁷⁹, C. Chen^{60a}, C.H. Chen⁷⁹, H. Chen^{15c},
 H. Chen²⁹, J. Chen^{60a}, J. Chen³⁹, J. Chen²⁶, S. Chen¹³⁶, S.J. Chen^{15c}, X. Chen^{15b}, Y. Chen^{60a},
 Y-H. Chen⁴⁶, H.C. Cheng^{63a}, H.J. Cheng^{15a}, A. Cheplakov⁸⁰, E. Cheremushkina¹²³,
 R. Cherkaoui El Moursli^{35e}, E. Cheu⁷, K. Cheung⁶⁴, T.J.A. Chevaléries¹⁴⁴, L. Chevalier¹⁴⁴, V. Chiarella⁵¹,
 G. Chiarelli^{72a}, G. Chiodini^{68a}, A.S. Chisholm²¹, A. Chitan^{27b}, I. Chiu¹⁶³, Y.H. Chiu¹⁷⁶, M.V. Chizhov⁸⁰,
 K. Choi¹¹, A.R. Chomont^{73a,73b}, Y.S. Chow¹²⁰, L.D. Christopher^{33f}, M.C. Chu^{63a}, X. Chu^{15a,15d},
 J. Chudoba¹⁴⁰, J.J. Chwastowski⁸⁵, L. Chytka¹³⁰, D. Cieri¹¹⁵, K.M. Ciesla⁸⁵, V. Cindro⁹², I.A. Cioara^{27b},
 A. Ciocio¹⁸, F. Cirotto^{70a,70b}, Z.H. Citron^{180,j}, M. Citterio^{69a}, D.A. Ciubotaru^{27b}, B.M. Ciungu¹⁶⁷,
 A. Clark⁵⁴, M.R. Clark³⁹, P.J. Clark⁵⁰, S.E. Clawson¹⁰¹, C. Clement^{45a,45b}, Y. Coadou¹⁰², M. Cobal^{67a,67c},
 A. Coccaro^{55b}, J. Cochran⁷⁹, R. Coelho Lopes De Sa¹⁰³, H. Cohen¹⁶¹, A.E.C. Coimbra³⁶, B. Cole³⁹,
 A.P. Colijn¹²⁰, J. Collot⁵⁸, P. Conde Muiño^{139a,139h}, S.H. Connell^{33c}, I.A. Connolly⁵⁷, S. Constantinescu^{27b},
 F. Conventi^{70a,am}, A.M. Cooper-Sarkar¹³⁴, F. Cormier¹⁷⁵, K.J.R. Cormier¹⁶⁷, L.D. Corpe⁹⁵,
 M. Corradi^{73a,73b}, E.E. Corrigan⁹⁷, F. Corriveau^{104,aa}, M.J. Costa¹⁷⁴, F. Costanza⁵, D. Costanzo¹⁴⁹,
 G. Cowan⁹⁴, J.W. Cowley³², J. Crane¹⁰¹, K. Cranmer¹²⁵, R.A. Creager¹³⁶, S. Crépé-Renaudin⁵⁸,
 F. Crescioli¹³⁵, M. Cristinziani²⁴, V. Croft¹⁷⁰, G. Crosetti^{41b,41a}, A. Cueto⁵, T. Cuhadar Donszelmann¹⁷¹,
 H. Cui^{15a,15d}, A.R. Cukierman¹⁵³, W.R. Cunningham⁵⁷, S. Czekierda⁸⁵, P. Czodrowski³⁶,

M.M. Czurylo^{61b}, M.J. Da Cunha Sargedas De Sousa^{60b}, J.V. Da Fonseca Pinto^{81b}, C. Da Via¹⁰¹,
 W. Dabrowski^{84a}, F. Dachs³⁶, T. Dado⁴⁷, S. Dahbi^{33f}, T. Dai¹⁰⁶, C. Dallapiccola¹⁰³, M. Dam⁴⁰,
 G. D'amen²⁹, V. D'Amico^{75a,75b}, J. Damp¹⁰⁰, J.R. Dandoy¹³⁶, M.F. Daneri³⁰, M. Danninger¹⁵², V. Dao³⁶,
 G. Darbo^{55b}, O. Dartsi⁵, A. Dattagupta¹³¹, T. Daubney⁴⁶, S. D'Auria^{69a,69b}, C. David^{168b}, T. Davidek¹⁴²,
 D.R. Davis⁴⁹, I. Dawson¹⁴⁹, K. De⁸, R. De Asmundis^{70a}, M. De Beurs¹²⁰, S. De Castro^{23b,23a},
 N. De Groot¹¹⁹, P. de Jong¹²⁰, H. De la Torre¹⁰⁷, A. De Maria^{15c}, D. De Pedis^{73a}, A. De Salvo^{73a},
 U. De Sanctis^{74a,74b}, M. De Santis^{74a,74b}, A. De Santo¹⁵⁶, J.B. De Vivie De Regie⁶⁵, D.V. Dedovich⁸⁰,
 A.M. Deiana⁴², J. Del Peso⁹⁹, Y. Delabat Diaz⁴⁶, D. Delgove⁶⁵, F. Deliot¹⁴⁴, C.M. Delitzsch⁷,
 M. Della Pietra^{70a,70b}, D. Della Volpe⁵⁴, A. Dell'Acqua³⁶, L. Dell'Asta^{74a,74b}, M. Delmastro⁵,
 C. Delporte⁶⁵, P.A. Delsart⁵⁸, D.A. DeMarco¹⁶⁷, S. Demers¹⁸³, M. Demichev⁸⁰, G. Demontigny¹¹⁰,
 S.P. Denisov¹²³, L. D'Eramo¹²¹, D. Derendarz⁸⁵, J.E. Derkaoui^{35d}, F. Derue¹³⁵, P. Dervan⁹¹, K. Desch²⁴,
 K. Dette¹⁶⁷, C. Deutsch²⁴, M.R. Devesa³⁰, P.O. Deviveiros³⁶, F.A. Di Bello^{73a,73b}, A. Di Ciaccio^{74a,74b},
 L. Di Ciaccio⁵, W.K. Di Clemente¹³⁶, C. Di Donato^{70a,70b}, A. Di Girolamo³⁶, G. Di Gregorio^{72a,72b},
 B. Di Micco^{75a,75b}, R. Di Nardo^{75a,75b}, K.F. Di Petrillo⁵⁹, R. Di Sipio¹⁶⁷, C. Diaconu¹⁰², F.A. Dias¹²⁰,
 T. Dias Do Vale^{139a}, M.A. Diaz^{146a}, F.G. Diaz Capriles²⁴, J. Dickinson¹⁸, M. Didenko¹⁶⁶, E.B. Diehl¹⁰⁶,
 J. Dietrich¹⁹, S. Díez Cornell⁴⁶, C. Diez Pardos¹⁵¹, A. Dimitrievska¹⁸, W. Ding^{15b}, J. Dingfelder²⁴,
 S.J. Dittmeier^{61b}, F. Dittus³⁶, F. Djama¹⁰², T. Djobava^{159b}, J.I. Djuvsland¹⁷, M.A.B. Do Vale¹⁴⁷,
 M. Dobre^{27b}, D. Dodsworth²⁶, C. Doglioni⁹⁷, J. Dolejsi¹⁴², Z. Dolezal¹⁴², M. Donadelli^{81c}, B. Dong^{60c},
 J. Donini³⁸, A. D'onofrio^{15c}, M. D'Onofrio⁹¹, J. Dopke¹⁴³, A. Doria^{70a}, M.T. Dova⁸⁹, A.T. Doyle⁵⁷,
 E. Drechsler¹⁵², E. Dreyer¹⁵², T. Dreyer⁵³, A.S. Drobac¹⁷⁰, D. Du^{60b}, T.A. du Pree¹²⁰, Y. Duan^{60d},
 F. Dubinin¹¹¹, M. Dubovsky^{28a}, A. Dubreuil⁵⁴, E. Duchovni¹⁸⁰, G. Duckeck¹¹⁴, O.A. Ducu^{36,27b},
 D. Duda¹¹⁵, A. Dudarev³⁶, A.C. Dudder¹⁰⁰, E.M. Duffield¹⁸, M. D'uffizi¹⁰¹, L. Duflot⁶⁵, M. Dührssen³⁶,
 C. Dülsen¹⁸², M. Dumancic¹⁸⁰, A.E. Dumitriu^{27b}, M. Dunford^{61a}, S. Dungs⁴⁷, A. Duperrin¹⁰²,
 H. Duran Yildiz^{4a}, M. Düren⁵⁶, A. Durglishvili^{159b}, D. Duschinger⁴⁸, B. Dutta⁴⁶, D. Duvnjak¹,
 G.I. Dyckes¹³⁶, M. Dyndal³⁶, S. Dysch¹⁰¹, B.S. Dziedzic⁸⁵, M.G. Eggleston⁴⁹, T. Eifert⁸, G. Eigen¹⁷,
 K. Einsweiler¹⁸, T. Ekelof¹⁷², H. El Jarrari^{35e}, V. Ellajosyula¹⁷², M. Ellert¹⁷², F. Ellinghaus¹⁸²,
 A.A. Elliot⁹³, N. Ellis³⁶, J. Elmsheuser²⁹, M. Elsing³⁶, D. Emeliyanov¹⁴³, A. Emerman³⁹, Y. Enari¹⁶³,
 M.B. Epland⁴⁹, J. Erdmann⁴⁷, A. Ereditato²⁰, P.A. Erland⁸⁵, M. Errenst¹⁸², M. Escalier⁶⁵, C. Escobar¹⁷⁴,
 O. Estrada Pastor¹⁷⁴, E. Etzion¹⁶¹, G. Evans^{139a,139b}, H. Evans⁶⁶, M.O. Evans¹⁵⁶, A. Ezhilov¹³⁷,
 F. Fabbri⁵⁷, L. Fabbri^{23b,23a}, V. Fabiani¹¹⁹, G. Facini¹⁷⁸, R.M. Fakhrutdinov¹²³, S. Falciano^{73a}, P.J. Falke²⁴,
 S. Falke³⁶, J. Faltova¹⁴², Y. Fang^{15a}, Y. Fang^{15a}, G. Fanourakis⁴⁴, M. Fanti^{69a,69b}, M. Faraj^{67a,67c},
 A. Farbin⁸, A. Farilla^{75a}, E.M. Farina^{71a,71b}, T. Farooque¹⁰⁷, S.M. Farrington⁵⁰, P. Farthouat³⁶, F. Fassi^{35e},
 P. Fassnacht³⁶, D. Fassouliotis⁹, M. Faucci Giannelli⁵⁰, W.J. Fawcett³², L. Fayard⁶⁵, O.L. Fedin^{137,o},
 W. Fedorko¹⁷⁵, A. Fehr²⁰, M. Feickert¹⁷³, L. Feligioni¹⁰², A. Fell¹⁴⁹, C. Feng^{60b}, M. Feng⁴⁹,
 M.J. Fenton¹⁷¹, A.B. Fenyuk¹²³, S.W. Ferguson⁴³, J. Ferrando⁴⁶, A. Ferrante¹⁷³, A. Ferrari¹⁷²,
 P. Ferrari¹²⁰, R. Ferrari^{71a}, D.E. Ferreira de Lima^{61b}, A. Ferrer¹⁷⁴, D. Ferrere⁵⁴, C. Ferretti¹⁰⁶,
 F. Fiedler¹⁰⁰, A. Filipčič⁹², F. Filthaut¹¹⁹, K.D. Finelli²⁵, M.C.N. Fiolhais^{139a,139c,a}, L. Fiorini¹⁷⁴,
 F. Fischer¹¹⁴, J. Fischer¹⁰⁰, W.C. Fisher¹⁰⁷, T. Fitschen²¹, I. Fleck¹⁵¹, P. Fleischmann¹⁰⁶, T. Flick¹⁸²,
 B.M. Flierl¹¹⁴, L. Flores¹³⁶, L.R. Flores Castillo^{63a}, F.M. Follega^{76a,76b}, N. Fomin¹⁷, J.H. Foo¹⁶⁷,
 G.T. Forcolin^{76a,76b}, B.C. Forland⁶⁶, A. Formica¹⁴⁴, F.A. Förster¹⁴, A.C. Forti¹⁰¹, E. Fortin¹⁰²,
 M.G. Foti¹³⁴, D. Fournier⁶⁵, H. Fox⁹⁰, P. Francavilla^{72a,72b}, S. Francescato^{73a,73b}, M. Franchini^{23b,23a},
 S. Franchino^{61a}, D. Francis³⁶, L. Franco⁵, L. Franconi²⁰, M. Franklin⁵⁹, G. Frattari^{73a,73b}, A.N. Fray⁹³,
 P.M. Freeman²¹, B. Freund¹¹⁰, W.S. Freund^{81b}, E.M. Freundlich⁴⁷, D.C. Frizzell¹²⁸, D. Froidevaux³⁶,
 J.A. Frost¹³⁴, M. Fujimoto¹²⁶, C. Fukunaga¹⁶⁴, E. Fullana Torregrosa¹⁷⁴, T. Fusayasu¹¹⁶, J. Fuster¹⁷⁴,
 A. Gabrielli^{23b,23a}, A. Gabrielli³⁶, S. Gadatsch⁵⁴, P. Gadow¹¹⁵, G. Gagliardi^{55b,55a}, L.G. Gagnon¹¹⁰,
 G.E. Gallardo¹³⁴, E.J. Gallas¹³⁴, B.J. Gallop¹⁴³, R. Gamboa Goni⁹³, K.K. Gan¹²⁷, S. Ganguly¹⁸⁰,
 J. Gao^{60a}, Y. Gao⁵⁰, Y.S. Gao^{31,1}, F.M. Garay Walls^{146a}, C. García¹⁷⁴, J.E. García Navarro¹⁷⁴,

J.A. García Pascual^{15a}, C. Garcia-Argos⁵², M. Garcia-Sciveres¹⁸, R.W. Gardner³⁷, N. Garelli¹⁵³,
 S. Gargiulo⁵², C.A. Garner¹⁶⁷, V. Garonne¹³³, S.J. Gasiorowski¹⁴⁸, P. Gaspar^{81b}, A. Gaudiello^{55b,55a},
 G. Gaudio^{71a}, P. Gauzzi^{73a,73b}, I.L. Gavrilenko¹¹¹, A. Gavrilyuk¹²⁴, C. Gay¹⁷⁵, G. Gaycken⁴⁶, E.N. Gazis¹⁰,
 A.A. Geanta^{27b}, C.M. Gee¹⁴⁵, C.N.P. Gee¹⁴³, J. Geisen⁹⁷, M. Geisen¹⁰⁰, C. Gemme^{55b}, M.H. Genest⁵⁸,
 C. Geng¹⁰⁶, S. Gentile^{73a,73b}, S. George⁹⁴, T. Geralis⁴⁴, L.O. Gerlach⁵³, P. Gessinger-Befurt¹⁰⁰,
 G. Gessner⁴⁷, S. Ghasemi¹⁵¹, M. Ghasemi Bostanabad¹⁷⁶, M. Ghneimat¹⁵¹, A. Ghosh⁶⁵, A. Ghosh⁷⁸,
 B. Giacobbe^{23b}, S. Giagu^{73a,73b}, N. Giangiocomi^{23b,23a}, P. Giannetti^{72a}, A. Giannini^{70a,70b}, G. Giannini¹⁴,
 S.M. Gibson⁹⁴, M. Gignac¹⁴⁵, D.T. Gil^{84b}, B.J. Gilbert³⁹, D. Gillberg³⁴, G. Gilles¹⁸², N.E.K. Gillwald⁴⁶,
 D.M. Gingrich^{3,al}, M.P. Giordani^{67a,67c}, P.F. Giraud¹⁴⁴, G. Giugliarelli^{67a,67c}, D. Giugni^{69a}, F. Giuli^{74a,74b},
 S. Gkaitatzis¹⁶², I. Gkialas^{9,g}, E.L. Gkougkousis¹⁴, P. Gkountoumis¹⁰, L.K. Gladilin¹¹³, C. Glasman⁹⁹,
 J. Glatzer¹⁴, P.C.F. Glaysher⁴⁶, A. Glazov⁴⁶, G.R. Gledhill¹³¹, I. Gnesi^{41b,b}, M. Goblirsch-Kolb²⁶,
 D. Godin¹¹⁰, S. Goldfarb¹⁰⁵, T. Golling⁵⁴, D. Golubkov¹²³, A. Gomes^{139a,139b}, R. Goncalves Gama⁵³,
 R. Gonçalo^{139a,139c}, G. Gonella¹³¹, L. Gonella²¹, A. Gongadze⁸⁰, F. Gonnella²¹, J.L. Gonski³⁹,
 S. González de la Hoz¹⁷⁴, S. Gonzalez Fernandez¹⁴, R. Gonzalez Lopez⁹¹, C. Gonzalez Renteria¹⁸,
 R. Gonzalez Suarez¹⁷², S. Gonzalez-Sevilla⁵⁴, G.R. Gonzalvo Rodriguez¹⁷⁴, L. Goossens³⁶,
 N.A. Gorasia²¹, P.A. Gorbounov¹²⁴, H.A. Gordon²⁹, B. Gorini³⁶, E. Gorini^{68a,68b}, A. Gorišek⁹²,
 A.T. Goshaw⁴⁹, M.I. Gostkin⁸⁰, C.A. Gottardo¹¹⁹, M. Gouighri^{35b}, A.G. Goussiou¹⁴⁸, N. Govender^{33c},
 C. Goy⁵, I. Grabowska-Bold^{84a}, E.C. Graham⁹¹, J. Gramling¹⁷¹, E. Gramstad¹³³, S. Grancagnolo¹⁹,
 M. Grandi¹⁵⁶, V. Gratchev¹³⁷, P.M. Gravila^{27f}, F.G. Gravili^{68a,68b}, C. Gray⁵⁷, H.M. Gray¹⁸, C. Grefe²⁴,
 K. Gregersen⁹⁷, I.M. Gregor⁴⁶, P. Grenier¹⁵³, K. Grevtsov⁴⁶, C. Grieco¹⁴, N.A. Grieser¹²⁸, A.A. Grillo¹⁴⁵,
 K. Grimm^{31,k}, S. Grinstein^{14,w}, J.-F. Grivaz⁶⁵, S. Groh¹⁰⁰, E. Gross¹⁸⁰, J. Grosse-Knetter⁵³, Z.J. Grout⁹⁵,
 C. Grud¹⁰⁶, A. Grummer¹¹⁸, J.C. Grundy¹³⁴, L. Guan¹⁰⁶, W. Guan¹⁸¹, C. Gubbels¹⁷⁵, J. Guenther⁷⁷,
 A. Guerguichon⁶⁵, J.G.R. Guerrero Rojas¹⁷⁴, F. Guescini¹¹⁵, D. Guest¹⁷¹, R. Gugel¹⁰⁰, A. Guida⁴⁶,
 T. Guillemin⁵, S. Guindon³⁶, J. Guo^{60c}, W. Guo¹⁰⁶, Y. Guo^{60a}, Z. Guo¹⁰², R. Gupta⁴⁶, S. Gurbuz^{12c},
 G. Gustavino¹²⁸, M. Guth⁵², P. Gutierrez¹²⁸, C. Gutschow⁹⁵, C. Guyot¹⁴⁴, C. Gwenlan¹³⁴,
 C.B. Gwilliam⁹¹, E.S. Haaland¹³³, A. Haas¹²⁵, C. Haber¹⁸, H.K. Hadavand⁸, A. Hadef^{60a}, M. Haleem¹⁷⁷,
 J. Haley¹²⁹, J.J. Hall¹⁴⁹, G. Halladjian¹⁰⁷, G.D. Hallewell¹⁰², K. Hamano¹⁷⁶, H. Hamdaoui^{35e},
 M. Hamer²⁴, G.N. Hamity⁵⁰, K. Han^{60a,v}, L. Han^{15c}, L. Han^{60a}, S. Han¹⁸, Y.F. Han¹⁶⁷, K. Hanagaki^{82,t},
 M. Hance¹⁴⁵, D.M. Handl¹¹⁴, M.D. Hank³⁷, R. Hankache¹³⁵, E. Hansen⁹⁷, J.B. Hansen⁴⁰, J.D. Hansen⁴⁰,
 M.C. Hansen²⁴, P.H. Hansen⁴⁰, E.C. Hanson¹⁰¹, K. Hara¹⁶⁹, T. Harenberg¹⁸², S. Harkusha¹⁰⁸,
 P.F. Harrison¹⁷⁸, N.M. Hartman¹⁵³, N.M. Hartmann¹¹⁴, Y. Hasegawa¹⁵⁰, A. Hasib⁵⁰, S. Hassani¹⁴⁴,
 S. Haug²⁰, R. Hauser¹⁰⁷, L.B. Havener³⁹, M. Havranek¹⁴¹, C.M. Hawkes²¹, R.J. Hawkings³⁶,
 S. Hayashida¹¹⁷, D. Hayden¹⁰⁷, C. Hayes¹⁰⁶, R.L. Hayes¹⁷⁵, C.P. Hays¹³⁴, J.M. Hays⁹³, H.S. Hayward⁹¹,
 S.J. Haywood¹⁴³, F. He^{60a}, Y. He¹⁶⁵, M.P. Heath⁵⁰, V. Hedberg⁹⁷, A.L. Heggelund¹³³, C. Heidegger⁵²,
 K.K. Heidegger⁵², W.D. Heidorn⁷⁹, J. Heilman³⁴, S. Heim⁴⁶, T. Heim¹⁸, B. Heinemann^{46,aj},
 J.G. Heinlein¹³⁶, J.J. Heinrich¹³¹, L. Heinrich³⁶, J. Hejbal¹⁴⁰, L. Helary⁴⁶, A. Held¹²⁵, S. Hellesund¹³³,
 C.M. Helling¹⁴⁵, S. Hellman^{45a,45b}, C. Helsens³⁶, R.C.W. Henderson⁹⁰, Y. Heng¹⁸¹, L. Henkelmann³²,
 A.M. Henriques Correia³⁶, H. Herde²⁶, Y. Hernández Jiménez^{33f}, H. Herr¹⁰⁰, M.G. Herrmann¹¹⁴,
 T. Herrmann⁴⁸, G. Herten⁵², R. Hertenberger¹¹⁴, L. Hervas³⁶, T.C. Herwig¹³⁶, G.G. Hesketh⁹⁵,
 N.P. Hessey^{168a}, H. Hibi⁸³, S. Higashino⁸², E. Higón-Rodríguez¹⁷⁴, K. Hildebrand³⁷, J.C. Hill³²,
 K.K. Hill²⁹, K.H. Hiller⁴⁶, S.J. Hillier²¹, M. Hils⁴⁸, I. Hinchliffe¹⁸, F. Hinterkeuser²⁴, M. Hirose¹³²,
 S. Hirose¹⁶⁹, D. Hirschbuehl¹⁸², B. Hiti⁹², O. Hladík¹⁴⁰, J. Hobbs¹⁵⁵, N. Hod¹⁸⁰, M.C. Hodgkinson¹⁴⁹,
 A. Hoecker³⁶, D. Hohn⁵², D. Hohov⁶⁵, T. Holm²⁴, T.R. Holmes³⁷, M. Holzbock¹¹⁵, L.B.A.H. Hommels³²,
 T.M. Hong¹³⁸, J.C. Honig⁵², A. Hönl¹¹⁵, B.H. Hooberman¹⁷³, W.H. Hopkins⁶, Y. Horii¹¹⁷, P. Horn⁴⁸,
 L.A. Horyn³⁷, S. Hou¹⁵⁸, A. Hoummada^{35a}, J. Howarth⁵⁷, J. Hoya⁸⁹, M. Hrabovsky¹³⁰, J. Hrvnac⁶⁵,
 A. Hrynevich¹⁰⁹, T. Hryni'ova⁵, P.J. Hsu⁶⁴, S.-C. Hsu¹⁴⁸, Q. Hu²⁹, S. Hu^{60c}, Y.F. Hu^{15a,15d.an}, D.P. Huang⁹⁵,
 X. Huang^{15c}, Y. Huang^{60a}, Y. Huang^{15a}, Z. Hubacek¹⁴¹, F. Hubaut¹⁰², M. Huebner²⁴, F. Huegging²⁴,

T.B. Huffman¹³⁴, M. Huhtinen³⁶, R. Hulskens⁵⁸, R.F.H. Hunter³⁴, N. Huseynov^{80,ab}, J. Huston¹⁰⁷, J. Huth⁵⁹, R. Hyneman¹⁵³, S. Hyrych^{28a}, G. Iacobucci⁵⁴, G. Iakovidis²⁹, I. Ibragimov¹⁵¹, L. Iconomidou-Fayard⁶⁵, P. Iengo³⁶, R. Ignazzi⁴⁰, R. Iguchi¹⁶³, T. Iizawa⁵⁴, Y. Ikegami⁸², M. Ikeda⁸², N. Illic^{119,167,aa}, F. Iltzsche⁴⁸, H. Imam^{35a}, G. Introzzi^{71a,71b}, M. Iodice^{75a}, K. Iordanidou^{168a}, V. Ippolito^{73a,73b}, M.F. Isaacson¹⁷², M. Ishino¹⁶³, W. Islam¹²⁹, C. Issever^{19,46}, S. Istin¹⁶⁰, J.M. Iturbe Ponce^{63a}, R. Iuppa^{76a,76b}, A. Ivina¹⁸⁰, J.M. Izen⁴³, V. Izzo^{70a}, P. Jacka¹⁴⁰, P. Jackson¹, R.M. Jacobs⁴⁶, B.P. Jaeger¹⁵², V. Jain², G. Jäkel¹⁸², K.B. Jakobi¹⁰⁰, K. Jakobs⁵², T. Jakoubek¹⁸⁰, J. Jamieson⁵⁷, K.W. Janas^{84a}, R. Jansky⁵⁴, M. Janus⁵³, P.A. Janus^{84a}, G. Jarlskog⁹⁷, A.E. Jaspan⁹¹, N. Javadov^{80,ab}, T. Javůrek³⁶, M. Javurkova¹⁰³, F. Jeanneau¹⁴⁴, L. Jeanty¹³¹, J. Jejelava^{159a}, P. Jenni^{52,c}, N. Jeong⁴⁶, S. Jézéquel⁵, H. Ji¹⁸¹, J. Jia¹⁵⁵, Z. Jia^{15c}, H. Jiang⁷⁹, Y. Jiang^{60a}, Z. Jiang¹⁵³, S. Jiggins⁵², F.A. Jimenez Morales³⁸, J. Jimenez Pena¹¹⁵, S. Jin^{15c}, A. Jinaru^{27b}, O. Jinnouchi¹⁶⁵, H. Jivan^{33f}, P. Johansson¹⁴⁹, K.A. Johns⁷, C.A. Johnson⁶⁶, E. Jones¹⁷⁸, R.W.L. Jones⁹⁰, S.D. Jones¹⁵⁶, T.J. Jones⁹¹, J. Jongmanns^{61a}, J. Jovicevic³⁶, X. Ju¹⁸, J.J. Junggeburth¹¹⁵, A. Juste Rozas^{14,w}, A. Kaczmarcka⁸⁵, M. Kado^{73a,73b}, H. Kagan¹²⁷, M. Kagan¹⁵³, A. Kahn³⁹, C. Kahra¹⁰⁰, T. Kaji¹⁷⁹, E. Kajomovitz¹⁶⁰, C.W. Kalderon²⁹, A. Kaluza¹⁰⁰, A. Kamenshchikov¹²³, M. Kaneda¹⁶³, N.J. Kang¹⁴⁵, S. Kang⁷⁹, Y. Kano¹¹⁷, J. Kanzaki⁸², L.S. Kaplan¹⁸¹, D. Kar^{33f}, K. Karava¹³⁴, M.J. Kareem^{168b}, I. Karkanias¹⁶², S.N. Karpov⁸⁰, Z.M. Karpova⁸⁰, V. Kartvelishvili⁹⁰, A.N. Karyukhin¹²³, E. Kasimi¹⁶², A. Kastanas^{45a,45b}, C. Kato^{60d}, J. Katzy⁴⁶, K. Kawade¹⁵⁰, K. Kawagoe⁸⁸, T. Kawaguchi¹¹⁷, T. Kawamoto¹⁴⁴, G. Kawamura⁵³, E.F. Kay¹⁷⁶, S. Kazakos¹⁴, V.F. Kazanin^{122b,122a}, J.M. Keaveney^{33a}, R. Keeler¹⁷⁶, J.S. Keller³⁴, E. Kellermann⁹⁷, D. Kelsey¹⁵⁶, J.J. Kempster²¹, J. Kendrick²¹, K.E. Kennedy³⁹, O. Kepka¹⁴⁰, S. Kersten¹⁸², B.P. Kerševan⁹², S. Ketabchi Haghigat¹⁶⁷, M. Khader¹⁷³, F. Khalil-Zada¹³, M. Khandoga¹⁴⁴, A. Khanov¹²⁹, A.G. Kharlamov^{122b,122a}, T. Kharlamova^{122b,122a}, E.E. Khoda¹⁷⁵, A. Khodinov¹⁶⁶, T.J. Khoo⁷⁷, G. Khoriauli¹⁷⁷, E. Khramov⁸⁰, J. Khubua^{159b}, S. Kido⁸³, M. Kiehn³⁶, E. Kim¹⁶⁵, Y.K. Kim³⁷, N. Kimura⁹⁵, A. Kirchhoff⁵³, D. Kirchmeier⁴⁸, J. Kirk¹⁴³, A.E. Kiryunin¹¹⁵, T. Kishimoto¹⁶³, D.P. Kisliuk¹⁶⁷, V. Kitali⁴⁶, C. Kitsaki¹⁰, O. Kivernyk²⁴, T. Klapdor-Kleingrothaus⁵², M. Klassen^{61a}, C. Klein³⁴, M.H. Klein¹⁰⁶, M. Klein⁹¹, U. Klein⁹¹, K. Kleinknecht¹⁰⁰, P. Klimek³⁶, A. Klimentov²⁹, T. Klingl²⁴, T. Klioutchnikova³⁶, F.F. Klitzner¹¹⁴, P. Kluit¹²⁰, S. Kluth¹¹⁵, E. Kneringer⁷⁷, E.B.F.G. Knoops¹⁰², A. Knue⁵², D. Kobayashi⁸⁸, M. Kobel⁴⁸, M. Kocian¹⁵³, T. Kodama¹⁶³, P. Kodys¹⁴², D.M. Koeck¹⁵⁶, P.T. Koenig²⁴, T. Koffas³⁴, N.M. Köhler³⁶, M. Kolb¹⁴⁴, I. Koletsou⁵, T. Komarek¹³⁰, T. Kondo⁸², K. Köneke⁵², A.X.Y. Kong¹, A.C. König¹¹⁹, T. Kono¹²⁶, V. Konstantinides⁹⁵, N. Konstantinidis⁹⁵, B. Konya⁹⁷, R. Kopeliansky⁶⁶, S. Koperny^{84a}, K. Korcyl⁸⁵, K. Kordas¹⁶², G. Koren¹⁶¹, A. Korn⁹⁵, I. Korolkov¹⁴, E.V. Korolkova¹⁴⁹, N. Korotkova¹¹³, O. Kortner¹¹⁵, S. Kortner¹¹⁵, V.V. Kostyukhin^{149,166}, A. Kotsokechagia⁶⁵, A. Kotwal⁴⁹, A. Koulouris¹⁰, A. Kourkoumeli-Charalampidi^{71a,71b}, C. Kourkoumelis⁹, E. Kourlitis⁶, V. Kouskoura²⁹, R. Kowalewski¹⁷⁶, W. Kozanecki¹⁰¹, A.S. Kozhin¹²³, V.A. Kramarenko¹¹³, G. Kramberger⁹², D. Krasnopevtsev^{60a}, M.W. Krasny¹³⁵, A. Krasznahorkay³⁶, D. Krauss¹¹⁵, J.A. Kremer¹⁰⁰, J. Kretzschmar⁹¹, P. Krieger¹⁶⁷, F. Krieter¹¹⁴, A. Krishnan^{61b}, M. Krivos¹⁴², K. Krizka¹⁸, K. Kroeninger⁴⁷, H. Kroha¹¹⁵, J. Kroll¹⁴⁰, J. Kroll¹³⁶, K.S. Krowpman¹⁰⁷, U. Kruchonak⁸⁰, H. Krüger²⁴, N. Krumnack⁷⁹, M.C. Kruse⁴⁹, J.A. Krzysiak⁸⁵, A. Kubota¹⁶⁵, O. Kuchinskaia¹⁶⁶, S. Kuday^{4b}, D. Kuechler⁴⁶, J.T. Kuechler⁴⁶, S. Kuehn³⁶, T. Kuhl⁴⁶, V. Kukhtin⁸⁰, Y. Kulchitsky^{108,ae}, S. Kuleshov^{146b}, Y.P. Kulinich¹⁷³, M. Kuna⁵⁸, A. Kupco¹⁴⁰, T. Kupfer⁴⁷, O. Kuprash⁵², H. Kurashige⁸³, L.L. Kurchaninov^{168a}, Y.A. Kurochkin¹⁰⁸, A. Kurova¹¹², M.G. Kurth^{15a,15d}, E.S. Kuwertz³⁶, M. Kuze¹⁶⁵, A.K. Kvam¹⁴⁸, J. Kvita¹³⁰, T. Kwan¹⁰⁴, F. La Ruffa^{41b,41a}, C. Lacasta¹⁷⁴, F. Lacava^{73a,73b}, D.P.J. Lack¹⁰¹, H. Lacker¹⁹, D. Lacour¹³⁵, E. Ladygin⁸⁰, R. Lafaye⁵, B. Laforge¹³⁵, T. Lagouri^{146c}, S. Lai⁵³, I.K. Lakomiec^{84a}, J.E. Lambert¹²⁸, S. Lammers⁶⁶, W. Lampl⁷, C. Lampoudis¹⁶², E. Lançon²⁹, U. Landgraf⁵², M.P.J. Landon⁹³, V.S. Lang⁵², J.C. Lange⁵³, R.J. Langenberg¹⁰³, A.J. Lankford¹⁷¹, F. Lanni²⁹, K. Lantzsch²⁴, A. Lanza^{71a}, A. Lapertosa^{55b,55a}, J.F. Laporte¹⁴⁴, T. Lari^{69a}, F. Lasagni Manghi^{23b,23a}, M. Lassnig³⁶, V. Latonova¹⁴⁰, T.S. Lau^{63a}, A. Laudrain¹⁰⁰, A. Laurier³⁴, M. Lavorgna^{70a,70b}, S.D. Lawlor⁹⁴, M. Lazzaroni^{69a,69b}, B. Le¹⁰¹,

E. Le Guiriec¹⁰², A. Lebedev⁷⁹, M. LeBlanc⁷, T. LeCompte⁶, F. Ledroit-Guillon⁵⁸, A.C.A. Lee⁹⁵,
 C.A. Lee²⁹, G.R. Lee¹⁷, L. Lee⁵⁹, S.C. Lee¹⁵⁸, S. Lee⁷⁹, B. Lefebvre^{168a}, H.P. Lefebvre⁹⁴, M. Lefebvre¹⁷⁶,
 C. Leggett¹⁸, K. Lehmann¹⁵², N. Lehmann²⁰, G. Lehmann Miotto³⁶, W.A. Leight⁴⁶, A. Leisos^{162,u},
 M.A.L. Leite^{81c}, C.E. Leitgeb¹¹⁴, R. Leitner¹⁴², K.J.C. Leney⁴², T. Lenz²⁴, S. Leone^{72a},
 C. Leonidopoulos⁵⁰, A. Leopold¹³⁵, C. Leroy¹¹⁰, R. Les¹⁰⁷, C.G. Lester³², M. Levchenko¹³⁷, J. Levêque⁵,
 D. Levin¹⁰⁶, L.J. Levinson¹⁸⁰, D.J. Lewis²¹, B. Li^{15b}, B. Li¹⁰⁶, C-Q. Li^{60c,60d}, F. Li^{60c}, H. Li^{60a}, H. Li^{60b},
 J. Li^{60c}, K. Li¹⁴⁸, L. Li^{60c}, M. Li^{15a,15d}, Q. Li^{15a,15d}, Q.Y. Li^{60a}, S. Li^{60d,60c}, X. Li⁴⁶, Y. Li⁴⁶, Z. Li^{60b},
 Z. Li¹³⁴, Z. Li¹⁰⁴, Z. Li⁹¹, Z. Liang^{15a}, M. Liberatore⁴⁶, B. Liberti^{74a}, K. Lie^{63c}, S. Lim²⁹, C.Y. Lin³²,
 K. Lin¹⁰⁷, R.A. Linck⁶⁶, R.E. Lindley⁷, J.H. Lindon²¹, A. Linss⁴⁶, A.L. Lioni⁵⁴, E. Lipeles¹³⁶,
 A. Lipniacka¹⁷, T.M. Liss^{173,ak}, A. Lister¹⁷⁵, J.D. Little⁸, B. Liu⁷⁹, B.X. Liu¹⁵², H.B. Liu²⁹, J.B. Liu^{60a},
 J.K.K. Liu³⁷, K. Liu^{60d,60c}, M. Liu^{60a}, M.Y. Liu^{60a}, P. Liu^{15a}, X. Liu^{60a}, Y. Liu⁴⁶, Y. Liu^{15a,15d}, Y.L. Liu¹⁰⁶,
 Y.W. Liu^{60a}, M. Livan^{71a,71b}, A. Lleres⁵⁸, J. Llorente Merino¹⁵², S.L. Lloyd⁹³, C.Y. Lo^{63b},
 E.M. Lobodzinska⁴⁶, P. Loch⁷, S. Loffredo^{74a,74b}, T. Lohse¹⁹, K. Lohwasser¹⁴⁹, M. Lokajicek¹⁴⁰,
 J.D. Long¹⁷³, R.E. Long⁹⁰, I. Longarini^{73a,73b}, L. Longo³⁶, K.A.Looper¹²⁷, I. Lopez Paz¹⁰¹,
 A. Lopez Solis¹⁴⁹, J. Lorenz¹¹⁴, N. Lorenzo Martinez⁵, A.M. Lory¹¹⁴, P.J. Lösel¹¹⁴, A. Lösle⁵²,
 X. Lou^{45a,45b}, X. Lou^{15a}, A. Lounis⁶⁵, J. Love⁶, P.A. Love⁹⁰, J.J. Lozano Bahilo¹⁷⁴, M. Lu^{60a}, Y.J. Lu⁶⁴,
 H.J. Lubatti¹⁴⁸, C. Luci^{73a,73b}, F.L. Lucio Alves^{15c}, A. Lucotte⁵⁸, F. Luehring⁶⁶, I. Luise¹⁵⁵, L. Luminari^{73a},
 B. Lund-Jensen¹⁵⁴, N.A. Luongo¹³¹, M.S. Lutz¹⁶¹, D. Lynn²⁹, H. Lyons⁹¹, R. Lysak¹⁴⁰, E. Lytken⁹⁷,
 F. Lyu^{15a}, V. Lyubushkin⁸⁰, T. Lyubushkina⁸⁰, H. Ma²⁹, L.L. Ma^{60b}, Y. Ma⁹⁵, D.M. Mac Donell¹⁷⁶,
 G. Maccarrone⁵¹, A. Macchioli¹¹⁵, C.M. Macdonald¹⁴⁹, J.C. MacDonald¹⁴⁹, J. Machado Miguens¹³⁶,
 D. Madaffari¹⁷⁴, R. Madar³⁸, W.F. Mader⁴⁸, M. Madugoda Ralalage Don¹²⁹, N. Madysa⁴⁸, J. Maeda⁸³,
 T. Maeno²⁹, M. Maerker⁴⁸, V. Magerl⁵², N. Magini⁷⁹, J. Magro^{67a,67c,q}, D.J. Mahon³⁹, C. Maidantchik^{81b},
 T. Maier¹¹⁴, A. Maio^{139a,139b,139d}, K. Maj^{84a}, O. Majersky^{28a}, S. Majewski¹³¹, Y. Makida⁸², N. Makovec⁶⁵,
 B. Malaescu¹³⁵, Pa. Malecki⁸⁵, V.P. Maleev¹³⁷, F. Malek⁵⁸, D. Malito^{41b,41a}, U. Mallik⁷⁸, C. Malone³²,
 S. Maltezos¹⁰, S. Malyukov⁸⁰, J. Mamuzic¹⁷⁴, G. Mancini⁵¹, J.P. Mandalia⁹³, I. Mandić⁹²,
 L. Manhaes de Andrade Filho^{81a}, I.M. Maniatis¹⁶², J. Manjarres Ramos⁴⁸, K.H. Mankinen⁹⁷, A. Mann¹¹⁴,
 A. Manousos⁷⁷, B. Mansoulie¹⁴⁴, I. Manthos¹⁶², S. Manzoni¹²⁰, A. Marantis^{162,u}, G. Marceca³⁰,
 L. Marchese¹³⁴, G. Marchiori¹³⁵, M. Marcisovsky¹⁴⁰, L. Marcoccia^{74a,74b}, C. Marcon⁹⁷, M. Marjanovic¹²⁸,
 Z. Marshall¹⁸, M.U.F. Martensson¹⁷², S. Marti-Garcia¹⁷⁴, C.B. Martin¹²⁷, T.A. Martin¹⁷⁸, V.J. Martin⁵⁰,
 B. Martin dit Latour¹⁷, L. Martinelli^{75a,75b}, M. Martinez^{14,w}, P. Martinez Agullo¹⁷⁴,
 V.I. Martinez Outshoorn¹⁰³, S. Martin-Haugh¹⁴³, V.S. Martoiu^{27b}, A.C. Martyniuk⁹⁵, A. Marzin³⁶,
 S.R. Maschek¹¹⁵, L. Masetti¹⁰⁰, T. Mashimo¹⁶³, R. Mashinistov¹¹¹, J. Masik¹⁰¹, A.L. Maslennikov^{122b,122a},
 L. Massa^{23b,23a}, P. Massarotti^{70a,70b}, P. Mastrandrea^{72a,72b}, A. Mastroberardino^{41b,41a}, T. Masubuchi¹⁶³,
 D. Matakias²⁹, A. Matic¹¹⁴, N. Matsuzawa¹⁶³, P. Mättig²⁴, J. Maurer^{27b}, B. Maček⁹²,
 D.A. Maximov^{122b,122a}, R. Mazini¹⁵⁸, I. Maznas¹⁶², S.M. Mazza¹⁴⁵, J.P. Mc Gowan¹⁰⁴, S.P. Mc Kee¹⁰⁶,
 T.G. McCarthy¹¹⁵, W.P. McCormack¹⁸, E.F. McDonald¹⁰⁵, A.E. McDougall¹²⁰, J.A. McFayden¹⁸,
 G. Mchedlidze^{159b}, M.A. McKay⁴², K.D. McLean¹⁷⁶, S.J. McMahon¹⁴³, P.C. McNamara¹⁰⁵,
 C.J. McNicol¹⁷⁸, R.A. McPherson^{176,aa}, J.E. Mdhluli^{33f}, Z.A. Meadows¹⁰³, S. Meehan³⁶, T. Megy³⁸,
 S. Mehlhase¹¹⁴, A. Mehta⁹¹, B. Meirose⁴³, D. Melini¹⁶⁰, B.R. Mellado Garcia^{33f}, J.D. Mellenthin⁵³,
 M. Melo^{28a}, F. Meloni⁴⁶, A. Melzer²⁴, E.D. Mendes Gouveia^{139a,139e}, A.M. Mendes Jacques Da Costa²¹,
 L. Meng³⁶, X.T. Meng¹⁰⁶, S. Menke¹¹⁵, E. Meoni^{41b,41a}, S. Mergelmeyer¹⁹, S.A.M. Merkt¹³⁸,
 C. Merlassino¹³⁴, P. Mermod^{54,*}, L. Merola^{70a,70b}, C. Meroni^{69a}, G. Merz¹⁰⁶, O. Meshkov^{113,111},
 J.K.R. Meshreki¹⁵¹, J. Metcalfé⁶, A.S. Mete⁶, C. Meyer⁶⁶, J.-P. Meyer¹⁴⁴, M. Michetti¹⁹, R.P. Middleton¹⁴³,
 L. Mijović⁵⁰, G. Mikenberg¹⁸⁰, M. Mikestikova¹⁴⁰, M. Mikuž⁹², H. Mildner¹⁴⁹, A. Milic¹⁶⁷, C.D. Milke⁴²,
 D.W. Miller³⁷, L.S. Miller³⁴, A. Milov¹⁸⁰, D.A. Milstead^{45a,45b}, R.A. Mina¹⁵³, A.A. Minaenko¹²³,
 I.A. Minashvili^{159b}, L. Mince⁵⁷, A.I. Mincer¹²⁵, B. Mindur^{84a}, M. Mineev⁸⁰, Y. Minegishi¹⁶³, Y. Mino⁸⁶,
 L.M. Mir¹⁴, M. Mironova¹³⁴, K.P. Mistry¹³⁶, T. Mitani¹⁷⁹, J. Mitrevski¹¹⁴, V.A. Mitsou¹⁷⁴, M. Mittal^{60c},

O. Miu¹⁶⁷, A. Miucci²⁰, P.S. Miyagawa⁹³, A. Mizukami⁸², J.U. Mjörnmark⁹⁷, T. Mkrtchyan^{61a},
 M. Mlynarikova¹²¹, T. Moa^{45a,45b}, S. Mobius⁵³, K. Mochizuki¹¹⁰, P. Moder⁴⁶, P. Mogg¹¹⁴, S. Mohapatra³⁹,
 R. Moles-Valls²⁴, K. Mönig⁴⁶, E. Monnier¹⁰², A. Montalbano¹⁵², J. Montejo Berlingen³⁶, M. Montella⁹⁵,
 F. Monticelli⁸⁹, S. Monzani^{69a}, N. Morange⁶⁵, A.L. Moreira De Carvalho^{139a}, D. Moreno^{22a},
 M. Moreno Llácer¹⁷⁴, C. Moreno Martinez¹⁴, P. Morettini^{55b}, M. Morgenstern¹⁶⁰, S. Morgenstern⁴⁸,
 D. Mori¹⁵², M. Mori⁵⁹, M. Morinaga¹⁷⁹, V. Morisbak¹³³, A.K. Morley³⁶, G. Mornacchi³⁶, A.P. Morris⁹⁵,
 L. Morvaj¹⁵⁵, P. Moschovakos³⁶, B. Moser¹²⁰, M. Mosidze^{159b}, T. Moskalets¹⁴⁴, P. Moskvitina¹¹⁹,
 J. Moss^{31,m}, E.J.W. Moyse¹⁰³, S. Muanza¹⁰², J. Mueller¹³⁸, R.S.P. Mueller¹¹⁴, D. Muenstermann⁹⁰,
 G.A. Mullier⁹⁷, D.P. Mungo^{69a,69b}, J.L. Munoz Martinez¹⁴, F.J. Munoz Sanchez¹⁰¹, P. Murin^{28b},
 W.J. Murray^{178,143}, A. Murrone^{69a,69b}, J.M. Muse¹²⁸, M. Muškinja¹⁸, C. Mwewa^{33a}, A.G. Myagkov^{123,ag},
 A.A. Myers¹³⁸, G. Myers⁶⁶, J. Myers¹³¹, M. Myska¹⁴¹, B.P. Nachman¹⁸, O. Nackenhorst⁴⁷, A.Nag Nag⁴⁸,
 K. Nagai¹³⁴, K. Nagano⁸², Y. Nagasaka⁶², J.L. Nagle²⁹, E. Nagy¹⁰², A.M. Nairz³⁶, Y. Nakahama¹¹⁷,
 K. Nakamura⁸², T. Nakamura¹⁶³, H. Nanjo¹³², F. Napolitano^{61a}, R.F. Naranjo Garcia⁴⁶, R. Narayan⁴²,
 I. Naryshkin¹³⁷, M. Naseri³⁴, T. Naumann⁴⁶, G. Navarro^{22a}, P.Y. Nechaeva¹¹¹, F. Nechansky⁴⁶,
 T.J. Neep²¹, A. Negri^{71a,71b}, M. Negrini^{23b}, C. Nellist¹¹⁹, C. Nelson¹⁰⁴, M.E. Nelson^{45a,45b}, S. Nemecek¹⁴⁰,
 M. Nessi^{36,e}, M.S. Neubauer¹⁷³, F. Neuhaus¹⁰⁰, M. Neumann¹⁸², R. Newhouse¹⁷⁵, P.R. Newman²¹,
 C.W. Ng¹³⁸, Y.S. Ng¹⁹, Y.W.Y. Ng¹⁷¹, B. Ngair^{35e}, H.D.N. Nguyen¹⁰², T. Nguyen Manh¹¹⁰, E. Nibigira³⁸,
 R.B. Nickerson¹³⁴, R. Nicolaïdou¹⁴⁴, D.S. Nielsen⁴⁰, J. Nielsen¹⁴⁵, M. Niemeyer⁵³, N. Nikiforou¹¹,
 V. Nikolaenko^{123,ag}, I. Nikolic-Audit¹³⁵, K. Nikolopoulos²¹, P. Nilsson²⁹, H.R. Nindhito⁵⁴, A. Nisati^{73a},
 N. Nishu^{60c}, R. Nisius¹¹⁵, I. Nitsche⁴⁷, T. Nitta¹⁷⁹, T. Nobe¹⁶³, D.L. Noel³², Y. Noguchi⁸⁶, I. Nomidis¹³⁵,
 M.A. Nomura²⁹, M. Nordberg³⁶, J. Novak⁹², T. Novak⁹², O. Novgorodova⁴⁸, R. Novotny¹⁴¹, L. Nozka¹³⁰,
 K. Ntekas¹⁷¹, E. Nurse⁹⁵, F.G. Oakham^{34,al}, H. Oberlack¹¹⁵, J. Ocariz¹³⁵, A. Ochi⁸³, I. Ochoa³⁹,
 J.P. Ochoa-Ricoux^{146a}, K. O'Connor²⁶, S. Oda⁸⁸, S. Odaka⁸², S. Oerdekk⁵³, A. Ogrodnik^{84a}, A. Oh¹⁰¹,
 C.C. Ohm¹⁵⁴, H. Oide¹⁶⁵, M.L. Ojeda¹⁶⁷, H. Okawa¹⁶⁹, Y. Okazaki⁸⁶, M.W. O'Keefe⁹¹, Y. Okumura¹⁶³,
 A. Olariu^{27b}, L.F. Oleiro Seabra^{139a}, S.A. Olivares Pino^{146a}, D. Oliveira Damazio²⁹, J.L. Oliver¹,
 M.J.R. Olsson¹⁷¹, A. Olszewski⁸⁵, J. Olszowska⁸⁵, Ö.O. Öncel²⁴, D.C. O'Neil¹⁵², A.P. O'neill¹³⁴,
 A. Onofre^{139a,139e}, P.U.E. Onyisi¹¹, H. Oppen¹³³, R.G. Oreamuno Madriz¹²¹, M.J. Oreglia³⁷,
 G.E. Orellana⁸⁹, D. Orestano^{75a,75b}, N. Orlando¹⁴, R.S. Orr¹⁶⁷, V. O'Shea⁵⁷, R. Ospanov^{60a},
 G. Otero y Garzon³⁰, H. Otono⁸⁸, P.S. Ott^{61a}, G.J. Ottino¹⁸, M. Ouchrif^{35d}, J. Ouellette²⁹,
 F. Ould-Saada¹³³, A. Ouraou^{144,*}, Q. Ouyang^{15a}, M. Owen⁵⁷, R.E. Owen¹⁴³, V.E. Ozcan^{12c}, N. Ozturk⁸,
 J. Pacalt¹³⁰, H.A. Pacey³², K. Pachal⁴⁹, A. Pacheco Pages¹⁴, C. Padilla Aranda¹⁴, S. Pagan Griso¹⁸,
 G. Palacino⁶⁶, S. Palazzo⁵⁰, S. Palestini³⁶, M. Palka^{84b}, P. Palni^{84a}, C.E. Pandini⁵⁴,
 J.G. Panduro Vazquez⁹⁴, P. Pani⁴⁶, G. Panizzo^{67a,67c}, L. Paolozzi⁵⁴, C. Papadatos¹¹⁰, K. Papageorgiou^{9,g},
 S. Parajuli⁴², A. Paramonov⁶, C. Paraskevopoulos¹⁰, D. Paredes Hernandez^{63b}, S.R. Paredes Saenz¹³⁴,
 B. Parida¹⁸⁰, T.H. Park¹⁶⁷, A.J. Parker³¹, M.A. Parker³², F. Parodi^{55b,55a}, E.W. Parrish¹²¹, J.A. Parsons³⁹,
 U. Parzefall⁵², L. Pascual Dominguez¹³⁵, V.R. Pascuzzi¹⁸, J.M.P. Pasner¹⁴⁵, F. Pasquali¹²⁰,
 E. Pasqualucci^{73a}, S. Passaggio^{55b}, F. Pastore⁹⁴, P. Pasuwan^{45a,45b}, S. Pataraia¹⁰⁰, J.R. Pater¹⁰¹,
 A. Pathak^{181,i}, J. Patton⁹¹, T. Pauly³⁶, J. Pearkes¹⁵³, B. Pearson¹¹⁵, M. Pedersen¹³³, L. Pedraza Diaz¹¹⁹,
 R. Pedro^{139a}, T. Peiffer⁵³, S.V. Peleganchuk^{122b,122a}, O. Penc¹⁴⁰, C. Peng^{63b}, H. Peng^{60a}, B.S. Peralva^{81a},
 M.M. Pereo⁶⁵, A.P. Pereira Peixoto^{139a}, L. Pereira Sanchez^{45a,45b}, D.V. Perepelitsa²⁹, E. Perez Codina^{168a},
 F. Peri¹⁹, L. Perini^{69a,69b}, H. Pernegger³⁶, S. Perrella³⁶, A. Perrevoort¹²⁰, K. Peters⁴⁶, R.F.Y. Peters¹⁰¹,
 B.A. Petersen³⁶, T.C. Petersen⁴⁰, E. Petit¹⁰², V. Petousis¹⁴¹, C. Petridou¹⁶², F. Petrucci^{75a,75b}, M. Pettee¹⁸³,
 N.E. Pettersson¹⁰³, K. Petukhova¹⁴², A. Peyaud¹⁴⁴, R. Pezoa^{146d}, L. Pezzotti^{71a,71b}, T. Pham¹⁰⁵,
 P.W. Phillips¹⁴³, M.W. Phipps¹⁷³, G. Piacquadio¹⁵⁵, E. Pianori¹⁸, A. Picazio¹⁰³, R.H. Pickles¹⁰¹,
 R. Piegaia³⁰, D. Pietreanu^{27b}, J.E. Pilcher³⁷, A.D. Pilkington¹⁰¹, M. Pinamonti^{67a,67c}, J.L. Pinfold³,
 C. Pitman Donaldson⁹⁵, M. Pitt¹⁶¹, L. Pizzimento^{74a,74b}, A. Pizzini¹²⁰, M.-A. Pleier²⁹, V. Plesanovs⁵²,
 V. Pleskot¹⁴², E. Plotnikova⁸⁰, P. Podberezko^{122b,122a}, R. Poettgen⁹⁷, R. Poggi⁵⁴, L. Poggioli¹³⁵,

I. Pogrebnyak¹⁰⁷, D. Pohl²⁴, I. Pokharel⁵³, G. Polesello^{71a}, A. Poley^{152,168a}, A. Policicchio^{73a,73b},
 R. Polifka¹⁴², A. Polini^{23b}, C.S. Pollard⁴⁶, V. Polychronakos²⁹, D. Ponomarenko¹¹², L. Pontecorvo³⁶,
 S. Popa^{27a}, G.A. Popeneciu^{27d}, L. Portales⁵, D.M. Portillo Quintero⁵⁸, S. Pospisil¹⁴¹, K. Potamianos⁴⁶,
 I.N. Potrap⁸⁰, C.J. Potter³², H. Potti¹¹, T. Poulsen⁹⁷, J. Poveda¹⁷⁴, T.D. Powell¹⁴⁹, G. Pownall⁴⁶,
 M.E. Pozo Astigarraga³⁶, A. Prades Ibanez¹⁷⁴, P. Pralavorio¹⁰², M.M. Prapa⁴⁴, S. Prell⁷⁹, D. Price¹⁰¹,
 M. Primavera^{68a}, M.L. Proffitt¹⁴⁸, N. Proklova¹¹², K. Prokofiev^{63c}, F. Prokoshin⁸⁰, S. Protopopescu²⁹,
 J. Proudfoot⁶, M. Przybycien^{84a}, D. Pudzha¹³⁷, A. Puri¹⁷³, P. Puzo⁶⁵, D. Pyatiizbyantseva¹¹², J. Qian¹⁰⁶,
 Y. Qin¹⁰¹, A. Quadt⁵³, M. Queitsch-Maitland³⁶, M. Racko^{28a}, F. Ragusa^{69a,69b}, G. Rahal⁹⁸, J.A. Raine⁵⁴,
 S. Rajagopalan²⁹, A. Ramirez Morales⁹³, K. Ran^{15a,15d}, D.M. Rauch⁴⁶, F. Rauscher¹¹⁴, S. Rave¹⁰⁰,
 B. Ravina⁵⁷, I. Ravinovich¹⁸⁰, J.H. Rawling¹⁰¹, M. Raymond³⁶, A.L. Read¹³³, N.P. Readioff¹⁴⁹,
 M. Reale^{68a,68b}, D.M. Rebuzzi^{71a,71b}, G. Redlinger²⁹, K. Reeves⁴³, D. Reikher¹⁶¹, A. Reiss¹⁰⁰, A. Rej¹⁵¹,
 C. Rembser³⁶, A. Renardi⁴⁶, M. Renda^{27b}, M.B. Rendel¹¹⁵, A.G. Rennie⁵⁷, S. Resconi^{69a},
 E.D. Ressegue¹⁸, S. Rettie⁹⁵, B. Reynolds¹²⁷, E. Reynolds²¹, O.L. Rezanova^{122b,122a}, P. Reznicek¹⁴²,
 E. Ricci^{76a,76b}, R. Richter¹¹⁵, S. Richter⁴⁶, E. Richter-Was^{84b}, M. Ridel¹³⁵, P. Rieck¹¹⁵, O. Rifki⁴⁶,
 M. Rijssenbeek¹⁵⁵, A. Rimoldi^{71a,71b}, M. Rimoldi⁴⁶, L. Rinaldi^{23b}, T.T. Rinn¹⁷³, G. Ripellino¹⁵⁴, I. Riu¹⁴,
 P. Rivadeneira⁴⁶, J.C. Rivera Vergara¹⁷⁶, F. Rizatdinova¹²⁹, E. Rizvi⁹³, C. Rizzi³⁶, S.H. Robertson^{104,aa},
 M. Robin⁴⁶, D. Robinson³², C.M. Robles Gajardo^{146d}, M. Robles Manzano¹⁰⁰, A. Robson⁵⁷,
 A. Rocchi^{74a,74b}, C. Roda^{72a,72b}, S. Rodriguez Bosca¹⁷⁴, A. Rodriguez Rodriguez⁵²,
 A.M. Rodríguez Vera^{168b}, S. Roe³⁶, J. Roggel¹⁸², O. Røhne¹³³, R. Röhrlig¹¹⁵, R.A. Rojas^{146d}, B. Roland⁵²,
 C.P.A. Roland⁶⁶, J. Roloff²⁹, A. Romaniouk¹¹², M. Romano^{23b,23a}, N. Rompotis⁹¹, M. Ronzani¹²⁵,
 L. Roos¹³⁵, S. Rosati^{73a}, G. Rosin¹⁰³, B.J. Rosser¹³⁶, E. Rossi⁴⁶, E. Rossi^{75a,75b}, E. Rossi^{70a,70b},
 L.P. Rossi^{55b}, L. Rossini⁴⁶, R. Rosten¹⁴, M. Rotaru^{27b}, B. Rottler⁵², D. Rousseau⁶⁵, G. Rovelli^{71a,71b},
 A. Roy¹¹, D. Roy^{33f}, A. Rozanov¹⁰², Y. Rozen¹⁶⁰, X. Ruan^{33f}, T.A. Ruggeri¹, F. Rühr⁵²,
 A. Ruiz-Martinez¹⁷⁴, A. Rummller³⁶, Z. Rurikova⁵², N.A. Rusakovich⁸⁰, H.L. Russell¹⁰⁴, L. Rustige^{38,47},
 J.P. Rutherford⁷, E.M. Rüttinger¹⁴⁹, M. Rybar¹⁴², G. Rybkin⁶⁵, E.B. Rye¹³³, A. Ryzhov¹²³,
 J.A. Sabater Iglesias⁴⁶, P. Sabatini¹⁷⁴, L. Sabetta^{73a,73b}, S. Sacerdoti⁶⁵, H.F-W. Sadrozinski¹⁴⁵,
 R. Sadykov⁸⁰, F. Safai Tehrani^{73a}, B. Safarzadeh Samani¹⁵⁶, M. Safdari¹⁵³, P. Saha¹²¹, S. Saha¹⁰⁴,
 M. Sahinsoy¹¹⁵, A. Sahu¹⁸², M. Saimpert³⁶, M. Saito¹⁶³, T. Saito¹⁶³, H. Sakamoto¹⁶³, D. Salamani⁵⁴,
 G. Salamanna^{75a,75b}, A. Salnikov¹⁵³, J. Salt¹⁷⁴, A. Salvador Salas¹⁴, D. Salvatore^{41b,41a}, F. Salvatore¹⁵⁶,
 A. Salvucci^{63a}, A. Salzburger³⁶, J. Samarati³⁶, D. Sammel⁵², D. Sampsonidis¹⁶², D. Sampsonidou¹⁶²,
 J. Sánchez¹⁷⁴, A. Sanchez Pineda^{67a,36,67c}, H. Sandaker¹³³, C.O. Sander⁴⁶, I.G. Sanderswood⁹⁰,
 M. Sandhoff¹⁸², C. Sandoval^{22b}, D.P.C. Sankey¹⁴³, M. Sannino^{55b,55a}, Y. Sano¹¹⁷, A. Sansoni⁵¹,
 C. Santoni³⁸, H. Santos^{139a,139b}, S.N. Santpur¹⁸, A. Santra¹⁷⁴, K.A. Saoucha¹⁴⁹, A. Sapronov⁸⁰,
 J.G. Saraiva^{139a,139d}, O. Sasaki⁸², K. Sato¹⁶⁹, F. Sauerburger⁵², E. Sauvan⁵, P. Savard^{167,al}, R. Sawada¹⁶³,
 C. Sawyer¹⁴³, L. Sawyer^{96,af}, I. Sayago Galvan¹⁷⁴, C. Sbarra^{23b}, A. Sbrizzi^{67a,67c}, T. Scanlon⁹⁵,
 J. Schaarschmidt¹⁴⁸, P. Schacht¹¹⁵, D. Schaefer³⁷, L. Schaefer¹³⁶, U. Schäfer¹⁰⁰, A.C. Schaffer⁶⁵,
 D. Schaile¹¹⁴, R.D. Schamberger¹⁵⁵, E. Schanet¹¹⁴, C. Scharf¹⁹, N. Scharmburg¹⁰¹, V.A. Schegelsky¹³⁷,
 D. Scheirich¹⁴², F. Schenck¹⁹, M. Schernau¹⁷¹, C. Schiavi^{55b,55a}, L.K. Schildgen²⁴, Z.M. Schillaci²⁶,
 E.J. Schioppa^{68a,68b}, M. Schioppa^{41b,41a}, K.E. Schleicher⁵², S. Schlenker³⁶, K.R. Schmidt-Sommerfeld¹¹⁵,
 K. Schmieden¹⁰⁰, C. Schmitt¹⁰⁰, S. Schmitt⁴⁶, L. Schoeffel¹⁴⁴, A. Schoening^{61b}, P.G. Scholer⁵²,
 E. Schopf¹³⁴, M. Schott¹⁰⁰, J.F.P. Schouwenberg¹¹⁹, J. Schovancova³⁶, S. Schramm⁵⁴, F. Schroeder¹⁸²,
 A. Schulte¹⁰⁰, H-C. Schultz-Coulon^{61a}, M. Schumacher⁵², B.A. Schumm¹⁴⁵, Ph. Schune¹⁴⁴,
 A. Schwartzman¹⁵³, T.A. Schwarz¹⁰⁶, Ph. Schwemling¹⁴⁴, R. Schwienhorst¹⁰⁷, A. Sciandra¹⁴⁵,
 G. Sciolla²⁶, M. Scornajenghi^{41b,41a}, F. Scuri^{72a}, F. Scutti¹⁰⁵, L.M. Scyboz¹¹⁵, C.D. Sebastiani⁹¹,
 K. Sedlaczek⁴⁷, P. Seema¹⁹, S.C. Seidel¹¹⁸, A. Seiden¹⁴⁵, B.D. Seidlitz²⁹, T. Seiss³⁷, C. Seitz⁴⁶,
 J.M. Seixas^{81b}, G. Sekhniaidze^{70a}, S.J. Sekula⁴², N. Semprini-Cesari^{23b,23a}, S. Sen⁴⁹, C. Serfon²⁹,
 L. Serin⁶⁵, L. Serkin^{67a,67b}, M. Sessa^{60a}, H. Severini¹²⁸, S. Sevova¹⁵³, F. Sforza^{55b,55a}, A. Sfyrla⁵⁴,

E. Shabalina⁵³, J.D. Shahinian¹³⁶, N.W. Shaikh^{45a,45b}, D. Shaked Renous¹⁸⁰, L.Y. Shan^{15a}, M. Shapiro¹⁸, A. Sharma³⁶, A.S. Sharma¹, P.B. Shatalov¹²⁴, K. Shaw¹⁵⁶, S.M. Shaw¹⁰¹, M. Shehade¹⁸⁰, Y. Shen¹²⁸, A.D. Sherman²⁵, P. Sherwood⁹⁵, L. Shi⁹⁵, C.O. Shimmin¹⁸³, Y. Shimogama¹⁷⁹, M. Shimojima¹¹⁶, J.D. Shinner⁹⁴, I.P.J. Shipsey¹³⁴, S. Shirabe¹⁶⁵, M. Shiyakova^{80,y}, J. Shlomi¹⁸⁰, A. Shmeleva¹¹¹, M.J. Shochet³⁷, J. Shojaei¹⁰⁵, D.R. Shope¹⁵⁴, S. Shrestha¹²⁷, E.M. Shrif^{33f}, M.J. Shroff¹⁷⁶, E. Shulga¹⁸⁰, P. Sicho¹⁴⁰, A.M. Sickles¹⁷³, E. Sideras Haddad^{33f}, O. Sidiropoulou³⁶, A. Sidoti^{23b,23a}, F. Siegert⁴⁸, Dj. Sijacki¹⁶, M.Jr. Silva¹⁸¹, M.V. Silva Oliveira³⁶, S.B. Silverstein^{45a}, S. Simion⁶⁵, R. Simonello¹⁰⁰, C.J. Simpson-allsop²¹, S. Simsek^{12b}, P. Sinervo¹⁶⁷, V. Sinetckii¹¹³, S. Singh¹⁵², M. Sioli^{23b,23a}, I. Siral¹³¹, S.Yu. Sivoklokov¹¹³, J. Sjölin^{45a,45b}, A. Skaf⁵³, E. Skorda⁹⁷, P. Skubic¹²⁸, M. Slawinska⁸⁵, K. Sliwa¹⁷⁰, R. Slovak¹⁴², V. Smakhtin¹⁸⁰, B.H. Smart¹⁴³, J. Smiesko^{28b}, N. Smirnov¹¹², S.Yu. Smirnov¹¹², Y. Smirnov¹¹², L.N. Smirnova^{113,r}, O. Smirnova⁹⁷, E.A. Smith³⁷, H.A. Smith¹³⁴, M. Smizanska⁹⁰, K. Smolek¹⁴¹, A. Smykiewicz⁸⁵, A.A. Snesarev¹¹¹, H.L. Snoek¹²⁰, I.M. Snyder¹³¹, S. Snyder²⁹, R. Sobie^{176,aa}, A. Soffer¹⁶¹, A. Søgaard⁵⁰, F. Sohns⁵³, C.A. Solans Sanchez³⁶, E.Yu. Soldatov¹¹², U. Soldevila¹⁷⁴, A.A. Solodkov¹²³, A. Soloshenko⁸⁰, O.V. Solovyanov¹²³, V. Solovyev¹³⁷, P. Sommer¹⁴⁹, H. Son¹⁷⁰, A. Sonay¹⁴, W. Song¹⁴³, W.Y. Song^{168b}, A. Sopczak¹⁴¹, A.L. Sopio⁹⁵, F. Sopkova^{28b}, S. Sottocornola^{71a,71b}, R. Soualah^{67a,67c}, A.M. Soukharev^{122b,122a}, D. South⁴⁶, S. Spagnolo^{68a,68b}, M. Spalla¹¹⁵, M. Spangenberg¹⁷⁸, F. Spanò⁹⁴, D. Sperlich⁵², T.M. Spieker^{61a}, G. Spigo³⁶, M. Spina¹⁵⁶, D.P. Spiteri⁵⁷, M. Spousta¹⁴², A. Stabile^{69a,69b}, B.L. Stamas¹²¹, R. Stamen^{61a}, M. Stamenkovic¹²⁰, A. Stampekis²¹, E. Stanecka⁸⁵, B. Stanislaus¹³⁴, M.M. Stanitzki⁴⁶, M. Stankaityte¹³⁴, B. Stapf¹²⁰, E.A. Starchenko¹²³, G.H. Stark¹⁴⁵, J. Stark⁵⁸, P. Staroba¹⁴⁰, P. Starovoitov^{61a}, S. Stärz¹⁰⁴, R. Staszewski⁸⁵, G. Stavropoulos⁴⁴, M. Stegler⁴⁶, P. Steinberg²⁹, A.L. Steinhebel¹³¹, B. Stelzer^{152,168a}, H.J. Stelzer¹³⁸, O. Stelzer-Chilton^{168a}, H. Stenzel⁵⁶, T.J. Stevenson¹⁵⁶, G.A. Stewart³⁶, M.C. Stockton³⁶, G. Stoicea^{27b}, M. Stolarski^{139a}, S. Stonjek¹¹⁵, A. Straessner⁴⁸, J. Strandberg¹⁵⁴, S. Strandberg^{45a,45b}, M. Strauss¹²⁸, T. Strebler¹⁰², P. Strizenec^{28b}, R. Ströhmer¹⁷⁷, D.M. Strom¹³¹, R. Stroynowski⁴², A. Strubig^{45a,45b}, S.A. Stucci²⁹, B. Stugu¹⁷, J. Stupak¹²⁸, N.A. Styles⁴⁶, D. Su¹⁵³, W. Su^{60c,148}, X. Su^{60a}, V.V. Sulin¹¹¹, M.J. Sullivan⁹¹, D.M.S. Sultan⁵⁴, S. Sultansoy^{4c}, T. Sumida⁸⁶, S. Sun¹⁰⁶, X. Sun¹⁰¹, C.J.E. Suster¹⁵⁷, M.R. Sutton¹⁵⁶, S. Suzuki⁸², M. Svatos¹⁴⁰, M. Swiatlowski^{168a}, S.P. Swift², T. Swirski¹⁷⁷, A. Sydorenko¹⁰⁰, I. Sykora^{28a}, M. Sykora¹⁴², T. Sykora¹⁴², D. Ta¹⁰⁰, K. Tackmann^{46,x}, J. Taenzer¹⁶¹, A. Taffard¹⁷¹, R. Tafirout^{168a}, E. Tagiev¹²³, R.H.M. Taibah¹³⁵, R. Takashima⁸⁷, K. Takeda⁸³, T. Takeshita¹⁵⁰, E.P. Takeva⁵⁰, Y. Takubo⁸², M. Talby¹⁰², A.A. Talyshев^{122b,122a}, K.C. Tam^{63b}, N.M. Tamir¹⁶¹, J. Tanaka¹⁶³, R. Tanaka⁶⁵, S. Tapia Araya¹⁷³, S. Tapprogge¹⁰⁰, A. Tarek Abouelfadl Mohamed¹⁰⁷, S. Tarem¹⁶⁰, K. Tariq^{60b}, G. Tarna^{27b,d}, G.F. Tartarelli^{69a}, P. Tas¹⁴², M. Tasevsky¹⁴⁰, E. Tassi^{41b,41a}, A. Tavares Delgado^{139a}, Y. Tayalati^{35e}, A.J. Taylor⁵⁰, G.N. Taylor¹⁰⁵, W. Taylor^{168b}, H. Teagle⁹¹, A.S. Tee⁹⁰, R. Teixeira De Lima¹⁵³, P. Teixeira-Dias⁹⁴, H. Ten Kate³⁶, J.J. Teoh¹²⁰, K. Terashi¹⁶³, J. Terron⁹⁹, S. Terzo¹⁴, M. Testa⁵¹, R.J. Teuscher^{167,aa}, S.J. Thais¹⁸³, N. Themistokleous⁵⁰, T. Theveneaux-Pelzer⁴⁶, F. Thiele⁴⁰, D.W. Thomas⁹⁴, J.O. Thomas⁴², J.P. Thomas²¹, E.A. Thompson⁴⁶, P.D. Thompson²¹, E. Thomson¹³⁶, E.J. Thorpe⁹³, R.E. Tiese Torres⁵³, V.O. Tikhomirov^{111,ah}, Yu.A. Tikhonov^{122b,122a}, S. Timoshenko¹¹², P. Tipton¹⁸³, S. Tisserant¹⁰², K. Todome^{23b,23a}, S. Todorova-Nova¹⁴², S. Todt⁴⁸, J. Tojo⁸⁸, S. Tokár^{28a}, K. Tokushuku⁸², E. Tolley¹²⁷, R. Tombs³², K.G. Tomiwa^{33f}, M. Tomoto^{82,117}, L. Tompkins¹⁵³, P. Tornambe¹⁰³, E. Torrence¹³¹, H. Torres⁴⁸, E. Torró Pastor¹⁷⁴, M. Toscani³⁰, C. Tosciri¹³⁴, J. Toth^{102,z}, D.R. Tovey¹⁴⁹, A. Traeet¹⁷, C.J. Treado¹²⁵, T. Trefzger¹⁷⁷, F. Tresoldi¹⁵⁶, A. Tricoli²⁹, I.M. Trigger^{168a}, S. Trincaz-Duvold¹³⁵, D.A. Trischuk¹⁷⁵, W. Trischuk¹⁶⁷, B. Trocmé⁵⁸, A. Trofymov⁶⁵, C. Troncon^{69a}, F. Trovato¹⁵⁶, L. Truong^{33c}, M. Trzebinski⁸⁵, A. Trzupek⁸⁵, F. Tsai⁴⁶, J.C.-L. Tseng¹³⁴, P.V. Tsiareshka^{108,ae}, A. Tsirigotis^{162,u}, V. Tsiskaridze¹⁵⁵, E.G. Tskhadadze^{159a}, M. Tsopoulou¹⁶², I.I. Tsukerman¹²⁴, V. Tsulaia¹⁸, S. Tsuno⁸², D. Tsybychev¹⁵⁵, Y. Tu^{63b}, A. Tudorache^{27b}, V. Tudorache^{27b}, T.T. Tulbure^{27a}, A.N. Tuna⁵⁹, S. Turchikhin⁸⁰, D. Turgeman¹⁸⁰, I. Turk Cakir^{4b,s}, R.J. Turner²¹, R. Turra^{69a}, P.M. Tuts³⁹, S. Tzamarias¹⁶²,

E. Tzovara¹⁰⁰, K. Uchida¹⁶³, F. Ukegawa¹⁶⁹, G. Unal³⁶, M. Unal¹¹, A. Undrus²⁹, G. Unel¹⁷¹,
 F.C. Ungaro¹⁰⁵, Y. Unno⁸², K. Uno¹⁶³, J. Urban^{28b}, P. Urquijo¹⁰⁵, G. Usai⁸, Z. Uysal^{12d}, V. Vacek¹⁴¹,
 B. Vachon¹⁰⁴, K.O.H. Vadla¹³³, T. Vafeiadis³⁶, A. Vaidya⁹⁵, C. Valderanis¹¹⁴, E. Valdes Santurio^{45a,45b},
 M. Valente^{168a}, S. Valentini^{23b,23a}, A. Valero¹⁷⁴, L. Valéry⁴⁶, R.A. Vallance²¹, A. Vallier³⁶,
 J.A. Valls Ferrer¹⁷⁴, T.R. Van Daalen¹⁴, P. Van Gemmeren⁶, S. Van Stroud⁹⁵, I. Van Vulpen¹²⁰,
 M. Vanadia^{74a,74b}, W. Vandelli³⁶, M. Vandenbroucke¹⁴⁴, E.R. Vandewall¹²⁹, A. Vaniachine¹⁶⁶,
 D. Vannicola^{73a,73b}, R. Vari^{73a}, E.W. Varnes⁷, C. Varni^{55b,55a}, T. Varol¹⁵⁸, D. Varouchas⁶⁵, K.E. Varvell¹⁵⁷,
 M.E. Vasile^{27b}, G.A. Vasquez¹⁷⁶, F. Vazeille³⁸, D. Vazquez Furelos¹⁴, T. Vazquez Schroeder³⁶, J. Veatch⁵³,
 V. Vecchio¹⁰¹, M.J. Veen¹²⁰, L.M. Veloce¹⁶⁷, F. Veloso^{139a,139c}, S. Veneziano^{73a}, A. Ventura^{68a,68b},
 A. Verbytskyi¹¹⁵, V. Vercesi^{71a}, M. Verducci^{72a,72b}, C.M. Vergel Infante⁷⁹, C. Vergis²⁴, W. Verkerke¹²⁰,
 A.T. Vermeulen¹²⁰, J.C. Vermeulen¹²⁰, C. Vernier¹⁵³, P.J. Verschueren⁹⁴, M.C. Vetterli^{152,al},
 N. Viaux Maira^{146d}, T. Vickey¹⁴⁹, O.E. Vickey Boeriu¹⁴⁹, G.H.A. Viehhäuser¹³⁴, L. Vigani^{61b},
 M. Villa^{23b,23a}, M. Villaplana Perez³, E.M. Villhauer⁵⁰, E. Vilucchi⁵¹, M.G. Vinchter³⁴, G.S. Virdee²¹,
 A. Vishwakarma⁵⁰, C. Vittori^{23b,23a}, I. Vivarelli¹⁵⁶, M. Vogel¹⁸², P. Vokac¹⁴¹, S.E. von Buddenbrock^{33f},
 E. Von Toerne²⁴, V. Vorobel¹⁴², K. Vorobev¹¹², M. Vos¹⁷⁴, J.H. Vossebeld⁹¹, M. Vozak¹⁰¹, N. Vranjes¹⁶,
 M. Vranjes Milosavljevic¹⁶, V. Vrba^{141,*}, M. Vreeswijk¹²⁰, N.K. Vu¹⁰², R. Vuillermet³⁶, I. Vukotic³⁷,
 S. Wada¹⁶⁹, P. Wagner²⁴, W. Wagner¹⁸², J. Wagner-Kuhr¹¹⁴, S. Wahdan¹⁸², H. Wahlberg⁸⁹, R. Wakasa¹⁶⁹,
 V.M. Walbrecht¹¹⁵, J. Walder¹⁴³, R. Walker¹¹⁴, S.D. Walker⁹⁴, W. Walkowiak¹⁵¹, V. Wallangen^{45a,45b},
 A.M. Wang⁵⁹, A.Z. Wang¹⁸¹, C. Wang^{60a}, C. Wang^{60c}, F. Wang¹⁸¹, H. Wang¹⁸, H. Wang³, J. Wang^{63a},
 P. Wang⁴², Q. Wang¹²⁸, R.-J. Wang¹⁰⁰, R. Wang^{60a}, R. Wang⁶, S.M. Wang¹⁵⁸, W.T. Wang^{60a}, W. Wang^{15c},
 W.X. Wang^{60a}, Y. Wang^{60a}, Z. Wang¹⁰⁶, C. Wanotayaroj⁴⁶, A. Warburton¹⁰⁴, C.P. Ward³², R.J. Ward²¹,
 N. Warrack⁵⁷, A.T. Watson²¹, M.F. Watson²¹, G. Watts¹⁴⁸, B.M. Waugh⁹⁵, A.F. Webb¹¹, C. Weber²⁹,
 M.S. Weber²⁰, S.A. Weber³⁴, S.M. Weber^{61a}, A.R. Weidberg¹³⁴, J. Weingarten⁴⁷, M. Weirich¹⁰⁰,
 C. Weiser⁵², P.S. Wells³⁶, T. Wenaus²⁹, B. Wendland⁴⁷, T. Wengler³⁶, S. Wenig³⁶, N. Wermes²⁴,
 M. Wessels^{61a}, T.D. Weston²⁰, K. Whalen¹³¹, A.M. Wharton⁹⁰, A.S. White¹⁰⁶, A. White⁸, M.J. White¹,
 D. Whiteson¹⁷¹, B.W. Whitmore⁹⁰, W. Wiedenmann¹⁸¹, C. Wiel⁴⁸, M. Wielers¹⁴³, N. Wieseotte¹⁰⁰,
 C. Wiglesworth⁴⁰, L.A.M. Wiik-Fuchs⁵², H.G. Wilkens³⁶, L.J. Wilkins⁹⁴, H.H. Williams¹³⁶,
 S. Williams³², S. Willocq¹⁰³, P.J. Windischhofer¹³⁴, I. Wingerter-Seez⁵, E. Winkels¹⁵⁶, F. Winklmeier¹³¹,
 B.T. Winter⁵², M. Wittgen¹⁵³, M. Wobisch⁹⁶, A. Wolf¹⁰⁰, R. Wölker¹³⁴, J. Wollrath⁵², M.W. Wolter⁸⁵,
 H. Wolters^{139a,139c}, V.W.S. Wong¹⁷⁵, N.L. Woods¹⁴⁵, S.D. Worm⁴⁶, B.K. Wosiek⁸⁵, K.W. Woźniak⁸⁵,
 K. Wright⁵⁷, S.L. Wu¹⁸¹, X. Wu⁵⁴, Y. Wu^{60a}, J. Wuerzinger¹³⁴, T.R. Wyatt¹⁰¹, B.M. Wynne⁵⁰, S. Xella⁴⁰,
 J. Xiang^{63c}, X. Xiao¹⁰⁶, X. Xie^{60a}, I. Xiotidis¹⁵⁶, D. Xu^{15a}, H. Xu^{60a}, H. Xu^{60a}, L. Xu²⁹, T. Xu¹⁴⁴,
 W. Xu¹⁰⁶, Y. Xu^{15b}, Z. Xu^{60b}, Z. Xu¹⁵³, B. Yabsley¹⁵⁷, S. Yacoob^{33a}, D.P. Yallup⁹⁵, N. Yamaguchi⁸⁸,
 Y. Yamaguchi¹⁶⁵, A. Yamamoto⁸², M. Yamatani¹⁶³, T. Yamazaki¹⁶³, Y. Yamazaki⁸³, J. Yan^{60c}, Z. Yan²⁵,
 H.J. Yang^{60c,60d}, H.T. Yang¹⁸, S. Yang^{60a}, T. Yang^{63c}, X. Yang^{60b,58}, Y. Yang¹⁶³, Z. Yang^{106,60a},
 W-M. Yao¹⁸, Y.C. Yap⁴⁶, E. Yatsenko^{60c}, H. Ye^{15c}, J. Ye⁴², S. Ye²⁹, I. Yeletskikh⁸⁰, M.R. Yexley⁹⁰,
 E. Yigitbasi²⁵, P. Yin³⁹, K. Yorita¹⁷⁹, K. Yoshihara⁷⁹, C.J.S. Young³⁶, C. Young¹⁵³, J. Yu⁷⁹, R. Yuan^{60b,h},
 X. Yue^{61a}, M. Zaazoua^{35e}, B. Zabinski⁸⁵, G. Zacharis¹⁰, E. Zaffaroni⁵⁴, J. Zahreddine¹³⁵,
 A.M. Zaitsev^{123,ag}, T. Zakareishvili^{159b}, N. Zakharchuk³⁴, S. Zambito³⁶, D. Zanzi³⁶, S.V. Zeißner⁴⁷,
 C. Zeitnitz¹⁸², G. Zemaityte¹³⁴, J.C. Zeng¹⁷³, O. Zenin¹²³, T. Ženís^{28a}, D. Zerwas⁶⁵, M. Zgubić¹³⁴,
 B. Zhang^{15c}, D.F. Zhang^{15b}, G. Zhang^{15b}, J. Zhang⁶, K. Zhang^{15a}, L. Zhang^{15c}, L. Zhang^{60a}, M. Zhang¹⁷³,
 R. Zhang¹⁸¹, S. Zhang¹⁰⁶, X. Zhang^{60c}, X. Zhang^{60b}, Y. Zhang^{15a,15d}, Z. Zhang^{63a}, Z. Zhang⁶⁵, P. Zhao⁴⁹,
 Y. Zhao¹⁴⁵, Z. Zhao^{60a}, A. Zhemchugov⁸⁰, Z. Zheng¹⁰⁶, D. Zhong¹⁷³, B. Zhou¹⁰⁶, C. Zhou¹⁸¹, H. Zhou⁷,
 M.S. Zhou^{15a,15d}, M. Zhou¹⁵⁵, N. Zhou^{60c}, Y. Zhou⁷, C.G. Zhu^{60b}, C. Zhu^{15a,15d}, H.L. Zhu^{60a}, H. Zhu^{15a},
 J. Zhu¹⁰⁶, Y. Zhu^{60a}, X. Zhuang^{15a}, K. Zhukov¹¹¹, V. Zhulanov^{122b,122a}, D. Ziemska⁶⁶, N.I. Zimine⁸⁰,
 S. Zimmermann^{52,*}, Z. Zinonos¹¹⁵, M. Ziolkowski¹⁵¹, L. Živković¹⁶, G. Zobernig¹⁸¹, A. Zoccoli^{23b,23a},
 K. Zoch⁵³, T.G. Zorbas¹⁴⁹, R. Zou³⁷, L. Zwalinski³⁶.

- ¹Department of Physics, University of Adelaide, Adelaide; Australia.
- ²Physics Department, SUNY Albany, Albany NY; United States of America.
- ³Department of Physics, University of Alberta, Edmonton AB; Canada.
- ⁴(*a*) Department of Physics, Ankara University, Ankara; (*b*) Istanbul Aydin University, Application and Research Center for Advanced Studies, Istanbul; (*c*) Division of Physics, TOBB University of Economics and Technology, Ankara; Turkey.
- ⁵LAPP, Univ. Savoie Mont Blanc, CNRS/IN2P3, Annecy ; France.
- ⁶High Energy Physics Division, Argonne National Laboratory, Argonne IL; United States of America.
- ⁷Department of Physics, University of Arizona, Tucson AZ; United States of America.
- ⁸Department of Physics, University of Texas at Arlington, Arlington TX; United States of America.
- ⁹Physics Department, National and Kapodistrian University of Athens, Athens; Greece.
- ¹⁰Physics Department, National Technical University of Athens, Zografou; Greece.
- ¹¹Department of Physics, University of Texas at Austin, Austin TX; United States of America.
- ¹²(*a*) Bahcesehir University, Faculty of Engineering and Natural Sciences, Istanbul; (*b*) Istanbul Bilgi University, Faculty of Engineering and Natural Sciences, Istanbul; (*c*) Department of Physics, Bogazici University, Istanbul; (*d*) Department of Physics Engineering, Gaziantep University, Gaziantep; Turkey.
- ¹³Institute of Physics, Azerbaijan Academy of Sciences, Baku; Azerbaijan.
- ¹⁴Institut de Física d'Altes Energies (IFAE), Barcelona Institute of Science and Technology, Barcelona; Spain.
- ¹⁵(*a*) Institute of High Energy Physics, Chinese Academy of Sciences, Beijing; (*b*) Physics Department, Tsinghua University, Beijing; (*c*) Department of Physics, Nanjing University, Nanjing; (*d*) University of Chinese Academy of Science (UCAS), Beijing, China.
- ¹⁶Institute of Physics, University of Belgrade, Belgrade; Serbia.
- ¹⁷Department for Physics and Technology, University of Bergen, Bergen; Norway.
- ¹⁸Physics Division, Lawrence Berkeley National Laboratory and University of California, Berkeley CA; United States of America.
- ¹⁹Institut für Physik, Humboldt Universität zu Berlin, Berlin; Germany.
- ²⁰Albert Einstein Center for Fundamental Physics and Laboratory for High Energy Physics, University of Bern, Bern; Switzerland.
- ²¹School of Physics and Astronomy, University of Birmingham, Birmingham; United Kingdom.
- ²²(*a*) Facultad de Ciencias y Centro de Investigaciones, Universidad Antonio Nariño, Bogotá; (*b*) Departamento de Física, Universidad Nacional de Colombia, Bogotá, Colombia; Colombia.
- ²³(*a*) INFN Bologna and Universita' di Bologna, Dipartimento di Fisica; (*b*) INFN Sezione di Bologna; Italy.
- ²⁴Physikalisch Institut, Universität Bonn, Bonn; Germany.
- ²⁵Department of Physics, Boston University, Boston MA; United States of America.
- ²⁶Department of Physics, Brandeis University, Waltham MA; United States of America.
- ²⁷(*a*) Transilvania University of Brasov, Brasov; (*b*) Horia Hulubei National Institute of Physics and Nuclear Engineering, Bucharest; (*c*) Department of Physics, Alexandru Ioan Cuza University of Iasi, Iasi; (*d*) National Institute for Research and Development of Isotopic and Molecular Technologies, Physics Department, Cluj-Napoca; (*e*) University Politehnica Bucharest, Bucharest; (*f*) West University in Timisoara, Timisoara; Romania.
- ²⁸(*a*) Faculty of Mathematics, Physics and Informatics, Comenius University, Bratislava; (*b*) Department of Subnuclear Physics, Institute of Experimental Physics of the Slovak Academy of Sciences, Kosice; Slovak Republic.
- ²⁹Physics Department, Brookhaven National Laboratory, Upton NY; United States of America.
- ³⁰Departamento de Física, Universidad de Buenos Aires, Buenos Aires; Argentina.
- ³¹California State University, CA; United States of America.

- ³²Cavendish Laboratory, University of Cambridge, Cambridge; United Kingdom.
- ³³^(a)Department of Physics, University of Cape Town, Cape Town;^(b)iThemba Labs, Western Cape;^(c)Department of Mechanical Engineering Science, University of Johannesburg, Johannesburg;^(d)National Institute of Physics, University of the Philippines Diliman;^(e)University of South Africa, Department of Physics, Pretoria;^(f)School of Physics, University of the Witwatersrand, Johannesburg; South Africa.
- ³⁴Department of Physics, Carleton University, Ottawa ON; Canada.
- ³⁵^(a)Faculté des Sciences Ain Chock, Réseau Universitaire de Physique des Hautes Energies - Université Hassan II, Casablanca;^(b)Faculté des Sciences, Université Ibn-Tofail, Kénitra;^(c)Faculté des Sciences Semlalia, Université Cadi Ayyad, LPHEA-Marrakech;^(d)LPMR, Faculté des Sciences, Université Mohamed Premier, Oujda;^(e)Faculté des sciences, Université Mohammed V, Rabat; Morocco.
- ³⁶CERN, Geneva; Switzerland.
- ³⁷Enrico Fermi Institute, University of Chicago, Chicago IL; United States of America.
- ³⁸LPC, Université Clermont Auvergne, CNRS/IN2P3, Clermont-Ferrand; France.
- ³⁹Nevis Laboratory, Columbia University, Irvington NY; United States of America.
- ⁴⁰Niels Bohr Institute, University of Copenhagen, Copenhagen; Denmark.
- ⁴¹^(a)Dipartimento di Fisica, Università della Calabria, Rende;^(b)INFN Gruppo Collegato di Cosenza, Laboratori Nazionali di Frascati; Italy.
- ⁴²Physics Department, Southern Methodist University, Dallas TX; United States of America.
- ⁴³Physics Department, University of Texas at Dallas, Richardson TX; United States of America.
- ⁴⁴National Centre for Scientific Research "Demokritos", Agia Paraskevi; Greece.
- ⁴⁵^(a)Department of Physics, Stockholm University;^(b)Oskar Klein Centre, Stockholm; Sweden.
- ⁴⁶Deutsches Elektronen-Synchrotron DESY, Hamburg and Zeuthen; Germany.
- ⁴⁷Lehrstuhl für Experimentelle Physik IV, Technische Universität Dortmund, Dortmund; Germany.
- ⁴⁸Institut für Kern- und Teilchenphysik, Technische Universität Dresden, Dresden; Germany.
- ⁴⁹Department of Physics, Duke University, Durham NC; United States of America.
- ⁵⁰SUPA - School of Physics and Astronomy, University of Edinburgh, Edinburgh; United Kingdom.
- ⁵¹INFN e Laboratori Nazionali di Frascati, Frascati; Italy.
- ⁵²Physikalisch Institut, Albert-Ludwigs-Universität Freiburg, Freiburg; Germany.
- ⁵³II. Physikalisch Institut, Georg-August-Universität Göttingen, Göttingen; Germany.
- ⁵⁴Département de Physique Nucléaire et Corpusculaire, Université de Genève, Genève; Switzerland.
- ⁵⁵^(a)Dipartimento di Fisica, Università di Genova, Genova;^(b)INFN Sezione di Genova; Italy.
- ⁵⁶II. Physikalisch Institut, Justus-Liebig-Universität Giessen, Giessen; Germany.
- ⁵⁷SUPA - School of Physics and Astronomy, University of Glasgow, Glasgow; United Kingdom.
- ⁵⁸LPSC, Université Grenoble Alpes, CNRS/IN2P3, Grenoble INP, Grenoble; France.
- ⁵⁹Laboratory for Particle Physics and Cosmology, Harvard University, Cambridge MA; United States of America.
- ⁶⁰^(a)Department of Modern Physics and State Key Laboratory of Particle Detection and Electronics, University of Science and Technology of China, Hefei;^(b)Institute of Frontier and Interdisciplinary Science and Key Laboratory of Particle Physics and Particle Irradiation (MOE), Shandong University, Qingdao;^(c)School of Physics and Astronomy, Shanghai Jiao Tong University, Key Laboratory for Particle Astrophysics and Cosmology (MOE), SKLPPC, Shanghai;^(d)Tsung-Dao Lee Institute, Shanghai; China.
- ⁶¹^(a)Kirchhoff-Institut für Physik, Ruprecht-Karls-Universität Heidelberg, Heidelberg;^(b)Physikalisches Institut, Ruprecht-Karls-Universität Heidelberg, Heidelberg; Germany.
- ⁶²Faculty of Applied Information Science, Hiroshima Institute of Technology, Hiroshima; Japan.
- ⁶³^(a)Department of Physics, Chinese University of Hong Kong, Shatin, N.T., Hong Kong;^(b)Department of Physics, University of Hong Kong, Hong Kong;^(c)Department of Physics and Institute for Advanced

- Study, Hong Kong University of Science and Technology, Clear Water Bay, Kowloon, Hong Kong; China.
- ⁶⁴Department of Physics, National Tsing Hua University, Hsinchu; Taiwan.
- ⁶⁵IJCLab, Université Paris-Saclay, CNRS/IN2P3, 91405, Orsay; France.
- ⁶⁶Department of Physics, Indiana University, Bloomington IN; United States of America.
- ⁶⁷^(a)INFN Gruppo Collegato di Udine, Sezione di Trieste, Udine;^(b)ICTP, Trieste;^(c)Dipartimento Politecnico di Ingegneria e Architettura, Università di Udine, Udine; Italy.
- ⁶⁸^(a)INFN Sezione di Lecce;^(b)Dipartimento di Matematica e Fisica, Università del Salento, Lecce; Italy.
- ⁶⁹^(a)INFN Sezione di Milano;^(b)Dipartimento di Fisica, Università di Milano, Milano; Italy.
- ⁷⁰^(a)INFN Sezione di Napoli;^(b)Dipartimento di Fisica, Università di Napoli, Napoli; Italy.
- ⁷¹^(a)INFN Sezione di Pavia;^(b)Dipartimento di Fisica, Università di Pavia, Pavia; Italy.
- ⁷²^(a)INFN Sezione di Pisa;^(b)Dipartimento di Fisica E. Fermi, Università di Pisa, Pisa; Italy.
- ⁷³^(a)INFN Sezione di Roma;^(b)Dipartimento di Fisica, Sapienza Università di Roma, Roma; Italy.
- ⁷⁴^(a)INFN Sezione di Roma Tor Vergata;^(b)Dipartimento di Fisica, Università di Roma Tor Vergata, Roma; Italy.
- ⁷⁵^(a)INFN Sezione di Roma Tre;^(b)Dipartimento di Matematica e Fisica, Università Roma Tre, Roma; Italy.
- ⁷⁶^(a)INFN-TIFPA;^(b)Università degli Studi di Trento, Trento; Italy.
- ⁷⁷Institut für Astro- und Teilchenphysik, Leopold-Franzens-Universität, Innsbruck; Austria.
- ⁷⁸University of Iowa, Iowa City IA; United States of America.
- ⁷⁹Department of Physics and Astronomy, Iowa State University, Ames IA; United States of America.
- ⁸⁰Joint Institute for Nuclear Research, Dubna; Russia.
- ⁸¹^(a)Departamento de Engenharia Elétrica, Universidade Federal de Juiz de Fora (UFJF), Juiz de Fora;^(b)Universidade Federal do Rio De Janeiro COPPE/EE/IF, Rio de Janeiro;^(c)Instituto de Física, Universidade de São Paulo, São Paulo; Brazil.
- ⁸²KEK, High Energy Accelerator Research Organization, Tsukuba; Japan.
- ⁸³Graduate School of Science, Kobe University, Kobe; Japan.
- ⁸⁴^(a)AGH University of Science and Technology, Faculty of Physics and Applied Computer Science, Krakow;^(b)Marian Smoluchowski Institute of Physics, Jagiellonian University, Krakow; Poland.
- ⁸⁵Institute of Nuclear Physics Polish Academy of Sciences, Krakow; Poland.
- ⁸⁶Faculty of Science, Kyoto University, Kyoto; Japan.
- ⁸⁷Kyoto University of Education, Kyoto; Japan.
- ⁸⁸Research Center for Advanced Particle Physics and Department of Physics, Kyushu University, Fukuoka ; Japan.
- ⁸⁹Instituto de Física La Plata, Universidad Nacional de La Plata and CONICET, La Plata; Argentina.
- ⁹⁰Physics Department, Lancaster University, Lancaster; United Kingdom.
- ⁹¹Oliver Lodge Laboratory, University of Liverpool, Liverpool; United Kingdom.
- ⁹²Department of Experimental Particle Physics, Jožef Stefan Institute and Department of Physics, University of Ljubljana, Ljubljana; Slovenia.
- ⁹³School of Physics and Astronomy, Queen Mary University of London, London; United Kingdom.
- ⁹⁴Department of Physics, Royal Holloway University of London, Egham; United Kingdom.
- ⁹⁵Department of Physics and Astronomy, University College London, London; United Kingdom.
- ⁹⁶Louisiana Tech University, Ruston LA; United States of America.
- ⁹⁷Fysiska institutionen, Lunds universitet, Lund; Sweden.
- ⁹⁸Centre de Calcul de l’Institut National de Physique Nucléaire et de Physique des Particules (IN2P3), Villeurbanne; France.
- ⁹⁹Departamento de Física Teorica C-15 and CIAFF, Universidad Autónoma de Madrid, Madrid; Spain.
- ¹⁰⁰Institut für Physik, Universität Mainz, Mainz; Germany.

- ¹⁰¹School of Physics and Astronomy, University of Manchester, Manchester; United Kingdom.
- ¹⁰²CPPM, Aix-Marseille Université, CNRS/IN2P3, Marseille; France.
- ¹⁰³Department of Physics, University of Massachusetts, Amherst MA; United States of America.
- ¹⁰⁴Department of Physics, McGill University, Montreal QC; Canada.
- ¹⁰⁵School of Physics, University of Melbourne, Victoria; Australia.
- ¹⁰⁶Department of Physics, University of Michigan, Ann Arbor MI; United States of America.
- ¹⁰⁷Department of Physics and Astronomy, Michigan State University, East Lansing MI; United States of America.
- ¹⁰⁸B.I. Stepanov Institute of Physics, National Academy of Sciences of Belarus, Minsk; Belarus.
- ¹⁰⁹Research Institute for Nuclear Problems of Byelorussian State University, Minsk; Belarus.
- ¹¹⁰Group of Particle Physics, University of Montreal, Montreal QC; Canada.
- ¹¹¹P.N. Lebedev Physical Institute of the Russian Academy of Sciences, Moscow; Russia.
- ¹¹²National Research Nuclear University MEPhI, Moscow; Russia.
- ¹¹³D.V. Skobeltsyn Institute of Nuclear Physics, M.V. Lomonosov Moscow State University, Moscow; Russia.
- ¹¹⁴Fakultät für Physik, Ludwig-Maximilians-Universität München, München; Germany.
- ¹¹⁵Max-Planck-Institut für Physik (Werner-Heisenberg-Institut), München; Germany.
- ¹¹⁶Nagasaki Institute of Applied Science, Nagasaki; Japan.
- ¹¹⁷Graduate School of Science and Kobayashi-Maskawa Institute, Nagoya University, Nagoya; Japan.
- ¹¹⁸Department of Physics and Astronomy, University of New Mexico, Albuquerque NM; United States of America.
- ¹¹⁹Institute for Mathematics, Astrophysics and Particle Physics, Radboud University/Nikhef, Nijmegen; Netherlands.
- ¹²⁰Nikhef National Institute for Subatomic Physics and University of Amsterdam, Amsterdam; Netherlands.
- ¹²¹Department of Physics, Northern Illinois University, DeKalb IL; United States of America.
- ¹²²^(a)Budker Institute of Nuclear Physics and NSU, SB RAS, Novosibirsk; ^(b)Novosibirsk State University Novosibirsk; Russia.
- ¹²³Institute for High Energy Physics of the National Research Centre Kurchatov Institute, Protvino; Russia.
- ¹²⁴Institute for Theoretical and Experimental Physics named by A.I. Alikhanov of National Research Centre "Kurchatov Institute", Moscow; Russia.
- ¹²⁵Department of Physics, New York University, New York NY; United States of America.
- ¹²⁶Ochanomizu University, Otsuka, Bunkyo-ku, Tokyo; Japan.
- ¹²⁷Ohio State University, Columbus OH; United States of America.
- ¹²⁸Homer L. Dodge Department of Physics and Astronomy, University of Oklahoma, Norman OK; United States of America.
- ¹²⁹Department of Physics, Oklahoma State University, Stillwater OK; United States of America.
- ¹³⁰Palacký University, Joint Laboratory of Optics, Olomouc; Czech Republic.
- ¹³¹Institute for Fundamental Science, University of Oregon, Eugene, OR; United States of America.
- ¹³²Graduate School of Science, Osaka University, Osaka; Japan.
- ¹³³Department of Physics, University of Oslo, Oslo; Norway.
- ¹³⁴Department of Physics, Oxford University, Oxford; United Kingdom.
- ¹³⁵LPNHE, Sorbonne Université, Université de Paris, CNRS/IN2P3, Paris; France.
- ¹³⁶Department of Physics, University of Pennsylvania, Philadelphia PA; United States of America.
- ¹³⁷Konstantinov Nuclear Physics Institute of National Research Centre "Kurchatov Institute", PNPI, St. Petersburg; Russia.
- ¹³⁸Department of Physics and Astronomy, University of Pittsburgh, Pittsburgh PA; United States of

America.

¹³⁹(*a*) Laboratório de Instrumentação e Física Experimental de Partículas - LIP, Lisboa; ^(b)Departamento de Física, Faculdade de Ciências, Universidade de Lisboa, Lisboa; ^(c)Departamento de Física, Universidade de Coimbra, Coimbra; ^(d)Centro de Física Nuclear da Universidade de Lisboa, Lisboa; ^(e)Departamento de Física, Universidade do Minho, Braga; ^(f)Departamento de Física Teórica y del Cosmos, Universidad de Granada, Granada (Spain); ^(g)Dep Física and CEFITEC of Faculdade de Ciências e Tecnologia, Universidade Nova de Lisboa, Caparica; ^(h)Instituto Superior Técnico, Universidade de Lisboa, Lisboa; Portugal.

¹⁴⁰Institute of Physics of the Czech Academy of Sciences, Prague; Czech Republic.

¹⁴¹Czech Technical University in Prague, Prague; Czech Republic.

¹⁴²Charles University, Faculty of Mathematics and Physics, Prague; Czech Republic.

¹⁴³Particle Physics Department, Rutherford Appleton Laboratory, Didcot; United Kingdom.

¹⁴⁴IRFU, CEA, Université Paris-Saclay, Gif-sur-Yvette; France.

¹⁴⁵Santa Cruz Institute for Particle Physics, University of California Santa Cruz, Santa Cruz CA; United States of America.

¹⁴⁶(*a*) Departamento de Física, Pontificia Universidad Católica de Chile, Santiago; ^(b)Universidad Andres Bello, Department of Physics, Santiago; ^(c)Instituto de Alta Investigación, Universidad de Tarapacá, Arica; ^(d)Departamento de Física, Universidad Técnica Federico Santa María, Valparaíso; Chile.

¹⁴⁷Universidade Federal de São João del Rei (UFSJ), São João del Rei; Brazil.

¹⁴⁸Department of Physics, University of Washington, Seattle WA; United States of America.

¹⁴⁹Department of Physics and Astronomy, University of Sheffield, Sheffield; United Kingdom.

¹⁵⁰Department of Physics, Shinshu University, Nagano; Japan.

¹⁵¹Department Physik, Universität Siegen, Siegen; Germany.

¹⁵²Department of Physics, Simon Fraser University, Burnaby BC; Canada.

¹⁵³SLAC National Accelerator Laboratory, Stanford CA; United States of America.

¹⁵⁴Department of Physics, Royal Institute of Technology, Stockholm; Sweden.

¹⁵⁵Departments of Physics and Astronomy, Stony Brook University, Stony Brook NY; United States of America.

¹⁵⁶Department of Physics and Astronomy, University of Sussex, Brighton; United Kingdom.

¹⁵⁷School of Physics, University of Sydney, Sydney; Australia.

¹⁵⁸Institute of Physics, Academia Sinica, Taipei; Taiwan.

¹⁵⁹(*a*) E. Andronikashvili Institute of Physics, Iv. Javakhishvili Tbilisi State University, Tbilisi; ^(b)High Energy Physics Institute, Tbilisi State University, Tbilisi; Georgia.

¹⁶⁰Department of Physics, Technion, Israel Institute of Technology, Haifa; Israel.

¹⁶¹Raymond and Beverly Sackler School of Physics and Astronomy, Tel Aviv University, Tel Aviv; Israel.

¹⁶²Department of Physics, Aristotle University of Thessaloniki, Thessaloniki; Greece.

¹⁶³International Center for Elementary Particle Physics and Department of Physics, University of Tokyo, Tokyo; Japan.

¹⁶⁴Graduate School of Science and Technology, Tokyo Metropolitan University, Tokyo; Japan.

¹⁶⁵Department of Physics, Tokyo Institute of Technology, Tokyo; Japan.

¹⁶⁶Tomsk State University, Tomsk; Russia.

¹⁶⁷Department of Physics, University of Toronto, Toronto ON; Canada.

¹⁶⁸(*a*) TRIUMF, Vancouver BC; ^(b)Department of Physics and Astronomy, York University, Toronto ON; Canada.

¹⁶⁹Division of Physics and Tomonaga Center for the History of the Universe, Faculty of Pure and Applied Sciences, University of Tsukuba, Tsukuba; Japan.

¹⁷⁰Department of Physics and Astronomy, Tufts University, Medford MA; United States of America.

- ¹⁷¹Department of Physics and Astronomy, University of California Irvine, Irvine CA; United States of America.
- ¹⁷²Department of Physics and Astronomy, University of Uppsala, Uppsala; Sweden.
- ¹⁷³Department of Physics, University of Illinois, Urbana IL; United States of America.
- ¹⁷⁴Instituto de Física Corpuscular (IFIC), Centro Mixto Universidad de Valencia - CSIC, Valencia; Spain.
- ¹⁷⁵Department of Physics, University of British Columbia, Vancouver BC; Canada.
- ¹⁷⁶Department of Physics and Astronomy, University of Victoria, Victoria BC; Canada.
- ¹⁷⁷Fakultät für Physik und Astronomie, Julius-Maximilians-Universität Würzburg, Würzburg; Germany.
- ¹⁷⁸Department of Physics, University of Warwick, Coventry; United Kingdom.
- ¹⁷⁹Waseda University, Tokyo; Japan.
- ¹⁸⁰Department of Particle Physics and Astrophysics, Weizmann Institute of Science, Rehovot; Israel.
- ¹⁸¹Department of Physics, University of Wisconsin, Madison WI; United States of America.
- ¹⁸²Fakultät für Mathematik und Naturwissenschaften, Fachgruppe Physik, Bergische Universität Wuppertal, Wuppertal; Germany.
- ¹⁸³Department of Physics, Yale University, New Haven CT; United States of America.
- ^a Also at Borough of Manhattan Community College, City University of New York, New York NY; United States of America.
- ^b Also at Centro Studi e Ricerche Enrico Fermi; Italy.
- ^c Also at CERN, Geneva; Switzerland.
- ^d Also at CPPM, Aix-Marseille Université, CNRS/IN2P3, Marseille; France.
- ^e Also at Département de Physique Nucléaire et Corpusculaire, Université de Genève, Genève; Switzerland.
- ^f Also at Departament de Fisica de la Universitat Autonoma de Barcelona, Barcelona; Spain.
- ^g Also at Department of Financial and Management Engineering, University of the Aegean, Chios; Greece.
- ^h Also at Department of Physics and Astronomy, Michigan State University, East Lansing MI; United States of America.
- ⁱ Also at Department of Physics and Astronomy, University of Louisville, Louisville, KY; United States of America.
- ^j Also at Department of Physics, Ben Gurion University of the Negev, Beer Sheva; Israel.
- ^k Also at Department of Physics, California State University, East Bay; United States of America.
- ^l Also at Department of Physics, California State University, Fresno; United States of America.
- ^m Also at Department of Physics, California State University, Sacramento; United States of America.
- ⁿ Also at Department of Physics, King's College London, London; United Kingdom.
- ^o Also at Department of Physics, St. Petersburg State Polytechnical University, St. Petersburg; Russia.
- ^p Also at Department of Physics, University of Fribourg, Fribourg; Switzerland.
- ^q Also at Dipartimento di Matematica, Informatica e Fisica, Università di Udine, Udine; Italy.
- ^r Also at Faculty of Physics, M.V. Lomonosov Moscow State University, Moscow; Russia.
- ^s Also at Giresun University, Faculty of Engineering, Giresun; Turkey.
- ^t Also at Graduate School of Science, Osaka University, Osaka; Japan.
- ^u Also at Hellenic Open University, Patras; Greece.
- ^v Also at IJCLab, Université Paris-Saclay, CNRS/IN2P3, 91405, Orsay; France.
- ^w Also at Institutio Catalana de Recerca i Estudis Avancats, ICREA, Barcelona; Spain.
- ^x Also at Institut für Experimentalphysik, Universität Hamburg, Hamburg; Germany.
- ^y Also at Institute for Nuclear Research and Nuclear Energy (INRNE) of the Bulgarian Academy of Sciences, Sofia; Bulgaria.
- ^z Also at Institute for Particle and Nuclear Physics, Wigner Research Centre for Physics, Budapest; Hungary.

- ^{aa} Also at Institute of Particle Physics (IPP); Canada.
- ^{ab} Also at Institute of Physics, Azerbaijan Academy of Sciences, Baku; Azerbaijan.
- ^{ac} Also at Instituto de Fisica Teorica, IFT-UAM/CSIC, Madrid; Spain.
- ^{ad} Also at Istanbul University, Dept. of Physics, Istanbul; Turkey.
- ^{ae} Also at Joint Institute for Nuclear Research, Dubna; Russia.
- ^{af} Also at Louisiana Tech University, Ruston LA; United States of America.
- ^{ag} Also at Moscow Institute of Physics and Technology State University, Dolgoprudny; Russia.
- ^{ah} Also at National Research Nuclear University MEPhI, Moscow; Russia.
- ^{ai} Also at Physics Department, An-Najah National University, Nablus; Palestine.
- ^{aj} Also at Physikalisches Institut, Albert-Ludwigs-Universität Freiburg, Freiburg; Germany.
- ^{ak} Also at The City College of New York, New York NY; United States of America.
- ^{al} Also at TRIUMF, Vancouver BC; Canada.
- ^{am} Also at Universita di Napoli Parthenope, Napoli; Italy.
- ^{an} Also at University of Chinese Academy of Sciences (UCAS), Beijing; China.
- * Deceased